ISTANBUL TECHNICAL UNIVERSITY ★ GRADUATE SCHOOL OF SCIENCE ENGINEERING AND TECHNOLOGY

SYNTHESIS AND CHARACTERIZATION OF ORGANIC-INORGANIC HYBRID MATERIALS

Ph.D. THESIS

Müfide Duriye KARAHASANOĞLU

Polymer Science and Technology

Polymer Science and Technology

MARCH 2015

ISTANBUL TECHNICAL UNIVERSITY ★ GRADUATE SCHOOL OF SCIENCE ENGINEERING AND TECHNOLOGY

SYNTHESIS AND CHARACTERIZATION OF ORGANIC-INORGANIC HYBRID MATERIALS

Ph.D. THESIS

Müfide Duriye KARAHASANOĞLU
(515052007)

Polymer Science and Technology

Polymer Science and Technology

Thesis Advisor: Prof. Dr. İ. Ersin SERHATLI

MARCH 2015

İSTANBUL TEKNİK ÜNİVERSİTESİ ★ FEN BİLİMLERİ ENSTİTÜSÜ

ORGANİK-İNORGANİK HİBRİT MALZEMELERİN SENTEZİ VE KARAKTERİZASYONU

DOKTORA TEZİ

Müfide Duriye KARAHASANOĞLU
(515052007)

Polimer Bilimi ve Teknolojileri

Polimer Bilimi ve Teknolojileri

Tez Danışmanı: Prof. Dr. İ. Ersin SERHATLI

MART 2015

Müfide Duriye Karahasanoğlu, a Ph.D. student of ITU Graduate School of Science Engineering and Technology student ID 515052007, successfully defended the thesis entitled "SYNTHESIS AND CHARACTERIZATION OF ORGANIC-INORGANIC HYBRID MATERIALS", which she prepared after fulfilling the requirements specified in the associated legislations, before the jury whose signatures are below.

Thesis Advisor :	**Prof. Dr. İbrahim Ersin SERHATLI** Istanbul Technical University	.....
Jury Members :	**Prof. Dr. Hacer Ayşen ÖNEN** Istanbul Technical University	.....
	Prof. Dr. Ahmet AKAR Istanbul Technical University	.....
	Prof. Dr. Yusuf MENCELOĞLU Sabancı University	.....
	Prof. Dr. Tarık EREN Yıldız Technical University	.....

Date of Submission : 16 January 2015
Date of Defense : 04 March 2015

To my father,

FOREWORD

I would like to thank my thesis supervisor, Professor İ. Ersin Serhatlı for giving me the opportunity to work in his group and I appreciate for his effort, time and suggestions for my thesis. For all of her support and valuable comments, I wish to thank Professor H. Ayşen Önen.

I would like to thank Professor Yusuf Menceloğlu, the member of my thesis committee, for his suggestions and contribution to this thesis.

I wish to give my sincere thanks to all the research assistants of Chemistry Department of ITU whom I worked with and also to all the faculty members and the staff of the department.

Furthermore, I want to give my warm thanks to Gökçe Merey, Burçin Gacal, Demet G. Çolak, Tuba Çakır Çanak for being right next to me and also to Argun T. Gökçeören, Abdullah Aydoğan, Cüneyt Ünlü, Armağan Atsay and Ufuk S. Günay for all their support.

Additionaly, I would also like to thank Ömer F. Vurur and all members and the students of POLMAG laboratory for sharing together the good and the bad as time brought us.

I am grateful for having my family, and I would specially thank to my mother for her patience and consistency in believing in me and her support at every condition. Her wisdom and generosity were my great fortune during my PhD.

For my father's memory, I would like to dedicate my thesis to my father who always encouraged me to do whatever I want in any circumstance and inherited me the passion for the truth and for searching ultimate reality.

January 2015

Müfide D. Karahasanoğlu
Chemist, M.Sc.

TABLE OF CONTENTS

Page

ABBREVIATIONS

SNP	**:** Silica nanoparticles
MMA	**:** Methyl Methacrylate
PMMA	**:** Poly(methyl metacrylate)
EA	**:** Epoxy acrylate
TDI	**:** Toluene diisocyanate
DMF	**:** N,N-dimehthylformamide
DBTL	**:** Dibutylytin dilaurate
THF	**:** Tetrahydrofuran
TEOS	**:** Tetraethyl orthosilicate
IPTES	**:** 3-(triethoxysilyl)propyl isocyanate
MAPTMS	**:** 3-(trimethoxysilyl)propyl methacrylate
TEA	**:** Triethylamine
HDDA	**:** Hexane diol diacrylate
TPGDA	**:** Tripropylene glycol diacrylate
UV	**:** Ultraviole
SEM	**:** Scanning Electron Microscope
TEM	**:** Transmission Electron Microscope
FTIR	**:** Fourier-Transform Infrared Spectroscopy
NMR	**:** Nuclear Magnetic Resonance Spectroscopy
CP- NMR	**:** Cross Polarization Nuclear Magnetic Resonance Spectroscopy
MAS	**:** Magic angle spin
TGA	**:** Thermogravimetric Analysis
DSC	**:** Differential Scanning Calorimetry

LIST OF TABLES

Page

LIST OF FIGURES

Page

SYNTHESIS AND CHARACTERIZATION OF ORGANIC-INORGANIC HYBRID MATERIALS

SUMMARY

Organic–inorganic hybrids that combine the advantages of both kinds of materials, such as mechanical strength and thermal stability with the processability and flexibility of an organic polymer matrix, exhibit multifunctional characteristics. Hybrid materials with the desired properties can be obtained in many forms such as bulk, powder, nanocomposites, coatings, glasses, fibres, foams etc., depending on the forming process and a wide variety of components of hybrids such as metal oxides, alloys, ceramics, clay, rubber, resins, elastomers, natural materials. Through the combinations of different inorganic and organic components with appropriate processing methods hybrid materials can be developed with new properties for electrical, optical, biomedical, structural, or related applications.

In principle two different approaches are used for the formation of hybrid materials: First approach, well-defined preformed building blocks are applied that react with each other to form the final hybrid material in which the precursors of blocks still at least partially keep their original integrity and second approach, one or both structural units are formed from the precursors that are transformed into a novel (network) structure as in-situ method.

There are mainly two classes of hybrid materials; the one with weak interactions between the two components of hybrid materials, such as van der Waals, hydrogen bonding or weak electrostatic interactions and no strong interaction such as covalent bonds and the second having strong chemical interactions between the components of the hybrid materials such as covalently bonding.

Silica has attracted much interest due to their low toxicity, ease of formation in a wide range of sizes and morphologies, high stability, and the surface that can be further functionalized. This thesis based on the study of incorporation of silica nanoparticles and silicon dioxide network domains, as the inorganic components, with organic polymeric structures leading the formation of hybrid materials and, the characterization of the such materials. The interactions between the inorganic silicon dioxide and organic components were based on the strong chemical interaction as covalent bonding.

Silica nanoparticles leading to an extreme increase in interfacial area have been considered as a challenging reinforcement with a wide range of properties for hybrid materials. Their efficiency in polymeric matrices requires uniform dispersion and strong interfacial bonding between two component of the hybrids. Common strategies are being developed to improve the poor dispersion of nanoparticles in polymer matrices and also organic solvents for advanced interfacial bonding of nanoparticles and matrices. Coupling reactions of silica nanoparticles with silane coupling agents

having functional groups is one of the most common approaches for the modification of the surface of the silica particles.

As the first step of the coupling reaction, silane coupling agents hydrolyze to form silanols and during the hydrolysis step, condensation can also take place between silanols resulting in ormation of siloxane bridges (Si-O-Si). The condensation between the silanol groups of coupling agents decrease the number of free silanols of silane coupling agents that reduce the rate of possible condensation with the silanol groups of the silica particles. Hence, the formation of a siloxane network layer on the surface of the silica nanoparticles may also results in a variety of concentration of functional groups of silane coupling agents.

In the second step of coupling reaction of silica particles, the possibility of different type of condensation reactions between free silanol groups of coupling agents and silanol groups of silica nanoparticles may also result in inadequate concentration of functional groups grafted on the surface of silica particles. Seemingly effective coupling reactions of silica nanoparticles over the silane coupling agents may become challenging due to the such disadvantages. Direct functionalization of the surface of silica particles with reactive organic moieties can overcome such problems of silane coupling reactions and the limitation of high concentration of functional groups on the surface of silica particle. 2,4-toluene diisocyanate (TDI) having two reactive isocyanate groups takes the place of being a very effective organic moiety for reacting with the hydroxyl groups of silica particles resulting in surface grafting and also for bringing the ability for further reactions on the surface of silica particles.

Grafting of end-functional polymers on the surface of silica nanoparticle as “grafting to” method has been described as one of the main approaches and the “grafting from” method, where polymers are grown from either monomer functionalized or initiator functionalized surfaces of silica nanoparticles, has been described as another approach. By a free radical manner, in most of silica nanoparticles functionalized with the organic monomers, the polymerization proceeds both by surface monomers of nanoparticles and by the free monomers existing in polymerization medium resulting a high ratio of ungrafted polymer formation. For this reason, initiator grafted nanoparticles may be considered for the higher grafting ratios of polymers onto the nanoparticles surfaces.

In this study, firstly, well defined, mono-dispersed silica nanoparticles within desired size range was synthesized according to Stöber method as depicted in Figure 1. Physical and chemical structure of the nanoparticles such as particle size, specific surface area and hydroxyl number characterized clarifying their surface properties for the modification of silica nanoparticles.

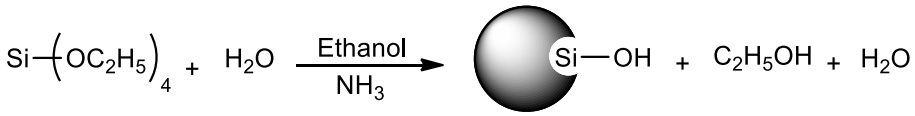

Figure 1 : Synthesis of silica nanoparticles by Stöber method.

After the definition of the silica nanoparticles, surface modification of the nanoparticles was achieved with the reaction over isocyanate groups of toluen di-isocyanate (TDI) in order to gain both improved dispersion in organic phase and further attachment possibility of benzoin photoinitiator moieties onto the surface of silica nanoparticles as represented in Figure 2.

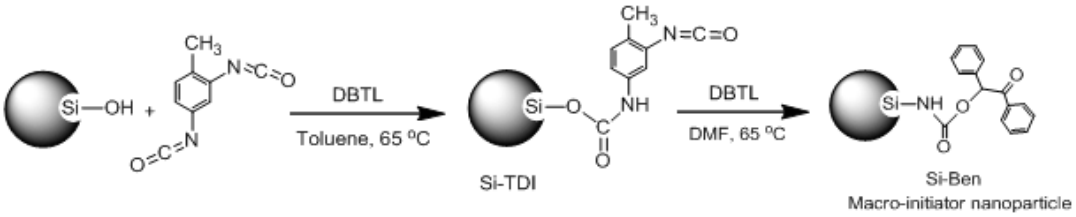

Figure 2 : Grafting of TDI and benzoin moeities onto the surface of silica nanoparticles

In the second stage, photopolymerization of methyl methacrylate (MMA) was achived over the benzoin photo-initiator attached succesfully onto the surface of silica nanoparticles. Since it was discovered by Dupont, photoinitiated polymerization has become an important industrial process. The main positive attributes of photochemical processes are that they offer a rapid conversion of formulated reactive liquids to solids by radical or cationic means. The photopolymerization of MMA by grafting from method was simply performed under UV radiation in the presence of benzoin functionalized silica macroitiators.

Well-defined, spherical silica nanoparticles grafted with TDI was also incorporated into preformed epoxy-acrylate resin over the covalent bonding between hydroxyl groups of epoxy resin and free isocyanate groups of Si-TDI by the formation of urethane linkage. Epoxy-acrylate resin forming networks with chemically incorporated silica naoparticles (EA-Si hybrid resin) was cured under UV treatment in the form of film. The effect of uniform, well-dispersed, covalently incorporated silica nanoparticles on the thermal, morphological and mechanical behavior of cured EA-Si hybrid film was also investigated.

In this thesis, the design of alkoxysilane precursor of aromatic amide-urethane structure was also aimed for the formation of silicon dioxide network domains and polymeric matrix together as hybrid material. For this purpose, preformed terephthalic acid chloride was reacted with m-amino phenol yielding aromatic amid containing dihydroxy monomer, N^1,N^4-bis(3-hydroxyphenyl), and the reaction of the synthesized monomer with amino propyl trimethoxysilane (IPTES), formed alkoxysilane containing aromatic amide-urethane macromonomer, over the urethane linkage. Synthesized macromonomer (Figure 3) characterized by ^{1}HNMR indicating the high purity, has the potential to form hybrid materials by owning the organic and inorganic precursor in the same macromonomer. Aromatic amide-urethane alkoxy silane based sol-gel was prepared and incorparated into epoxy acrylate resin formulations following UV curing process. The resulting epoxy acrylate hybrid material was determined and thermal and morphological properties of the hybrid material were characterized.

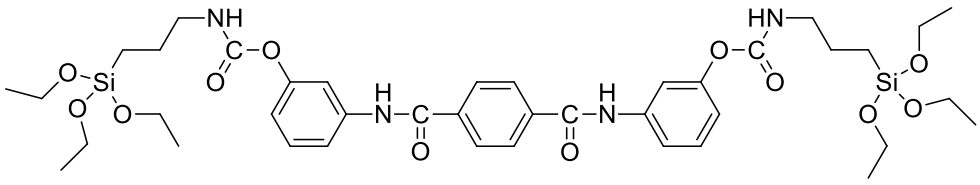

Figure 3 : Alkoxysilane modified aromatic amide-urethane precursor.

ORGANİK-İNORGANİK HİBRİT MALZEMELERİN SENTEZİ VE KARAKTERİZASYONU

ÖZET

Mekanik dayanıklılık ve termal kararlılık özellikleri ile organik polimer matrislerinin işlenebilirlik ve esneklik özelliklerini birleştiren organik-inorganik hibrit malzemeler çok fonksiyonlu karakterler gösterirler. İstenilen özelliklere sahip hibrit malzemeler oluşum süreçlerine göre kalıp, toz, nanokompozit, kaplama, cam, elyaf, köpük ve benzeri pek çok şekilde elde edilebilirler ve metal oksit, alaşım, seramik, kil, kauçuk, reçine, elastomer ve doğal malzemeler gibi geniş çapta hibrit bileşenlerden oluşurlar. Farklı inorganik ve organik bileşenlerin uygun işleme yöntemleri kullanılarak birleştirilmesi ile elektrik, optik, biomedikal, yapı ile ilgili ve daha pek çok uygulama alanlarında yeni özelliklere sahip hibrit malzemeler geliştirilebilir.

Prensip olarak hibrit malzemelerin oluşumu için kullanılan iki farklı yaklaşım vardır. İlkinde özellikleri iyi belirlenerek önceden oluşturulmuş yapılar birbirleriyle reaksiyona girerek istenilen hibrit malzemeyi oluşturur. Burada her iki yapının önceki orijinal özellikleri bir miktar korunmaktadır. İkinci yaklaşımda ise hibriti oluşturan yapılardan biri ya da her ikisi birden ilk hallerinden başlayarak kullanılır ve insitü olarak özgün yapılara (ağ yapısı) dönüştürülür.

Temel olarak iki tür hibrit malzeme vardır. Birincisi, hibrit malzemeyi oluşturan iki bileşenin birbirine van der Waals kuvvetleri, hidrojen bağı ya da zayıf elektrostatik etkileşimler gibi zayıf etkileşimlerle bağlandığı, kovalent bağlar gibi kuvvetli etkileşimlerin olmadığı malzemelerdir. İkinci tip ise hibrit malzemeyi oluşturan bileşenlerin kovalent bağ gibi güçlü etkileşimlerle birbirine bağlandığı malzemelerdir.

Bu tez çalışması, inorganik bileşen olarak silika (silikon dioksit) nanopartikülleri ve silikon dioksit ağ örgüsü ile organik polimerik yapıların birleşimiyle oluşan hibrit malzemeler ve bu malzemelerin karakterizasyonuna dayanmaktadır. İnorganik silikon dioksit ile organik yapının etkileşimi kovalent bağ ile oluşan güçlü bir etkileşimdir. Silikalar düşük toksisiteye sahip olmaları, farklı boyut ve morfolojilere sahip olacak şekilde kolaylıkla sentezlenebilmeleri, yüksek kararlılıkları ve fonksiyonlandırılabilir yüzeyleri sayesinde oldukça ilgi çekmektedirler.

Geniş yüzey alanı yaratabilen silika nanopartiküller, hibrit materyallerin farklı farklı özelliklere sahip olmasını sağlayan ilgi çekici örnekler olarak görülmüştür. Polimer matrisleri içinde gösterdikleri etki, homojen dağılıp dağılmadıklarına ve hibriti oluşturan iki bileşen arasında güçlü yüzey etkileşimleri sağlayıp sağlayamamalarına bağlıdır. Nanopartiküllerin polimer matrisi içinde zayıf dağılımlarını üstesinden gelebilmek için ortak stratejiler geliştirilmiş ve ayrıca nanopartikül ve matris arasındaki yüzey etkileşimini artırmak için çeşitli organik çözücüler kullanılmıştır. Silika partiküllerinin yüzey modifikasyonunu sağlamak için kullanılan en genel

yaklaşım, silika nanopartiküllerin fonksiyonel grup içeren birleştirici silan bileşikleriyle kenetlenme reaksiyonlarıdır.

Kenetlenme reaksiyonlarının ilk aşaması, silan kenetlenme bileşiklerinin hidrolizi sonucu silanol (mono, di ve trisilanol) oluşumudur ve hidroliz aşamasında bu silanol grupları arasında gerçekleşen kondenzasyon sonucu dimer, oligomer veya siloksan (Si-O-Si) ağı oluşur. Silanol grupları arasında gerçekleşen kondenzasyon reaksiyonları, silan bileşiklerindeki serbest silanollerin sayısını azaltır ve bu nedenle fonksiyonel grup içeren silan yapıların içeren silika nanopartikülleri ile silanol gruplarının kondenzasyon hızı düşer. Silika nanopartiküllerinin yüzeyinde siloksan ağının oluşması silan bileşiklerindeki fonksiyonel grupların çeşitli şekillerde azalmasına neden olur.

Kenetlenme reaksiyonlarının ikinci aşamasında ise, kenetlenme bileşiklerinin serbest silanol grupları, silika nanopartiküllerinin silanol grupları ile kondense olur. Kenetlenme bileşiklerinin serbest silanol grupları ile silika nanopartiküllerin silanol grupları arasında gerçekleşebilecek olan farklı tip kondenzasyon reaksiyonları silika partiküllerinin yüzeyindeki fonksiyonel grupların azalmasına neden olabilir. Silan kenetlenme bileşiklerinin reaksiyonlarına göre daha etkin görünen silika nanopartiküllerin kenetlenme reaksiyonları pek çok dezavantaj yüzünden zorlayıcı olabilmektedir. Silika partiküllerin yüzeylerinin toluendiizosiyanat (TDI) gibi reaktif organik yapılarla doğrudan fonksiyonlandırılması, silan kenetlenme reaksiyonları ve silika yüzeyindeki fonksiyonel grup sayısının sınırlandırılması gibi problemleri çözmek için avantaj sağlayabilir. Oldukça reaktif iki izosiyanat grubu taşıyan toluendiizosiyanat, silika taneciklerindeki hidroksil gruplarıyla reaksiyona girerek oldukça etkin bir organik yapı olarak davranmaktadır. Böylelikle silika yüzeyinin fonksiyonlandırılması ve sonrasında izosiyanat gruplarıyla gerçekleştirilebilecek sonraki aşama reaksiyonları mümkün olmaktadır.

Silika nanopartiküllerin yüzeyinde bulunan ve fonksiyonel uç grup içeren polimerlerin uç grup üzerinden yeniden fonksiyonlandırılması en çok uygulanan yöntemlerdendir. Monomer ya da başlatıcı ile fonksiyonlandırılmış silika nanopartikül yüzeylerinde polimerleşme reaksiyonlarının gerçekleştirilmesi uygulanan bir diğer yöntemdir. Serbest radikallerin olması durumunda polimerleşme, organik monomerler tarafından fonksiyonlandırılan silika nanopartiküllerde hem nanopartiküllerin yüzey monomerleri hem de polimerizasyon ortamında bulunan serbest monomerler ile gerçekleşir ve bu durum yüksek oranda fonksiyonlandırılmadan kalan polimer oluşumuna neden olur. Bu nedenle, nanopartiküllerin yüzeyinde daha çok polimerin oluşabilmesi için başlatıcı ile fonksiyonlandırılmış nanopartiküllerin kullanımı düşünülebilir.

Bu çalışmada ilk olarak, iyi karakterize edilmiş, homojen dağılımlı silika nanopartiküller Stöber yöntemi kullanılarak istenilen boyut aralığında Şekil 1'de gösterildiği gibi sentezlenmiştir. Sentezlenen silika nanopartiküllerin tanecik boyutu, spesifik yüzey alanı ve hidroksil sayısı gibi fiziksel ve kimyasal özellikleri incelenerek modifikasyon için gerekli yüzey özellikleri belirlenmiştir.

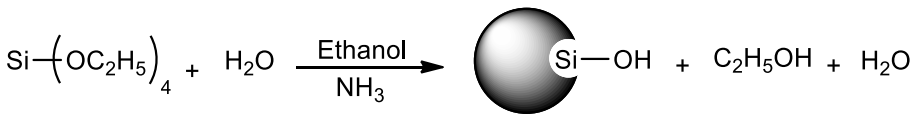

Şekil 1 : Stöber yöntemi ile silika nanopartiküllerin sentezi.

Taneciklerin tanımlanmasından sonra yüzey modifikasyonu, nanopartiküllerin organik fazda daha iyi dağılımının sağlanması ve sonrasında benzoin fotobaşlatıcının bağlanabilmesi için toluendiizosiyanata ait izosiyanat gruplarının reaksiyonları ile sağlanmıştır (Şekil 2).

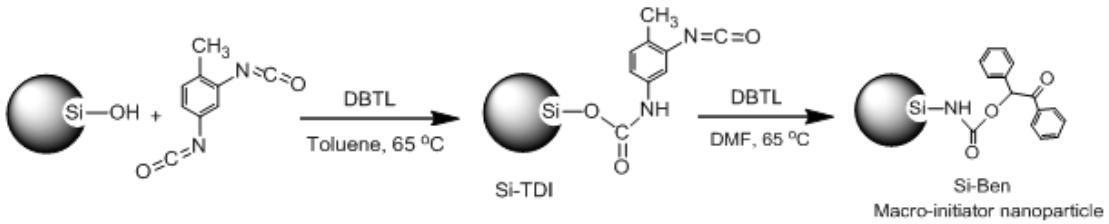

Şekil 2 : TDI ve benzoinin silika nanopartiküllerin yüzeyine bağlanması.

Çalışmanın ikinci aşamasında, silika nanopartiküllerinin yüzeyinde önceden bağlanmış olan benzoin fotobaşlatıcı ile metil metaakrilat (MMA) fotopolimerizasyonu başarıyla gerçekleştirilmiştir. Dupont firması tarafından keşfedildiğinden beri fotobaşlatıcılı polimerizasyon endüstriyel üretimde önemli bir yere sahiptir. Fotokimyasal süreçlerin en önemli olumlu tarafı, reaktif sıvıları hızlı bir şekilde radikalik ya da katyonik olarak katıya dönüştürebilmeleridir. Önceden fotobaşlatıcı bağlanıp sonradan MMA fotopolimerizasyonunun gerçekleştirildiği bu yöntemde polimerizasyon, benzoin fonksiyonu bağlanmış silika makrobaşlatıcılar ile basitçe UV ışığı altında gerçekleştirilmiştir.

TDI ile fonksiyonlandırılmış, homojen dağılımlı, küresel silika nanopartiküller (Si-TDI), önceden oluşturulmuş epoksi-akrilat reçinelerine de epoksi reçinelerin hidroksil grupları ve Si-TDI'ın serbest izosiyanat grupları arasında kovalent bağ kurarak üretan köprüleri üzerinden bağlanmışlardır. İyi tanımlanmış, kimyasal olarak bağlanmış silika nanopartiküller ile ağ yapısı oluşturan epoksi-akrilat reçineleri UV altında kürlenerek film oluşturmuşlardır. Sentezlenen hibrit epoksi-akrilat filmlerin ısısal, morfolojiik ve mekanik özellikleri incelenmiştir.

Ayrıca silikon dioksit ağ yapısı ve polimer matrisin beraber oluşumu ile gerçekleştirilen sol-jel reaksiyonu da hibrit malzemelerin sentezi için uygulanmıştır. Bu amaçla, terefitalik asit klorür amino fenol ile reaksiyona sokularak aromatik amit fonksiyonu içeren dihidroksi ön yapıları oluşturulmuştur ve ön yapılar aminopropil trimetoksisilan ile modifiye edilerek Şekil 3'te gösterilen iyi tasarlanmış makromonomeri oluşturmuştur. Alkoksisilan ile reaksiyondan elde edilen bu makromonomer hibrit malzemelerin sentezi için kullanılmıştır. Aromatik amit-üretan alkoksi silan yapılı monomerden soljel hazırlanmış ve epoksi akrilat reçine formülasyonlarına dahil edilmiştir, formülasyonların UV ışığı altında kürlenmeleriyle hibrit malzeme elde edilmiştir. Elde edilen hibrit epoksi akrilat malzemenin karekterizayonu yapılmış ve ısısal ve morfolojik özelllikleri incelenmiştir.

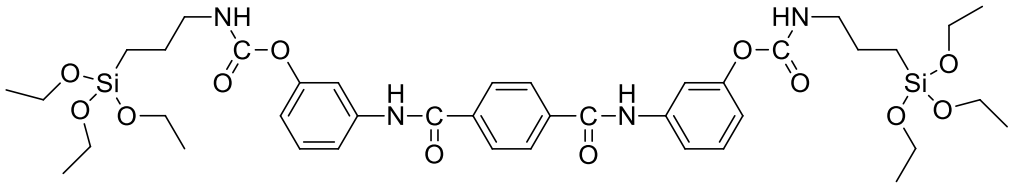

Şekil 3 : Alkoksisilan modifiye makromonomer.

1. INTRODUCTION

Organic–inorganic hybrids exhibit multifunctional characteristics and show superior properties compared to their pure compenents. In principle, two different methodologies can be used for the formation of hybrid materials as building blocks and in-situ both having their advantages and disadvantages [1]. Building blocks are well-defined preformed structural units that react with each other to form the final hybrid material in which the precursors still at least partially keep their original molecular integrity throughout the material formation. Contrary to the building block approach, the in-situ formation of the hybrid materials is based on the chemical transformation of the precursors throughout the formation of hybrid materials, which often show different properties from the original precursors.

Beside the molecular building blocks, nanosized building blocks can also be used to form nanocomposites. Inorganic nanoparticles have already had an impact in fields such as surface coatings, mechanics, optics, electricity, magnetism, medicine, aerospace, thermodynamics and bionics [2]. One of particular interest to nanocomposite materials is the fact that nanostructure containg materials have higher surface areas than do normal materials, with a decrease in the size, the surface area per unit volume increases, which enhances the properties due to the available surface area.

Silica nanoparticles have attracted much interest due to their low toxicity, chemical inertness ease of formation in a wide range of sizes and morphologies, high stability, and the flexible and robust surface that can be further functionalized [3].

Sol-gel process, as a type of in-situ method, which enable the control of the preparation of multi-component systems over the mild reaction conditions lead to the significant interest in both scientific and industrial areas [4]. Sol-gel process is kind of an organic polycondensation reaction in which small molecules form usually three-dimensional crosslinked network structures by the loss of substituents. In particular, the silicon dioxide based sol-gel process is one of the major driving forces what has become the broad field of organic-inorganic hybrid materials.

The most common method for silica preparation is the sol-gel method and usually soluable silicates or alkoxysilanes are used as starting materials in aqueous solution. Hydrolysis and condensation steps of alkoxysilanes occur simultaneously during the siloxane (Si-O-Si) formation over acid or base catalyst. Changing one parameter can often lead to very different materials, such as water to precursor ratio and type of catalyst. Acid-catalyzed reactions can lead to an open network polymer-like micro structure while base catalyst reaction leading to highly crosslinked particle-like structure same as in Stöber method [5]. Hence, for a well-defined material the reaction conditions have to be fine-tuned.

Preparation of silica nanoparticles by Stöber is based on the hydrolysis and polycondensation of tetraethylorthosilicates (TEOS) as silica precursor in the solution of water, ethanol and ammonia. Properties of Stöber silica particles such as surface area, pore volume, particle size and distribution, pore size and hydroxyl number that all affect the chemical and physical behavior of silica particles can be controlled by controlling the pH of the solution, composition of the reactants and temperature of the reaction which also influence the rate of hydrolysis.

The strong hydrophilic character and the tendency to agglomeration of silica particles mainly due to their high silanol content and, specific surface area cause the difficulty for the silica particle to become monodispersed in such organic and polymeric phases. It is possible to modify silica particles by obtaining desired properties in order to enable silica particles to gain organic/polymeric functionality. The most popular method is the surface functionalization of silica particles by silane coupling agents (organo-silanes), which contain both organic moieties and silane moeities (such as chloro and alkoxy silanes) in one precursor. Rarely, some organic moieties with multi functional groups are also employed to substitute the hydroxyl groups of silica particle in order to bring organic properties on the surface of silica particles. Both methods have their own advantages and disadvantages. Such organically modified silica particles may react with the oligomeric or polymeric components in a chemical manner and/or become well dispersed in organic or polymeric matrix having the opportunity for the further reactions leading the formation of hybrid materials [6].

Alkoxy silane precursors owning organic functionalities also have the ability to form simultaneously both the organic networks, polymeric components and inorganic SiO_2 network domains resulting in hybrid networks and polymers by the chemical and

physical interactions and hydrolysis and condensation reactions of the silanol groups of precursors [7, 8].

1.1 Purpose of Thesis

Incorparation of silica nanoparticles into polymeric hybrid materials as preformed building blocks makes it superior to the in-situ formed silica nanoparticles because of the possible well-defined and designed properties of the preformed nanoparticles. For this reason, in this work, well-defined silica nanoparticles of narrrow size distribution are aimed to synthesize. By the following well known Stöber method which is a type of sol-gel process, discussions on the effect of reaction parameters such as concentration of ammonia and the ratio of the reactants to eachother and also optimizing the synthesis conditions will help to obtain silica nanoparticles with determined final properties.

Efficient functionalization/modification of silica nanoparticles has the great importance for enabling both the well dispersiton of such nanoparticles into organic phase of the hybrid materials and also possible strong and chemical interactions of the nanoparticles with the organic precursor or polymer components of the hybrid.

In case of the use of organo-silanes as silica coupling agents some ambiguities may occur reducing the modification efficiency of the nanoparticles. For example, the possibility of different type of condensation reactions between free silanol groups of coupling agents and silanol groups of silica nanoparticles may result in inadequate concentration of functional groups on the surface of silica particles. In order to overcome such diffuculties, contrary to common coupling methods of silica particles with organo-silanes, toluene diisocynate (TDI) is considered to be an ideal activator for the surface modification of silica nanoparticles. TDI is a very active molecule to react with hydroxyl groups of silica particles because of having two isocyanate groups with different activities. Grafting of TDI onto silica nanoparticle surface may improve the dispersibility of the silica particles in organic phase of the hybrids and brings possibility for further reactions over the isocyane groups of TDI attached onto surface of silica particles such as reacting with benzoin moieties resulting in the form of macro-phoinitiator silica nanoparticles. It is possible to initiate polymerization with such silica nanoparticle macroinitiator system under UV radiance same as in

photopolymerization of MMA resulting in well dispersion of silica nanoparticles into polymer matrix that is also initiated by the particles themself.

Well-defined spherical silica nanoparticles functionalized with TDI can also be incorporated into preformed epoxy-acrylate resin over the covalent bonding between hydroxyl groups of epoxy-acrylate resin and free isocyanate groups of Si-TDI by the formation of urethane linkage having the possibility to obtain cured silica nanoparticles/epoxy-acrylate hybrid films as last.

In this thesis, we also aimed to synthesize a model alkoxysilane precursor of aromatic amide-urethane structure. For this purpose, preformed terephthalic acid chloride might react with the amino phenol yielding aromatic amid containing diphenol monomer, and the reaction of such monomer with amino propyl trimethoxysilane (IPTES) over the urethane linkage might form alkoxysilane containing aromatic amide-urethane precursor. Alkoxysilane incorparated aromatic amide-urethane macromonomer has the potential to form hybrid materials by owning the organic and inorganic component in the same precursor.

2. THEORETICAL PART

2.1 Hybrid Materials

Hybrid material is a material that formed by different types of materials. A wide variety of structure can be combined in any scale such as macroscopic or nanometer to form hybrid materials. Hybrid materials can be formed by simple mixing process over physical interactions such as in blends or by the chemical interactions of the components ranging from weak to strong. Commonly, the combined two moieties of hybrid materials are organic and inorganic in nature [9]. Here, in the scope of this thesis, hybrid materials will also refer to "organic-inorganic hybrid materials" and the combining level of organic-inorganic components of this study is at the nanometer or molecular level.

Hybrid materials with the desired properties can be obtained by a wide variety of inorganic components such as metal oxides, alloys, ceramics, clay, rubber, resins, elastomers, natural materials in a variety of forms such as bulk, powder, nanocomposites, coatings, glasses, fibres, foams etc., depending on the forming process. As briefly represented in Figure 2.1, through the combinations of different inorganic and organic components with appropriate processing methods, different types of hybrid materials can be developed by gaining new properties for electrical, optical, biomedical, structural, or related applications [10].

The origin and the chemical structure of the inorganic components of the hybrid materials have the major effect on the properties and well-determination of the final hybrid materials which is same for the organic components [11]. There is a wide variety of inorganic structure used as the inorganic constituent of hybrid materials including mainly; metals, metal oxides, alloys, ceramic and clay.

Due to its electronegativity, oxygen forms stable chemical bonds with almost all elements to give the corresponding oxides. Metal oxides typically contain an anion of oxygen and most of the earth's crust consists of solid oxides, the result of elements being oxidized by the oxygen in air or in water. Oxides of most metals adopt polymeric structures and some of the oxides are in molecule forms. Because metal-oxide bonds

are strong, the solids tend to be insoluble in solvents, though they are attacked by acids and bases. Metals can combine with other metal and non-metal to form alloys which are also widely used in many industries [12]. Metalloids such as silicon and germanium are usually too brittle to have any structural uses. They and their compounds are used in alloys, biological agents, catalysts, flame retardants, glasses, optical storage and optoelectronics, pyrotechnics, semiconductors, and electronics [13-16].

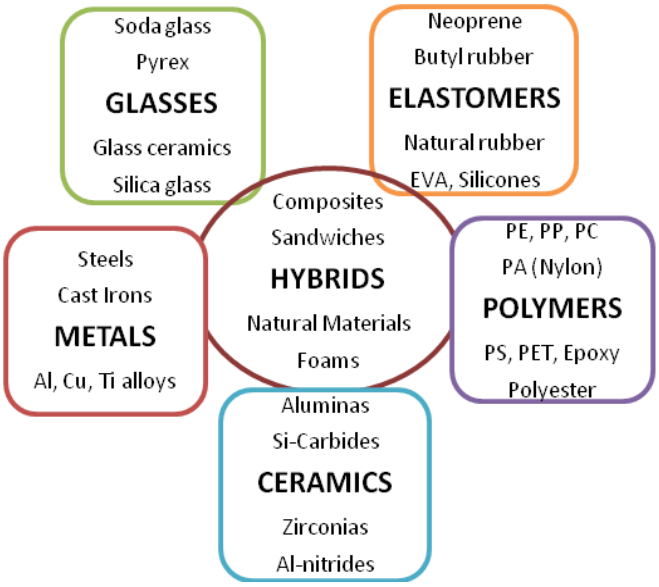

Figure 2.1 : Selected substituents typically used in hybrid materials.

Ceramic is an inorganic, nonmetallic or metalloid solid material which of the atoms primarily held by ionic and covalent bonds. The crystallinity of ceramic materials ranges from highly oriented to semi-crystalline, and often completely amorphous. Having such a large range of possible options for the composition-structure (types of elements and bonding, and levels of crystallinity) of a ceramic, ceramic materials gain big variance of properties such as hardness, toughness, thermal stability, electrical conductivity [17].

Clay is a natural rock or soil material with small grained particle size that combines minerals with traces of metal oxides and organic matter. Clay exhibits plastic behavior due to their water content in certain proportions and becomes firm, brittle and non–plastic through drying or firing with occurring permanent physical and chemical changes. Such changes convert clay into a ceramic material. Different types of clay can be produced with the use of different minerals and firing conditions. Clay is one of the oldest building materials on Earth and also used in many area such as for making

pottery, construction products, such as bricks, wall and floor tiles and even musical instruments paper pipes [18, 19].

The most obvious advantage of organic-inorganic hybrids is that they can favorably combine often dissimilar properties of organic and inorganic components in one material, such as mechanical strength and thermal stability with the processability and flexibility of an organic polymer matrix. Hybrid materials have brought the possiblity to carry out molecular design with high prediction even at the nanometer levels. By controlling individual components of hybrid materials at the molecular scale, instead of developing a totally new material, it is possible to obtain proper improvement in the materials characteristics.

Different synthetical approaches can be used and different properties that comes from both organic and inorganic materials can be combined. The desired function can be delivered from the organic or inorganic or from both components. The properties of the final hybrid materials are not only determined by the properties of the inorganic and organic component, but also by the phase morphology and the interfacial region between the components (Table 2.1).

Table 2.1 : Possible structure and properties of hybrid materials.

Type	Property
Matrix	Crystalline ↔ Amorphous Organic ↔ Inorganic
Building blocks	Molecules ↔ Macromolecules ↔ Particles ↔ Fibers
Interactions between components	Strong ↔ Weak

There are mainly two classes of hybrid material [10]: Class I hybrid materials are the ones having weak interactions between the two phases, such as van der Waals, hydrogen bonding or weak electrostatic interactions. Combination of inorganic clusters or particles with organic polymers is one of the examples of this type. There is no strong interaction such as covalent bonds between the components (Figure 2.2a). In this case, materials are formed by discrete inorganic moieties trapped in organic polymer depending on the functionalities of the components. For example, weak crosslinking may occur by the inorganic units via physical interactions or inorganic

units may be entrapped in a crosslinked polymer matrix. Another type of Class I hybrid materials are interpenetrating networks in which one network is formed in another network matrix without strong interactions. Class II hybrid materials are the ones having strong chemical interactions between the components. Class II hybrids are formed when the discrete inorganic building blocks, such as clusters, are covalently bonded to the organic polymers (Figure 2.2c) or inorganic and organic polymers are covalently connected with each other (Figure 2.2d).

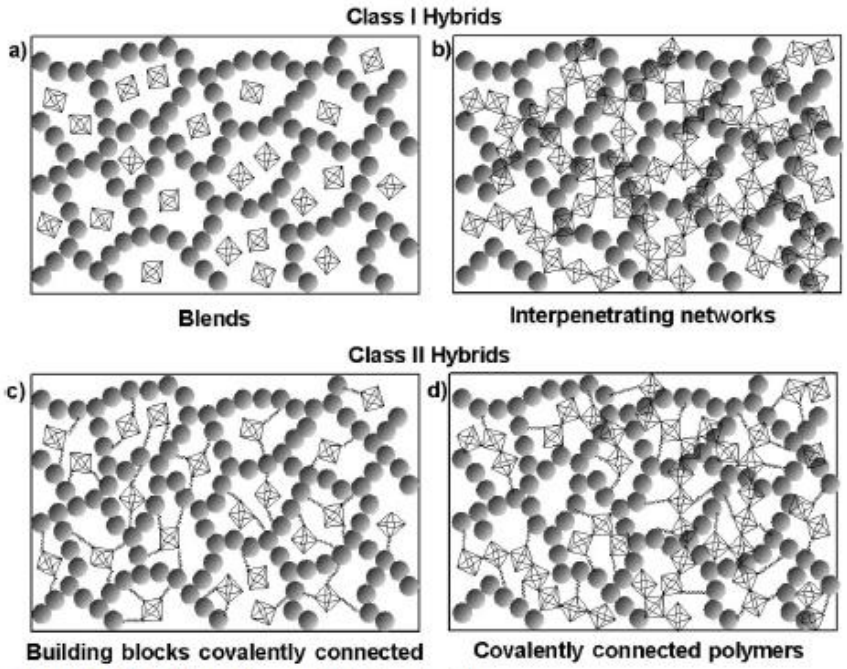

Figure 2.2 : Different types of interactions of the hybrid materials [10].

2.2 Synthesis and Properties of Hybrid Materials

There is almost no limit to the combinations of inorganic and organic components in the formation of hybrid materials. Because of the many possible combinations of components, this field is very creative, since it provides the opportunity to invent an almost unlimited set of new materials with a large spectrum of properties. Another driving force in the area of hybrid materials is the possibility to create multifunctional materials. Such examples, the incorporation of inorganic clusters or nanoparticles with specific optical, electronic or magnetic properties in organic polymer matrices [20-25].

The processing property of hybrid materials makes this material class interesting for many applications [26]. Contrary to pure solid state inorganic materials that often require a high temperature treatment for their processing, hybrid materials show a

more polymer-like handling, either because of their large organic content or because of the formation of crosslinked inorganic networks from small molecular precursors just like in polymerization reactions. These materials can be shaped in any form such as in bulk, in films [27]. The possibility of their processing as thin films can lead to property improvements of cheaper materials by a simple surface treatment, e.g. scratch resistant coatings [28]. Decorative coatings obtained by the embedment of organic dyes [29] in hybrid coatings one of the most prominent usage of hybrid materials in industry.

One of the major advantages of hybrid materials is that it is possible to include more than one function into a material by simply incorporating a second component with another property into the material formulation. In the case of scratch resistant coatings, for example, additional hydrophobic or antifogging [30] properties can be introduced.

Based on the inorganic structures, increased mechanical strength is one of the advantages of hybrid materials [31, 32]. Scratch-resistant coatings for plastic glasses are based on this principle. The enhancement of mechanical and thermal properties of polymers by the inclusion of inorganic moieties, especially in the form of nanocomposites, enables these materials to be used in the transportation industry or as fire retardant materials [33] for construction industry.

Medical materials are also one typical application area of hybrid materials, as their mechanical properties can be tailored in combination with their biocompatibility, functional organic molecules as well as biomolecules often show better stability and performance if introduced in an inorganic matrix [34, 35]. Nanocomposites are also used for dental filling materials. A high content of inorganic particles in these materials provides the necessary toughness and low shrinkage, while the organic components provide the curing properties combined with the paste-like behavior. Additional organic groups can improve the adhesion properties between the nanocomposites and the dentine [36, 37].

The optical transparency of the resulting hybrid materials and is highly dependent on the composition and molecular or nanoscale dimensions of the building blocks [15]. Silica is preferred as the inorganic component in such applications because of its low optical loss. Other inorganic components, for example zirconia [23], can incorporate high refractive index properties, or titania [24] in its rutile phase can be applied for

UV absorbers. Functional organic molecules can add third order nonlinear optical (NLO) properties and optical properties of hybrid materials play a major role in many high-tech applications [38-42]. Interesting electrical properties can be obtained by the incorporation of conjugated and conductive polymers and nanocomposite based devices for electronic and optoelectronic applications include photodiodes, solar cells, solid-state lithium batteries, supercapacitors, gas sensors and field effect transistors [43-48].

Mainly two different approaches are considered for the formation of hybrid materials: In one, well-defined preformed building blocks are applied to react with each other forming the final hybrid material. And in the other, one or both structural units are formed in situ from the precursors that are transformed into a network structure. Both methodologies have their advantages and disadvantages. In this thesis, sol-gel approach as an in situ method is considered apart from the two approaches.

2.2.1 Building block approach for hybrid materials

Building blocks at least partially keep their molecular integrity throughout the material formation, which means that structural units that are present in these sources for materials formation can be also find in the final material. Representative examples of such well-defined building blocks are modified inorganic clusters or nanoparticles with attached reactive organic groups [49].

Cluster compounds often consist of at least one functional group that allows an interaction with an organic matrix, for example by copolymerization. Depending on the number of groups that can interact, these building blocks are able to modify an organic matrix or form partially or fully crosslinked materials. For instance, two reactive groups can lead to the formation of chain structures. If the building blocks contain at least three reactive groups, they can be used for the formation of a crosslinked material [50].

Beside the molecular building blocks mentioned, nanosized building blocks, such as particles or nanorods, can also be used to form nanocomposites. The building block approach has one large advantage compared with the in situ formation of the hybrid materials since at least one structural unit of the blocks is well-defined and usually does not undergo significant structural changes during the matrix formation, better structure–property predictions are possible. Furthermore, the building blocks can be

designed in such a way for the best performance in the materials' formation, for example good solubility of inorganic compounds in organic monomers by surface groups showing a similar polarity as the monomers [51].

2.2.2 In situ formation of hybrid materials

Contrary to the building block approach, in situ formation of the hybrid materials is based on the chemical transformation of the precursors used throughout materials' preparation. In these cases, well-defined discrete molecules are transformed to multidimensional structures, which often show very different properties from the original precursors. Generally, simple and commercially available molecules are applied and the internal structure of the final material is determined by the composition of these precursors but also by the reaction conditions. Therefore, control over the reaction conditions is a significant step in this process. Changing one parameter can often lead to two very different materials. If, for example, the inorganic species is a silica derivative formed by the sol–gel process, the change from base to acid catalysis makes a large difference because base catalysis leads to a more particle-like microstructure while acid catalysis leads to a polymer-like microstructure. Hence, the final performance of the derived materials is strongly dependent on their processing and its optimization [52-54].

Many of the inorganic solid-state materials are formed using solid precursors and high temperature processes, which are often not compatible with the presence of organic groups because they decompose at elevated temperatures. Hence, these high temperature processes are not suitable for the in situ formation of hybrid materials. Reactions that employed should be more suitable for the hybrid formation in solutions and mild conditions. One of the most prominent processes, which fulfill these demands, is the sol–gel process. However, such rather low temperature processes often do not lead to the thermodynamically most stable structure but to kinetic products, which has some implications for the structures obtained. For example, low temperature derived inorganic materials are often amorphous or crystallinity is only observed on a very small length scale, i.e. the nanometer range.

2.2.3 Sol–Gel approach for hybrid materials

Compared with other inorganic network forming reactions, the sol–gel processes show mild reaction conditions and a broad solvent compatibility. These two characteristics

offer the possibility to carry out the inorganic network forming process in the presence of a preformed organic polymer or to carry out the organic polymerization before, during or after the sol–gel process. Sol-gel process is kind of an inorganic polycondensation reaction in which small molecules form polymeric structures by the loss of substituents. Usually a three-dimensional (3-D) crosslinked network is formed after the reaction. The often dissimilar reaction mechanisms of the sol–gel process and typical organic polymerizations allow the temporal separation of the two polymerization reactions which offers many advantages in the material formation [55, 56].

One major parameter in the synthesis of these materials derived by the sol–gel process is the identification of a solvent in which the organic macromolecules are soluble and which is compatible with either the monomers or preformed inorganic oligomers. Many commonly applied organic polymers, such as polystyrene or polymethacrylates, are immiscible with alcohols that released during the sol–gel process and which are also used as solvents, therefore phase separation is likely in these cases. This can be avoided if the solvent is switched from the typically used alcohols to, for example, THF in which many organic polymers are soluble and which is compatible with many sol–gel reactions. Phase separation can also be avoided if the polymers contain functional groups that are more compatible with the reaction conditions of the sol–gel process or even undergo an interaction with the inorganic material formed [57] .

The pH not only plays a major role in the mechanism but also for the microstructure of the final material. The pH used therefore has an effect on the kinetics, which is usually expressed by the gel point of the sol–gel reaction. Hence, for a well-defined material the reaction conditions have to be fine-tuned. Not only do the reaction conditions have a strong influence on the kinetics of the reaction but also the structure of the precursors. Generally, larger substituents decrease the reaction time due to steric hindrance. In addition, the substituents also play a role in the solubility of the precursor in the solvent [58].

After the gelation point which is the the transition from a sol to a gel, links between the sol particles are formed to such an extent that a solid material is obtained containing internal pores that incorporate the released alcohol. However at this point the reaction has not finished, but condensation reactions can go on for a long time until a final stage is reached. This process is called aging. During this reaction the material shrinks and

stiffens , thus xerogels are formed. This process is carried on in the drying process, where the material acquires a more compact structure and the associated crosslinking leads to an increased stiffness [59, 60].

2.3 Silica Hybrid Materials

In this thesis, for the incorporation of inorganic constituents in hybrid materials, we focused on silica (silicon dioxide) metal (metalloid) oxide, both in the form of monodispersed silica nanoparticles and in network structure of polymers with silicon dioxide domains.

2.3.1 Structure and properties of silica

Silicon is present in environment in different forms. It is not found in nascent form but also it is always present in combination with oxygen as in silica or hydroxides as in silicic acid. Silicon dioxide (silica) is one of the hardest and most common constituent of the earth's crust and is a basic component of soil, sand, gravel and most rock types including granite, sandstones and even exists in some living organisms. Silica (SiO_2) is found in nature most commonly in crystalline form mainly as quartz, trdymite, cristobalite. Various kinds of synthetic silica (colloidal silica, silica gels, pyrogenic (fumed) silica, precipitated silica, silica aeoregel etc.) are produced mostly in amorphous powder form (Figure 2.3) [61].

Silicon dioxide molecule is not really a molecule as it forms a giant covalent structure adopting a polymeric structure rather than a simple covalent structure. The oxidation and coordination numbers for silicon are both four. Because of its peculiarity, silicon atom bonds to four oxygen atoms rather than two oxygen atoms with double bonds. The structure of silica is three-dimensional arrays of linked tetrahedrons consisting of a silicon atom coordinated by four oxygen atoms in a way similar to tetrahedral structure of diamond. However, the empirical formula of silica is SiO_2 because the proportion of silicon to oxygen in silica is 1:2. The similarity in structure of quartz (crystalline SiO_2) and diamond explains the hardness, and transparency-translucency of quartz. The tetrahedrons are usually quite regular, and the silicon-oxygen bond distances are ~1.61 Å. It is chemically inert and does not affect redox reactions. Moreover, pure silica is optically transparent in the visible region and emitted light is not hindered, so that chemical reactions can be monitored spectroscopically.

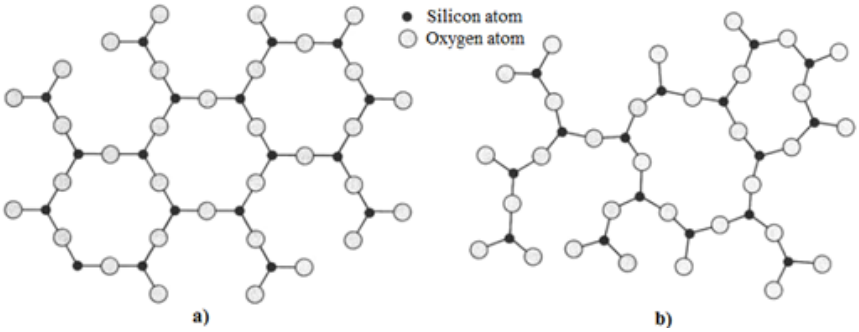

Figure 2.3 : Two dimensional representation of (a) crystalline (quartz) and (b) amorphous form of silica [61].

Silica is insoluble in all kinds of solvents and liquids except hydrofluoric acid. According to periodic table of the elements there is not enough electronegativity difference between silicon and oxygen to form ionic bonds of silicon dioxide. Silicon dioxide has no basic properties because it does not contain oxide ions and it does not react with acids. Instead, it is very weakly acidic, reacting only with hot and concentrated strong bases. The silanol groups on the surface of silicas determine acidic and basic behavior of silicas. Silicon dioxide does not react with water, because of the difficulty of breaking up the polymeric covalent structure.

Silicate is a silicon containing anionic compound. The great majority of silicates are oxides, forming minerals with other elements (mostly as cations) such as Mg_2SiO_4 (forsterite) and Fe_2SiO_4 (fayalite), but hexafluorosilicate (SiF_6^{2-}) and other silicate anions are also included. In vast majority of silicate structures silicon occupies a tetrahedral environment. Tetrahedral silicates sometimes occur as isolated SiO_4^{4-} centres, but most commonly are joined together in various ways, such as pairs ($Si_2O_7^{6-}$) and rings ($Si_6O_{18}^{12-}$). Commonly the silicate anions are chains, double chains, sheets, and three-dimensional frameworks (Figure 2.4).

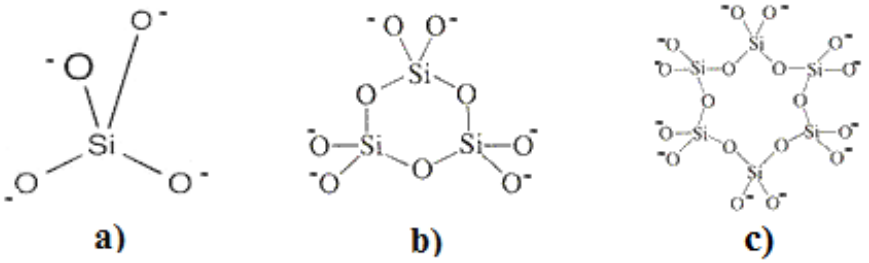

Figure 2.4 : Tetrahedral structure of (a) isolated (SiO_4^{4-}), (b) ($Si_3O_9^{6-}$) ring and (c) ($Si_6O_{18}^{12-}$) ring, oxide silicates.

Although the tetrahedron is the common coordination geometry for silicon compounds, silicon can adopt octahedral coordination geometry. Such examples are

hexafluorosilicate (SiF_6^{2-}), hexahydroxysilicate ($[Si(OH)_6]^{2-}$) and a dense polymorph silica, stishovite, being bound to six oxides, occurring rarely in nature [62].

The structure and main characteristics of silica are related to its particle size and distribution, its porosity, specific surface area and its purity determining the area of application. For example, monodisperse nonporous silica spheres can be used to prepare colloidal compounds for numerous applications and, mesoporous silica particles with well-defined pores can be used in drug delivery by encapsulating a drug and capping the pores [63]. However, it is difficult to get silica particles monodispersed in the polymer matrix, because silica particles agglomerate due to their specific surface area and volume.

Two principally different process technologies are used for synthetic silica: the thermal process leading to such as pyrogenic silica and the wet process yielding precipitated silica, silica gel, colloidal silica etc. Precipitated silica is a white and amorphous synthetic silicon dioxide and is mainly manufactured through a process of neutralization of sodium silicate solution with sulphuric acid following the precipitation stage. A range of silica varying in different properties and characteristics can be synthesized by altering the precipitation conditions. Silicagel is the porous form of silica and synthetically produced mainly by sodium silicate.

Synthetic amorphous silica in its pure form is a colourless to white used in a wide range of industrial applications and products also in consumer products including cosmetics, foods and pharmaceuticals. Silica gel, a highly porous amorphous form of silica used to remove moisture from gases and liquids, to thicken liquids, to impart a dull surface to paints and synthetic films, as filler in the manufacture of paint, rubber, plastics, and for many other purposes. The true density of silica is 2.2 grams per milliliter, but the porosity of silica gels gives them much lower bulk densities. Due to its mechanical resistance, high dielectric strength, and selectivity for chemical modification, amorphous silica has become a key material in a broad range of application as briefly represented in Table 2.2.

Recently, interest in the scientific research of silica nanoparticles has increased because of their easy preparation and their wide uses in various industrial applications, such as catalysis, pigments, pharmacy, electronic and thin film substrates, thermal

insulators, and humidity sensors [64-66]. Furthermore, molecular biologists employ silica in resins and optical beads to study the biomacromolecules.

Table 2.2 : Silica functionality in hybrid materials.

Usage	Property and Function
Tyres, shoe soles, technical rubber goods, silicones	Use as reinforcing filler for elastomers
Human and animal nutrition	Use as carrier for liquid active ingredients, as free flow agent for powders
Building, membranes	Miscellaneous functions
Paint, coating	Opacity, whiteness, brightness, flatting and scrub resistance, TiO_2 extender
Paper	Use as whiteness agent, to improve printability, defoamers for coalescing of foam bubbles.
Drug	tablet durability, stability, densification within the dosage matrix, minimize the amount of air of the powder
Food products.	Prevent caking Improve flow Efficiently absorb liquids, fats, and oils for powdered food applications will improve the flow behavior and storage stability of a broad variety of food products
Oral care (toothpaste)	Use as cleaning/polishing agent; use as thickening agent as an abrasive in toothpaste
Dentifrice	Cleaning/whitening thickener silicas is to control rheology
Rubber	Reinforcing agent imparts excellent retention of tensile and elongation properties after heat aging, increase tear and abrasion resistance, lower viscosity, improve flex/fatigue resistance

2.3.2 Synthesis of silica hybrid materials

The most common method for silica preparation is the sol-gel method [54]. In this process $Si(OH)_4$ molecules condense to form a siloxane network. Usually sodium silicate or any soluble silicate is used as a starting compound. Also alkoxysilanes are used commonly, in this case hydrolysis of alkoxy group precedes condensation with a neighbouring silanol in the aqueous alkoxide solution. During the sol–gel process, the

two steps of hydrolysis and polycondensation proceed in parallel rather than in sequence, and their relative rates determine the final structure of the sol–gel process. If tetraalkoxysilanes are used as precursors, hydrolysis and polycondensation proceed as follows;

$$\text{Hydrolysis:} \quad Si(OC_2H_5)_4 + 4H_2O \leftrightarrow Si(OH)_4 + 4C_2H_5OH \tag{2.1}$$

$$\text{Condensation step:} \quad Si(OH)_4 \leftrightarrow SiO_2 + 2H_2O \tag{2.2}$$

$$\text{The reaction proceeds as:} \quad Si(OC_2H_5)_4 + 2H_2O \leftrightarrow SiO_2 + 4C_2H_5OH \tag{2.3}$$

The reaction brings increase of viscosity of the medium and sol gets condensed to a gel at the point where elastic stress is supported. This gel is termed as hydrogel or alcogel (if alcohol used as a solvent). The hydrogel structure is controlled by temperature, pH, solvent, electrolyte and the type of starting salt or alkoxide. Controlling the factors either favours the growing of the particles or the linkage of particles to form chains. Condensation step allows to form stable particles of colloidal size. During the condensation step small three-dimensional siloxane network gradually gets formed. There are different aging and drying conditions and each condition results different porosity and surface area [67]. Figure 2.5 represents the sol-gel process with different type of final form and structure depending on the methods applied. Moisture, pressure and temperature all adversely affect powdered and granulated products.

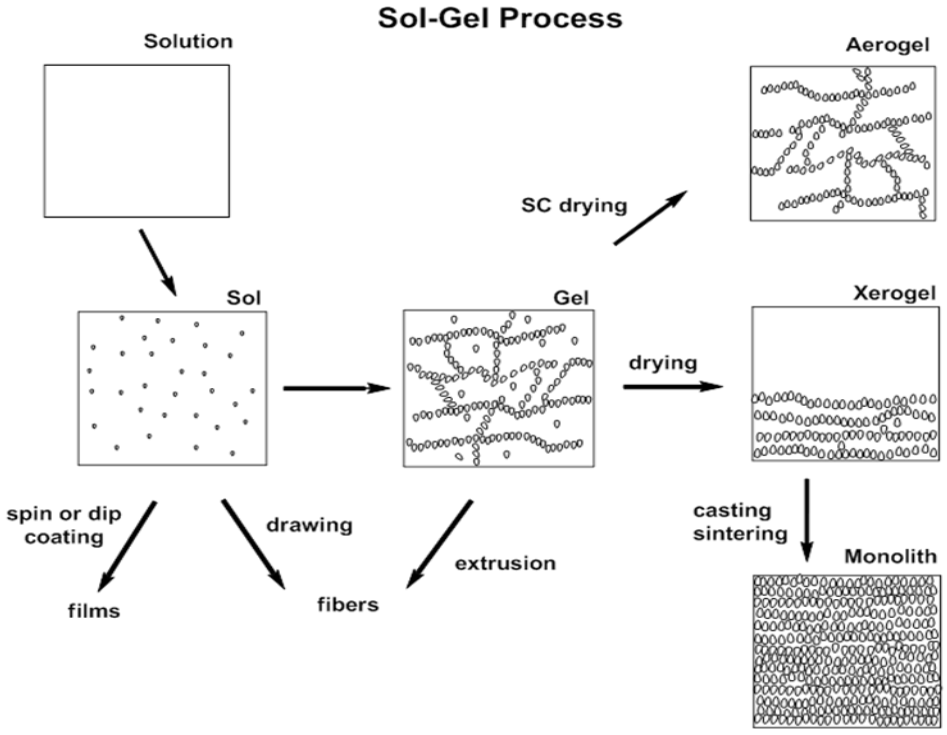

Figure 2.5 : Schematic formation of sol-gel process.

The type of solvent, reactant ratios, temperature, and type of catalyst are major factors affecting the relative rates of hydrolysis and condensation reactions, and thus determine the ultimate morphology and pore structures of the formed materials.

The process is catalyzed by acids or bases resulting in different reaction mechanismsm (Figure 2.6). Applying acid-catalyzed reactions, an open network structure is formed in the first steps of the reaction leading to condensation of small clusters afterwards. Contrarily, the base-catalyzed reaction leads to highly crosslinked sol particles already in the first steps. This can lead to variations in the homogeneity of the final hybrid materials as will be shown later. Commonly used catalysts are HCl, NaOH or NH_4OH, but fluorides can be also used as catalysts leading to fast reaction times [68].

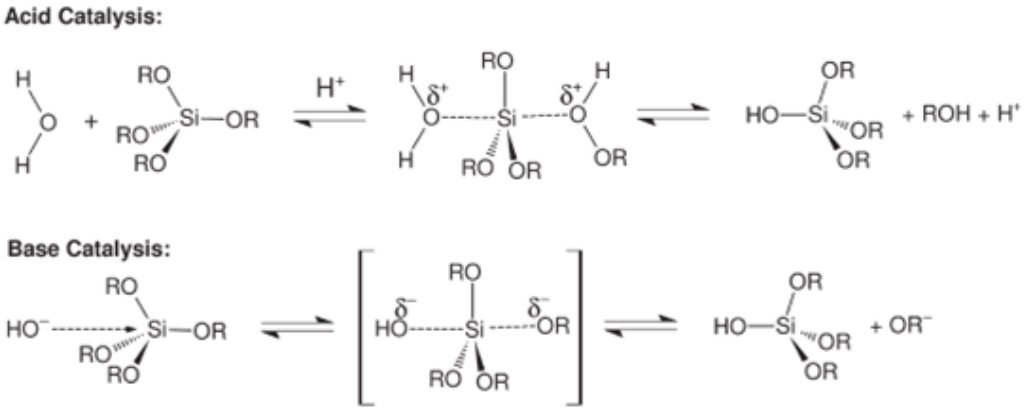

Figure 2.6 : Different mechanisms of silicon based sol-gel process based on acid and base catalyst.

Solvents which are not inert such as ethanol might increase the gelatin time. Might also effect the transparency. Even under the catalitic condition gelation might not occur. Trialkoxy structures might effect more than tetraalkoxy structures. Precursors with basic or acidic characteristics might led gelation (hydrolysis) without the need of catalyse. Solvent retards the gelation time even under the catalytic condition [69].

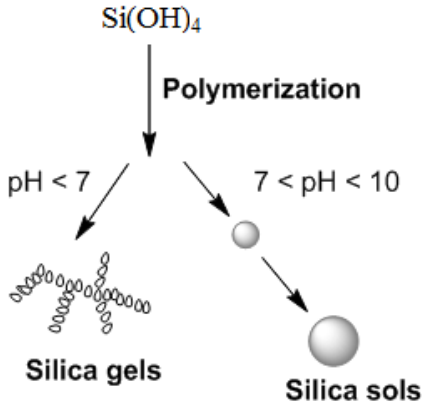

Figure 2.7 : The effect of pH on silica structure.

By controlling the pH and the reactive concentration of reaction it is possible to control the resulting structure of the sol–gel process and particle size due to the relative rate at which hydrolysis and condensation occur (Figure 2.7). Acid-catalyzed reactions can lead to an open network polymer-like networks, porous particle with small pores while base catalyst reaction leading to colloidal gel with large pores, highly crosslinked nonporous particle-like structure same as in Stöber method. Hence, for a well-defined material the reaction conditions have to be fine-tuned [70].

Some behaviors of acid catalysed sol-gel process are as follows; reaction rate decreases as more alkoxy groups are hydrolyzed, reaction is favored at terminal Si, linear polymer products are obtained such as fibers, $RSi(OR)_3$ is more reactive than $Si(OR)_4$, the gelation time (hydrolysis rate) for tetraethoxysilane (TEOS) precursor significantly decrease with the increased acid concentration. Some of the behaviors of base catalysed sol-gel process are also as follows; reaction rate increases as more alkoxy groups are hydrolyzed, reaction is favored at central Si, branched polymer products, spherical particles, powders, $RSi(OR)_3$ is less reactive than $Si(OR)_4$. It is possible to synthesize well defined Stöber type, spherical, white solid particles with $Si(OR)_4$ precursors.

If a homogeneous material is required, all parameters must be optimized. This is especially true if hybrid materials are the target, because undesired phase separations of organic and inorganic species in the materials or between the network and unreacted precursors weaken the materials' properties. This can often even be observed by the naked eye if the material turns opaque. The water to precursor ratio is also a major parameter in the sol–gel process. If tetraalkoxysilanes are used as precursors, two water molecules per starting compound are necessary to form completely condensed SiO_2. Applying a lower H_2O/Si ratio, would lead to an alkoxide containing final material. In hybrid organic-inorganic backbones, organic groups are less stable and more quickly. The monodispersity achieved in the final particles is thus due to size-dependent aggregation rates [71].

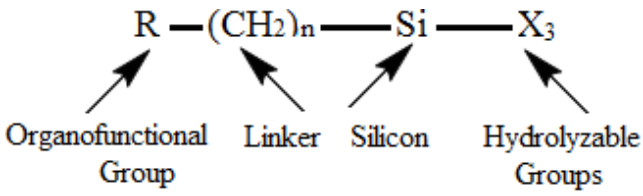

Figure 2.8 : A typical organosilane precursor.

Silane precursors also have the ability to form simultaneously both the organic networks by the chemical and physical interactions with organic monomers and polymeric components, and inorganic SiO_2 network domains by the hydrolysis and the condensation reactions between the silane groups of precursors resulting in hybrid networks and polymers. General representation of a typical organosilane precursor is seen in Figure 2.8. Organofunctional groups own a wide variety such as epoxy, isocyanate, acrylare, aliphatic, aromatic etc. and is chosen depending on the method of the process such as building block or in-situ formation, and also the functionality of organic monomers and polymeric components resulting in a desired form of hybrid material. The hydrolyzable groups -X are typically, alkoxy, acyloxy, amine, or chlorine. Alkoxy silane precursors are mostly methoxy and ethoxy and with their wide variety of organic functional groups have been widely used as coupling agents, silane crosslinkers and organic polymer modifiers commonly being followed by the application of sol-gel process that is resulted in the formation of hybrid materials with the silicon dioxide networks. Such hybrid materials gain improved thermal, mechanical, optical, surface etc. properties depending on the strructure, chemistry and the morphology of newly formed material [72-76].

2.4 Silica Nanoparticle Hybrids

2.4.1 Synthesis of silica nanoparticles

In recent years, there has been increasing interest and demand for hybrid materials with silica nanoparticles both in scientific field and in industry fields. The quality of these material are greatly influenced by the size and uniformity of the silica nanoparticles. Hence, the demand for silica nanoparticle of narrow size distribution and monodispersity has increased.

Mainly, for the effective synthesis process of silica particles, three types of methods are included. First is by using microemulsion method yielding silica spheres with a good average monodispersit. However, it requires large amounts of surfactants, hence, the particles need to be further cleaned to remove the remained surfactants. The second approach is the production of monodisperse small silica particles by the elemental silicon with water using ammonia as catalyst and the main disadvantage of this method is that, the elemental silicon must be activated by washing with aqueous hydrofluoric acid, pure water, alcohol and ether to remove silicon dioxide film from the particle

surface [77, 78]. As last, Stöber process is regarded as the simplest and most effective route to prepare monodisperse silica spheres with the use of reactants that are easly handled and with the reaction condition that is controllable and easy to be carried out.

Preparation of silica particles of desired properties was first demonstrated by Stöber et al. in 1968 [5]. A typical reaction mixture contained tetraethoxysilane (TEOS) as silica precursor, water, ethanol and ammonia. This method allows to produce colloidal silica spheres by the hydrolysis and condensation of silicon alkoxides, such as tetraethyl orthosilicate (TEOS), in alcohol solvents (e.g., ethanol) in the presence of water and a base catalyst (e.g., ammonia aqueous solution). By using the Stöber method, it is possible to achieve excellent control of particle size, narrow size distribution, smooth spherical morphology of the resulting silica, microporous silica. The spherical silica particles produced had a narrow size distribution and could be controlled by controlling the solution pH, composition of reactants and temperature. According to this model, when the synthesis of silicon dioxide particles starts with TEOS, the supersaturation of soluble product in the solution is initially created by the hydrolysis and condensation reactions. When the supersaturation rises above a critical level, a huge number of primary particles of silicon dioxide is suddenly produced by high nucleation rate in the supersaturation solution and then is quickly aggregated to form large stable particles. After that, the stable particles grow by aggregation of primary particles (Figure 2.9).

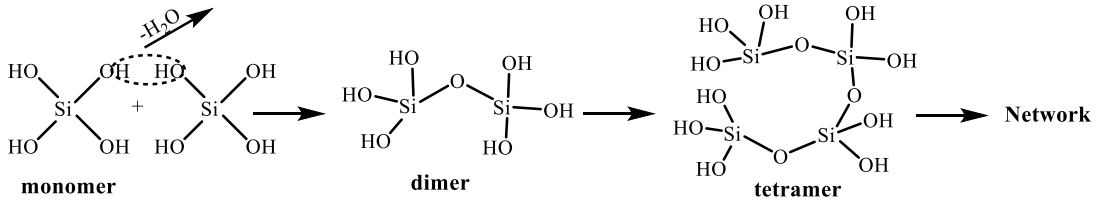

Figure 2.9 : Schematic formation of silica network.

The size of the particles is directly related to nucleation. The monomer is consumed in reaction either with monomers to produce nuclei or with existing particles. Factors that promote nucleation must result in smaller particles while factors that favor growth should have the opposite effect. Nucleation can be a kinetic phenomenon resulting from a low monomer-monomer reaction rate. It can also be a dynamic effect determined by the two competing processes, nucleation and growth.

In the latter case, hydrolysis plays a dominant role since it controls the availability of the hydrolyzed monomer. If nucleation is defined as the reaction between two monomers, then the nucleation rate is a second-order reaction in the concentration of the active (hydrolyzed) monomer, whereas growth is first order. Monomer-monomer reaction is significant only during the early stages of the process, when the concentration of grown particles (rate of growth) is low. Under conditions of low concentration of hydrolyzed monomer and in the presence of already grown particles, the main process of monomer consumption is growth. Therefore, hydrolysis has a direct effect upon nucleation and the resulting particle size, and if all other factors remain the same, factors that inhibit hydrolysis inhibit nucleation as well and produce larger particles.

The hydrolysis reaction, consists in replacing of the alkoxide groups (-OR) with hydroxyl groups (-OH) releasing of the corresponding ROH alcohol molecules (2.4). A complete hydrolysis is obtained when the stoichiometric molar ratio water: $Si(OR)_4$ is 4. Any intermediate species (-mono, -di and –tri hydroxy) can be formed as a result of partial hydrolysis. Subsequent condensation reactions occur between the silanol groups (Si-OH) (2.5) and also between silanol groups and alkoxide groups (2.6) producing siloxane bonds (Si-O-Si) and by-products as water and alcohol, respectively. Under most conditions, condensation can start before a complete hydrolysis. Conditions such as pH, H_2O/Si molar ratio (R) and catalyst can force complete hydrolysis before condensation begins [79].

$$\equiv Si-OC_2H_5 + H_2O \longrightarrow \equiv Si-OH + C_2H_5OH \quad (2.4)$$

$$\equiv Si-OH + \equiv Si-OH \longrightarrow \equiv Si-O-Si\equiv + H_2O \quad (2.5)$$

$$\equiv Si-OC_2H_5 + \equiv Si-OH \longrightarrow \equiv Si-O-Si\equiv + C_2H_5OH \quad (2.6)$$

LaMer and Dinega [69] hypothesize one of the proposed mechanisms for growth of colloidal silica particles. If all nucleation occurs in a short time and all particles grow at the same rate, monodisperse particles will be formed. They state that this mechanism explains why the particle size depends inversely on the reaction temperature. As the temperature is decreased, the rate-limiting hydrolysis step becomes slower. It then takes a smaller number of nuclei to relieve the supersaturation of silicic acid. Since fewer particles are nucleated, the final particle size must be larger, assuming that all

tetraethyl orthosilicate reacts. An increase in temperature is known to decrease the particle size and the particles become more monodisperse as the particle size is increased. The smaller particles (<l00 nm) are distorted spheres with rough surfaces, while the large particles appear to be perfectly monodisperse, smooth spheres.

A second mechanism for particle growth is coagulation of particles much smaller than the final product [80]. In order for colloidal particles to be stable, the interparticle repulsive forces must be greater than the van der Waals attractive forces. Stability of charged colloidal particles increases approximately linearly with particle size. The small particles formed first are marginally unstable and aggregate in order to lower the interfacial free energy. As large clusters are formed, they aggregate with freshly formed nuclei until they grow to a colloidally stable size. In an unpolar environment like a solvent or a resin the nanoparticles tend to reduce the interface, exposed to the unipolar matrix, by agglomeration. Once the inorganic surfaces come in contact with each other, condensation reactions of the hydroxyl groups take place, making the process almost irreversible.

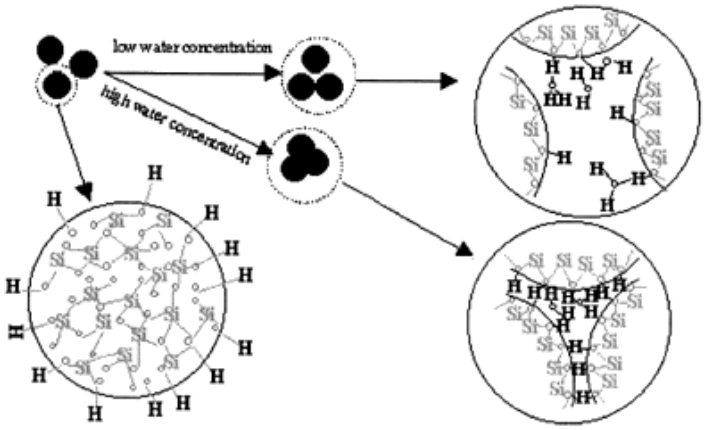

Figure 2.10 : Effect of water concentration on particle size and size distribution [82].

The higher ammonia and water concentration must attribute to the higher hydrolysis rate. Matsoukas and Gulari [81] reported that the effect of ammonia concentration is to promote hydrolysis, but also to promote the polymerization (condensation) rate, resulting in faster kinetics, and lager particle sizes. If high water concentration is applied, a high nucleation rate occurred, so a lot of small sub particles are prepared at a short period. But, the hydrogen bond of SiO_2 sub-particles under the condition of a higher water concentration is stronger than that of a lower water concentration because of excess water. Therefore, sub-particles in the higher water concentration agglomerate each other and grow into a large particle. Figure 2.10 illustrates the effect of the water

concentration on the particle size and its distribution [82]. A small amount of water leads to a slow hydrolysis due to the reduced reactant concentration. A large amount of water gives a slow hydrolysis due to the increased reactant dilution. It is sure that high concentration of water and ammonia attributes to broaden the particle size distribution. The faster kinetics observed under higher ammonia concentrations must be attributed to the higher hydrolysis rate. However, the effect of ammonia goes beyond increasing the rate of monomer release. This is evident by the fact that ammonia also promotes the formation of larger particles [83].

2.4.2 Chemical and physical nature of silica particles

The properties of a pure silica, are determined in the first place by: (i) the chemical activity of the surface which depends on the concentration and the distribution of different types of OH groups, and on the presence of siloxane bridges; and (ii) the porous structure of the silica.

The ultimate particles which make up the silicas can be regarded as polymers of silicic acid, consisting of interlinked SiO_4 tetrahedra. In the primary silica gel matrix, a core of silicon atoms joined together with oxygen atoms by silicon-oxygen-silicon (siloxane) bonds. In the 1930s, by Rideal [44] and Kiselev [52], and slightly later by Carman [53] carried out studies of the condensation processes of silicic acids and showed that silanol (≡Si-OH) groups should be present on the surface of silicates and silicas. At the surface, the structure terminates in either a siloxane group with the oxygen on the surface, or uncondensed hydroxyl group of several forms of silanol groups that gives polarity to silica gel. Hydroxyl groups are bound via the valence bond with Si atoms on the silica surface, and in some cases with Si atoms inside the particles of silica. At last, there is structurally bound water inside the silica skeleton (internal silanols) and very fine ultramicropores with less than 1 nm pore diameter [84].

The silanol types are isolated (free) silanols, where the surface silicon atom has three bonds into the bulk structure and the fourth bond attached to a single OH group, and vicinal (bridged) silanols, where two single silanol groups attached to different silicon atoms, are close enough to hydrogen bond. A third type of silanols, geminal silanols, consist of two hydroxyl groups, that are attached to one silicon atom. The geminal silanols are too close to hydrogen bond each other, whereas the free hydroxyl groups

are too far separated [85]. Surface hydroxyl groups are catagorized as seen in Figure 2.11. The surface of the amorphous silica gel may be covered by isolated as well as vicinal hydroxyl groups. The surface of amorphous silica is an oxide adsorbent and depends on the presence of silanol groups. Since the surface of silica is highly disordered, there is not a regular arrangement of hydroxyl groups.

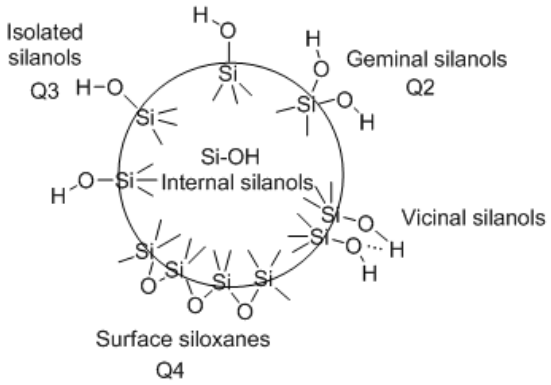

Figure 2.11 : Type of surface silanols [84].

On exposing silica to water, it is further able to adsorb water physically by means of hydrogen bonding. In fully hydroxylated non-porous silica species, a multilayer of adsorbed water is build up by increasing the partial pressure. The uptake of physically adsorbed water is termed hydration.

Dehydration is the term for the loss of physically adsorbed water because of temperature increase. The temperature at which dehydration is completed cannot be determined unambiguously. The porosity, the size and the morphology of the pores largeley influence the water desorption. It is now generally agreed that heating at 100 ^{o}C for prolonged period, removes all physically sorbed water on a non-porous silica [86]. A non-microporous silica has what is sometimes called an ‘open surface’ [87], leading to appoximately the same desorption behaviour as a non-porous silica. However, when microporosity is present, heating up to 200 ^{o}C might not be adequate to remove all physically absorbed water.

Dehyroxylation is the condensation of hydroxyl groups to form siloxane bonds. whereas in the region above 400^{o}C mainly isolated hydroxyls condense with increasing difficulty. Temperatures more than 1200 ^{o}C are required to remove all silanols [88].

Upon a preliminary activation of silica above 400 ^{o}C the concentration of the relatively hydrophobic siloxane bridges on the surface increases sharply, while the silanol

concentration drops as a function of temperature. Hydroxyl groups are capable of forming hydrogen bonds; thus they make such a surface hydrophilic at proper concentrations. The removal of the hydroxyl groups from the surface of silica leads to a decrease in the adsorption, and the surface acquires more and more hydrophobic properties [89, 90]. It is not easy to separate dehydration and dehydroxylation processes (Figure 2.12).

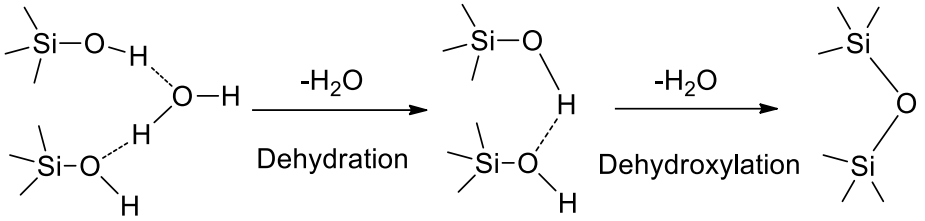

Figure 2.12 : Dehydration and dehydroxylation process of silica.

Rehydroxylation is the hydroxylation process of dehydroxylated silica after treatment with water or aqueous solutions. Complete rehydroxylation of the surface can only be achieved for silica samples which were subjected to a thermal treatment below 400 ^{o} C [91]. After calcination at higher temperatures, only partial rehydroxylation takes place.

The rehydroxylation process of silica procedes in two steps. In the first step, water molecules preadsorb on the hydrophilic silanol sites. In the second step, this preadsorbed water causes a bond breaking of a siloxane group, yielding two new silanols. It is because the surface silicon atoms tend to have a complete tetrahedral configuration, and in an aqueous medium their free valence becomes saturated with hydroxyl group.

Depending on the silica nature there are tecniques to characterize the physical and chemical properties silica surface and functional groups. NMR results are preferred over the infrared results because of the ambiguity in literature concerning the peak assignment of geminal hydroxyls in infrared spectroscopy and quantification problems. In principle high-resolution solid state NMR spectra can provide the same type of information that is available from corresponding solution NMR spectra, but special techniques/equipment are required. The combination of magic-angle spinning (MAS) and cross polarization (CP) provides ^{29}Si-NMR spectra with a high degree of structural resolution, permitting detailed study of structures and transformations at the silica surface [92, 93]. In ^{29}Si-NMR spectroscopy, silanols are not reffered to as free,

bridged and geminal silanols, instead, Q sites. Siloxane bridges are called Q^4 sites, single silanols Q^3 sites and geminal silanols Q^2 sites.

2.4.2.1 Surface properties of Silica Particles

The surface properties of silica based on physico-chemical model was conducted by Zhuravlev in detail [94-96]. The main advantage of this physico-chemical model is that it helps to determine the concentration and the distribution of different types of silanol and siloxane groups and to characterize the energetic heterogenity of the silica surface as a function of the pretreatment temperature of SiO2 samples. It is possible to determine the chemisorption of water (fast, weakly activated or slow, strongly activated) under the restoration of the hydroxyl covering and also to determine the OH groups inside the SiO_2 skeleton. The magnitude of the silanol number which is the number of OH groups per unit surface area, αOH, when the surface is hydroxylated to the maximum degree, is considered to be a physico-chemical constant. The silanol number αOH, expressed in OH groups nm^{-2}, is determined as in the following equation:

$$\alpha OH = \delta OH(s)\ NA \times 10^{-21} / S^{-1} \qquad (2.7)$$

Whereas, δOH(s) is the concentration of OH groups on SiO_2 surface referred to the unit mass of the sample (mmol of OH/g of SiO_2) found by the deuterio-exchange method with mass spectrometric analysis, S is the specific surface area with respect to krypton adsorption (m^2g^{-l}) and NA is the Avogadro number.

This constant has a numerical value: αOH,AVER = 4.6 (least-squares method) and αOH,AVER = 4.9 OH nm^{-2} (arithmetical mean) and is known in literature as the Kiselev–Zhuravlev constant [95].

Specific surface area (m^2/g), pore size distribution (based on pore volume and pore area) and particle size are the three parameters to fully characterize the physical properties of the silica matrix sufficiently. Surface area expresses the concentration of the reactive surface species in ($\#/nm^2$). It gives a microscopial image of the surface loading and is related to effects such as steric hindrance. The pore size distribution explains sorption characteristics of the silica and helps to understand the availability of reactive surface silanols towards the reacting molecules. Measurement of particle sizes gives information on surface area and porosity.

It has been established that adsorption and other surface properties per unit surface area of silica are identical (except for very fine pores). Brunauer-Emmet-Teller (BET) method is the most widespread method for determination of specific surface area (S). Argon, nitrogen and krypton are standard gases for BET surface area measurements of porous or non-porous materials and possess different advantages over each other in the use for different cases. Adsorption of nitrogen at 77 K is mostly measured over porous materials. BET analysis provides precise specific surface area evaluation of materials by nitrogen (or kyrpton and argon) multilayer adsorption measured as a function of relative pressure using a fully automated analyser. The technique encompasses external area and pore area evaluations to determine the total specific surface area in m^2/g yielding important information in studying the effects of surface porosity and particle size in many applications.

The surface of the solid is an array of adsorbtion sites according to Langmuir [97] and BET method [66] is based on a kinetic model of the adsorbtion process by Langmuir. A state of dynamic equilibrium is postulated, in which the rate of molecules arriving from the gas phase and condensing onto the bare sites (θ_0) is equal to the rate at which molcules evaporate from the occupied sites (θ_1).

Using the monolayer capacity, the specific surface area (S_{BET}) can be easily calculated according to

$$S_{BET} = \nu_m.a_m.N_A.10^{-20}\ (m^2/g) \qquad (2.8)$$

ν_m is the monolayer capacity of the surface (the number of moles of gas per gram of adsorbent, required to fomrm a monolayer) With N_A the Avogadro number ($6.02x10^{23}$ molecules/mol) and a_m the molecular cross-sectional area of the gas molecule. This value is commonly assumed to be about 0.162 nm^2 for nitrogen on an oxide surface [98].

In spite of some grounded criticism [99] (the BET model assumes energetically identical adsorbtion sites, neglects lateral interactions and assumes identical behaviour in all layers of the multilayer adsorbtion) and the proposal of alternative models [100, 101], the BET equation has retained utility. It is a relatively easy approach and the method is applicable to a great variety of adsorbtion isotherms.

Pore size characterization

Assuming that the external surface of a porous substrate is negligible and that the pores are cylindrically shaped, the average pore diameter of a substrate can be calculated by the Wheeler formula [102]:

$$r_p = 2.10^3 \, V_P / S_{BET} \quad (2.9)$$

Pore diameter and pore radius are expresse in nm. V_P is the volume (ml/g) of liquid adsorbate and can be calculated from the volume of adsorbed gas (V_a) by means of Gurvitsch rule [103]:

$$V_P = 1{,}54.10^{-3} \, . \, V_a \quad (2.10)$$

In the temperature range 200-400 ^oC, mainly vicinal hydroxyl groups condense at the surface, forming strained siloxane bridges. This process does not influence the pore structure parameters. above 600 ^oC, interparticle condensation of free hydroxyl groups occurs, which is combined with a rearrangement of silica gloubules to produce a more stable configuration. Obviously, this interparticle condensation is highly favoured by smaller pores, resulting a faster collapse of the pore structure. At the temperatures higher than 1200 ^oC, non-porous products are obtained.

Particle Size

The main methods for calculating particle size are dynamic light scattering, electron microscopy techniques such as scanning electron microscopy (SEM) and transmission electron microscopy (TEM), also atomic force microscopy.

Dynamic Light Scattering is a technique for measuring the size of particles typically in the sub micron region. The advantage of using dynamic scattering is the possibility to analyze samples containing broad distributions of species of widely differing molecular masses and to detect very small amounts of the higher mass species (<0.01% in many cases) [104].

DLS measures Brownian motion and relates this to the size of the particles. Brownian motion is the random movement of particles due to the bombardment by the solvent molecules that surround them. Normally DLS is concerned with measurement of particles suspended within a liquid.

The larger the particle, the slower the Brownian motion will be. Smaller particles are “kicked” further by the solvent molecules and move more rapidly. An accurately

known temperature is necessary for DLS because knowledge of the viscosity is required (because the viscosity of a liquid is related to its temperature). The temperature also needs to be stable, otherwise convection currents in the sample will cause non-random movements that will ruin the correct interpretation of size.

The size of a particle is calculated from the translational diffusion coefficient by using the Stokes- Einstein equation [105]; $d(H)= kT/3\pi\eta D$

where as, d(H)is hydrodynamic diameter, D is translational diffusion coefficient, k is Boltzmann's constant, T is absolute temperature and η is viscosity.

The diameter that is measured in DLS is a value that refers to how a particle diffuses within a fluid so it is referred to as a hydrodynamic diameter. The diameter that is obtained by this technique is the diameter of a sphere that has the same translational diffusion coefficient as the particle.

The translational diffusion coefficient will depend not only on the size of the particle "core", but also on any surface structure, as well as the concentration and type of ions in the medium.

Any change to the surface of a particle that affects the diffusion speed will correspondingly change the apparent size of the particle. An adsorbed polymer layer projecting out into the medium will reduce the diffusion speed more than if the polymer is lying flat on the surface. The nature of the surface and the polymer, as well as the ionic concentration of the medium can affect the polymer conformation, which in turn can change the apparent size by several nanometres.

Electron microscopy became one of the most important techniques to characterize the materials morphology on the nanometer and even on the atomic scale. Scanning electron microscopy (SEM) produces high resolution images of a sample surface. SEM images have a characteristic 3-D appearance and are therefore useful for judging the surface structure of the sample. The primary electrons coming from the source strike the surface and they are inelastically scattered by atoms in the sample.

The spatial resolution of the SEM techniques depends on various parameters, most of them are instrument related. Generally, the resolution goes down to 20nm to 1 nm, which is much lower than that of transmission electron microscopy (TEM) but SEM has some advantages compared with TEM. For example, a quite large area of the specimen can be imaged, bulk materials can be used as samples and, as mentioned, a

variety of analytical modes is available for measuring the composition and nature of the specimen [10].

In transmission electron microscopy (TEM) images are produced by focusing a beam of electrons onto a very thin specimen, which is partially transmitted by those electrons and carries information about the inner structure of the specimen. It is often difficult in TEM to receive details of a sample because of low contrast, which is based on the weak interaction with the electrons. Particularly samples that have a high content of organic components often reveal this problem, which can partially be overcome by the use of stains such as heavy metal compounds.

The dense electron clouds of the heavy atoms interact strongly with the electron beam. However, sometimes the organic components of the sample are not detected because they decompose in the electron beam; this can be avoided using cryogenic microscopy, which keeps the specimen at liquid nitrogen or liquid helium temperatures (cryo-TEM). One of the major limitations of TEM is the extensive sample preparation, which makes TEM analysis a relatively time consuming process ^{29}Si-NMR spectroscopy distinguishes single (either isolated or vicinal) from double (geminal) silanols due to the different behaviours during dehydration and rehydration process.

Hydroxyl Number

For determination of the OH groups titration [106, 107] is one of the methods to be used. It is time consuming and applied to relatively large samples (2 - 25g). This method is based on the reaction of the surface hydroxyl groups with a selectively reacting compound to form a covalently bonded surface species of known composition. It is subject to steric effects and stability of the reaction products are not known all the time [108]. Diborane, borontrichloride, diazomethane, organosilanes and organometallic compounds are used as reactive compounds.

Other modern and widely applied methods for hydroxyl determination of silica are infrared (IR) spectroscopy, thermogravimetric analysis (TGA) and nuclear magnetic resonance (NMR).

Although IR is a very simple and useful method sometimes it is difficult to distinguish between adsorbed water and surface hydroxyl groups. To determine the silanol number density, a calibration with different samples containing known amounts of OH groups is necessary [109]. Also, intergration may give errors due to band overlap and this

causes an underestimation of the fraction of free hydroxyl groups in the low treatment region. The region 1950- 1766 cm^{-1} is attributed to an overtone structure vibration. Its integrated value is used as a reference band to normalize all other integrations, since this band is found unaffected by the different treatments [94]. The assignment of the broad absorption region between 3740 and 3400 cm^{-1} has caused some discussion in the literature [95, 96]. The vibrations at 3730 - 3720 cm^{-1} and 3520 cm^{-1} have been assigned to the interaction of the oxygen of the hydroxyl group with the hydrogen of a neighbouring hydroxyl group. This vibration can thus be regarded as the O-H stretching vibration of the free silanol in a couple of hydrogen bonded hydroxyl groups, whereas the vibration band at 3520 cm^{-1} is attributed to the 'bonding' hydroxyl group (Table 2.3).

Table 2.3 : Infrared band assignments of stretching OH vibrations.

Frequency, cm^{-1}	**Species**
3746	Free OH
3742	Geminal OH
3730 – 3720	Hydrogen perturbed OH
3650	Intraglobular OH
3520	Oxygen perturbed OH
3400 – 3500	Molecular adsorbed H_2O

In an earlier report' it was shown that the ^{29}Si CP/MAS signals of surface silanol silicons, both SiOH and $Si(OH)_2$, are suitable for quantitative study. Q^n-terminology is used in NMR, where *n* indicates the number of bridging bonds (-O-Si) tied to the central Si atom: Q^4, surface siloxanes; Q^3, single silanols; Q^2, geminal silanols (silanediols) [114].

Table 2.4 : Silanol types with their approximate ^{29}Si CP MAS NMR peak position.

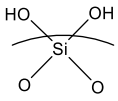	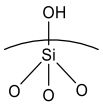	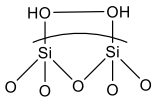
Geminal	**Isolated**	**Vicinal**
Q^2	Q^3	Q^3
-94 ppm	-100 ppm	-100 ppm

Distribution of Q^2 and Q^3 sites as a function of temperature can be obtained by the deconvolution of these peaks. Cross-polarization spectroscopy is not an automatically a quantitative technique. Maciel and Sindorf [113] provided methods and algorithms to perform quantitative measurements with CP / MAS ^{29}Si NMR. Approximate NMR peak positions for typical surface silanols are listed in Table 2.4.

Weight loss determination allows thermogravimetry analysis (TGA) to determine hydroxyl group content of silica particles [115, 116]. The limitation is that distinguishing of the hydrogen-bonded and isolated silanols on the basis of the thermograms is not possible due to the partly occuring simultaneous dehydroxylation reactions. Fully hydrolyzed, bare silica particles consist of siloxane network and surface silanol groups absorbing some amount of water due to hydrophilic character of silica particles. During the heat treatment all types of adjacent silanol groups (hydroxyl) condense to form siloxane bond with the release of water. Since siloxane bond (Si-O-Si) is stable at high temperatures, up to 1000 ^{o}C, weight losses of bare silica particles evaluated from thermogravimetric analysis belong (are due to) to silanol condensation (dehydroxylation) and the release of absorped water (dehydration). The condensation of all types of silanol groups occurs by the reaction of two adjacent silanol groups on the silica surface resulting in the release of one molecule of water and the formation of one siloxane group. The hydroxide group content, determined as moles of hydroxyls left per gram of silica (n_{OH}) at any temperature, can be calculated as follows:

$$n_{OH}\ (\text{mol/g } SiO_2) = 2\ n_{H2O} = 2(W_0\text{-}W_f\ )\ /100\ M_{H2O} \qquad (2.11)$$

Where the residue difference, W_0-W_f corresponds to the weight loss in any temperature region (T_0-T_{final}) and M_{H2O} is the molar mass of water.

Structurally bound water inside the silica and the ultramicropores of stoeber silica has no effect on the surface processes so it is necessary to consider those out of the hydroxyl coverage. The amount of absorbed water does not only depend on the structure of particles but also on storage condition and pre treatment of the particles. When silica samples are subjected to high temperatures under vacuum dehydration will occur resulting a general loss in weight corresponding to the evolution of molecular water because of the condensation of adjacent hydroxyl groups to form siloxane bridges.

It is necessary to distinguish OH groups on the surface of silica particles from the molecularly absorbed water. There is no agreement for the values of T_B, Boundary temperature that separates two processes; Dehydration and Dehydroxylation. Although there has been a wide discrepancy for T_B (120-600 ^{o}C), Oldlyha, Kiselev and Zhuravlev found T_B to be 190 ± 10 ^{o}C. But 200 ^{o}C would enable desorption of

mainly physically absorbed multi and mono-layered water. Temperature even up to 450 ^{o}C is required for desorption of high majority of hydrogen bonded water and structurally bound water inside and in ultramicropores of stoeber silica. T_B should be determined according to porous structure of silica sample.

2.4.3 Functionalization and hybrid formation of silica nanoparticles

Silica nanoparticles leading to an extreme increase in interfacial area have been considered as a challenging matter for foreign organic matrix. Their efficiency in polymeric matrices requires uniform dispersion and strong interfacial bonding between two component of the hybrids. Both the dispertion of nanoparticles in the organic polymer matrix and the interaction between nanoparticles and the polymers significantly assign the properties of the nanohybrids. Common strategies are being developed to improve the poor dispersion of nanoparticles in polymer matrices and also organic solvents for advanced interfacial bonding of nanoparticles and matrices. The simple mixing can be done by melt blending and solution blending. However, to fully disperse nanoparticles in the polymer matrix is a big challenge due to the strong tendency of nanoparticles to agglomerate [117]. Different approaches have been developed in order to obtain polymer-silica nanohybrids as represented briefly in Figure 2.13.

Surface modification of the silica nanoparticles is a general route to enhance the dispersion of the particles and to build up a strong interfacial interaction between the organic matrix and inorganic nanoparticles. Coupling reactions of silica nanoparticles with silane coupling agents having functional groups is one of the most common approaches for the modification of the surface of the silica particles [118-122].

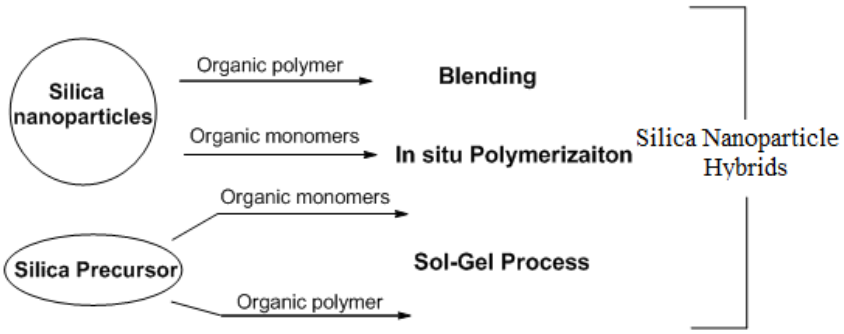

Figure 2.13 : Typical methods for the preparation of hybrid silica naoparticles.

Alkoxysilane coupling agents owns a wide variety of functional groups such as epoxy, isocyanate, acrylare, aliphatic, aromatic etc. as briefly listed in Table 2.5 and are

chosen to be applied depending on the functionality of organic monomers and polymeric components of the aimed hybrid material [8, 31, 62, 64, 123-131].

Table 2.5 : Typical silane coupling agents used for functionalization of silicas.

Name	Structure	Ref.
Methyltriethoxysilane	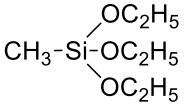	[62,123]
Phenyltrimethoxysilane	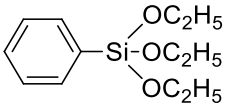	[124]
Vinyltriethoxysilane	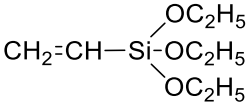	[8, 125]
5,6-Epoxyhexyltriethoxysilane	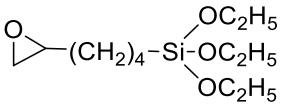	[31,126]
3-Glycidoxypropyltrimethoxysilane	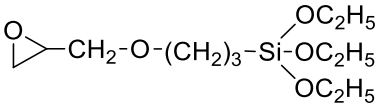	[31,126]
3-Aminopropyltrimethoxysilane	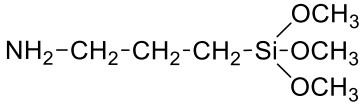	[127]
Mercaptopropyl triethoxysilane	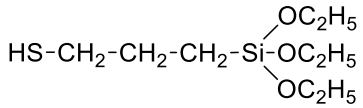	[128]
3-Isocyanatopropyltrimethoxysilane	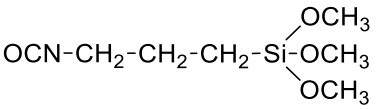	[129]
Methacryloxymethyltriethoxysilane	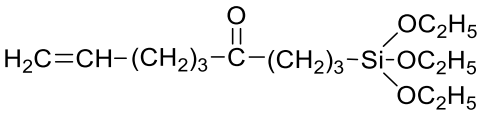	[130]
Dodecyl-triethoxysilane	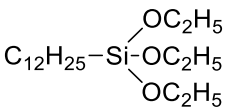	[64]
Dimethyldichlorosilane	$(CH_3)_2SiCl_2$	[131]

Alkoxysilane coupling agents are also applied depending on the grefting method of organic matrices such as"grafting to" and "grafting from". Grafting of end-functional polymers on the surface of silica nanoparticle as "grafting to" method has been reported in a serious of publications [132, 133]. The "grafting from" method, where

polymers are grown from either monomer functionalized or initiator functionalized surfaces of silica nanoparticles, has been described as another approach [134, 135].

As the first step of the coupling reaction by alkoxy silane coupling agents, agents hydrolyze to form silanols (mono, di and tri silanols) and during the hydrolysis step, condensation can also take place between these silanols resulting in dimer, oligomer or network formation of siloxane (Si-O-Si) [136]. The condensation between the silanol groups decrease the number of free silanols of silane coupling agents that reduce the condensation rate of silanol groups of the silica nanoparticles. The formation of a polysiloxane layer on silica nanoparticle surface may hinder the further desired reactions over the functional R' group of silane coupling agent due to the diffusion problem and also result in a variety of concentration of siloxane group on silica surface. Such concentration variety may also result in an inadequate concentration of silanol groups wich leads the further reaction on the surface of silica nanoparticles.

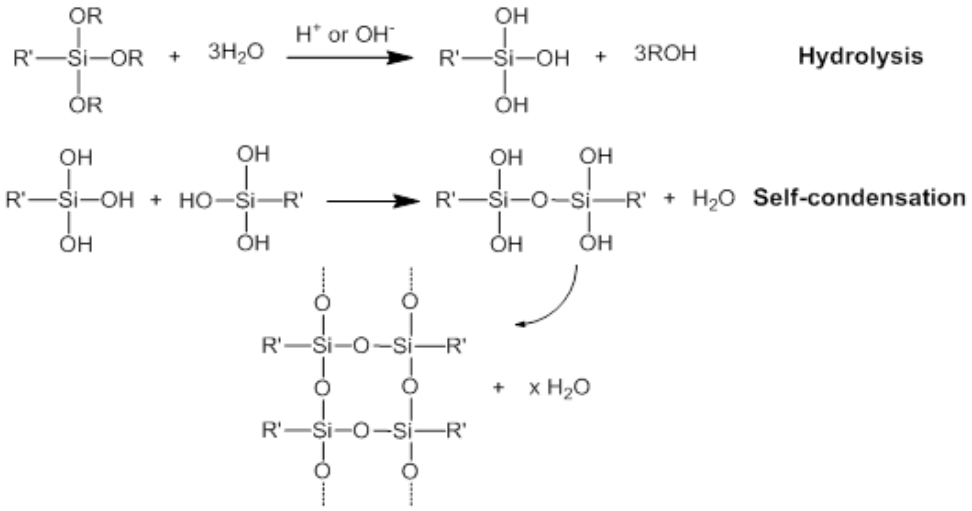

Figure 2.14 : Hydrolysis and self-condensation reactions of alkoxysilane precursors.

As the second step of coupling reaction of silica particles, the free silanol groups of coupling agents condense with the silanol groups of the silica nanoparticles. The possibility of different type of condensation reactions between free silanol groups of coupling agents and silanol groups of silica nanoparticles also may result in inadequate concentration of functional groups grafted on the surface of silica particles [137, 138]. Seemingly effective coupling reactions of silica nanoparticles over the silane coupling agents may become challenging due to the such disadvantages [139-141].

The condensation between the silanol groups aimed to be minimized to leave the silanols free for reacting with the hydroxyl groups of silica nanoparticles reasulting in the grafting of the agents. The competition of alkoxy hydrolysis of silane coupling agent and silanol condensation depend on the hydrolysis condition such as solvent, pH, temperature and the concentration of silanes. As a conclusion, seemingly effective coupling reactions between silica nanoparticles and the alkoxy silanes consisting of the hydrolysis and the condensation steps may become challenging owning some mentioned disadvantages. Direct functionalization of the surface of silica particles with reactive organic moieties can overcome such problems of silane coupling reactions and the limitation of high concentration of functional groups on the silica particle surface [142].

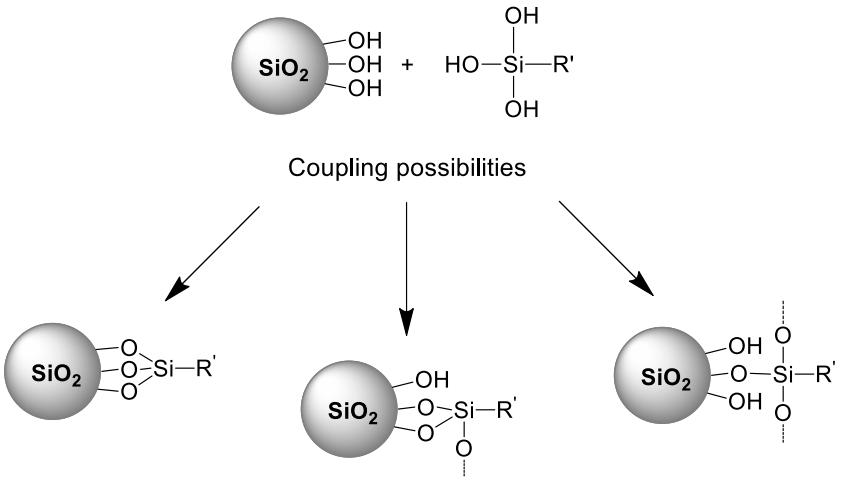

Figure 2.15 : Coupling possibilities of alkoxysilane precursors with silica particles.

In most of monomer grafted nanoparticle composite systems, the polymerization proceeds over both surface monomers of nanoparticles, and the free monomers existing in polymerization medium resulting in a high yield of ungrafted polymer. For this reason, initiator grafted nanoparticles may be considered for the higher grafting ratios of polymers onto the nanoparticles surfaces. By this manner chemical compounds with active groups are employed to substitute silanol groups of silica nanoparticles to form various functionalites on silica nanoparticle surfaces [143-145].

3. EXPERIMENTAL

3.1 Materials and Chemicals

3.1.1 Monomer

Methyl methacrylate (MMA, 99%, Aldrich)

It was first washed with dilute NaOH solution in order to remove inhibitor, and then dried with sodium sulfate ($NaSO_4$) and distilled over calcium hydride (CaH_2) at reduced pressure.

Hexanediol diacrylate (HDDA, 99%, Alfa-Aesar)

It was used as received.

3.1.2 Solvents

Toluene (99.8%, Aldrich)

It was distilled over sodium wire.

Tetrahydrofuran (THF, 99.8%, J.T. Baker)

It was dried over potassium hydroxide and distilled over sodium wire.

N,N'-Dimethylformamide (DMF, 99.5%, Aldrich)

It was distilled at reduced pressure after drying over calcium hydride.

Methanol (98%, Aldrich)

It was used as recieved for the precipitation of polymers.

Ethanol (99%, Aldrich)

It was used as received.

3.1.3 Other chemicals

Tetraethyl orthosilicate (TEOS, 98%, Aldrich)

It was used as received.

Toluene 2,4-diisocyanate (TDI, 98%, Aldrich)

It was used as received.

Ammonium hydroxide (NH_3, 25% aq., Merck)

It was used as received.

Potassium hydroxide (KOH, >85%, Aldrich)

It was used as received.

Acetic acid (glacial, 100%, Merck)

It was used as received.

Triethylamine (TEA) (J.T. Baker)

It was used as received.

3-Aminophenol (98.5%, Aldrich)

It was used as received.

Terephtalic acid (98%, Alfa-Aesar)

It was used as received.

Bisphenol A type epoxy resin (Marepoks 1721)

It was used as received.

Bisphenol A type epoxy acrylate resin (EM 621A-80, diluted in 20% TPGDA)

It was used as received.

3-(Triethoxysilyl)propyl isocyanate (IPTES, 96%, Aldrich)

It was used as received.

3-(Trimethoxysilyl)propyl methacrylate (MAPTMS, 98%, Aldrich)

It was used as received.

Dibutyltin dilaurate (DBTL, 95%, Aldrich)

It was used as received.

1-Hydroxycyclohexyl phenyl ketone (Irgacure 184, Ciba)

It was used as received.

3.2 Instrumentation

3.2.1 Infrared spectroscopy (IR)

Infrared analysis were performed with Fourier Transform Infrared (FTIR) Spectroscopy, Nicolet 850 FT-IR operating in the 4000-400 cm^{-1} range.

3.2.2 Nuclear magnetic resonance spectroscopy (NMR)

^{1}H NMR and ^{13}C NMR measurements in reiterated diethyl sulfoxide (DMSO-d6) and reiterated chloroform ($CDCl_3$-d1) were recorded with $Si(CH_3)_4$ as internal standard, on a Broker Spectrometer at 500 MHz.

3.2.3 Magic-angle spinning solid-state (MAS-NMR)

^{29}Si MAS and ^{13}C Cross Polarization Magic-Angle Spinning (CP/MAS) NMR measurements were carried out on a Bruker AVANCE 300 solid-state NMR spectrometer. The ^{13}C CP/MAS and ^{29}Si MAS NMR spectra were recorded at the resonance frequency of approximately 75.4 MHz and 59.6 MHz respectively with a 4 mm rotor spinning at 8.5 kHz using $\pi/2$ pulse width of 4.5 μs and 5 μs respectively and averaging over 15000 and 3000 scans respectively. The contact times were 2 ms and 3μs, and relaxation delays were 4 s and 7 s for ^{13}C CP/MAS and ^{29}Si MAS NMR measurements respectively.

3.2.4 Thermogravimetric analysis

Amount of organic groups and polymer incorporation in hybrid structures determined by Thermogravimetric analysis (TGA) using Q50 TGA analyzer from TA instruments under nitrogen with a ramp rate of 20 ^{o}C/min.

3.2.5 Differantial scanning calorimetry

Differantial scanning calorimetry (DSC) analyses were performed on a Q10 TA instrument DSC with a heating rate of 10^{o}C/min under nitrogen flow.

3.2.6 Scanning electron microscopy (SEM)

Particle size and distribution analysis were carried out with Scanning Electron Microscopy (SEM), Philips XL30 ESEM-FEG.

3.2.7 Transmission electron microscopy (TEM)

Transmission electron microscopy (TEM) analysis was performed with a JEOL JEM-2000 FX microscope operating at 120 kV for PMMA grafted silica nanoparticle composite. The sample for TEM observations was prepared by placing a drop of dilute particle dispersion on carbon-coated copper grids and letting it dry at room temperature.

3.2.8 Brunauer-Emmett-Teller (BET) Surface area analysis

Specific surface area (SSA) of nanoparticles was determined by BET model with the data provided by Nova 2200e model (Quantachrome) instrument, samples preheated at 160 ^{o}C for 2 h and degassed.

3.2.9 Stress-strain

Stress–strain tests were carried out by Zwick Z010 Universal Tensile Tester under a 50 N load cell with a crosshead speed of 2 mm/min at room temperature. Reported data for each sample is the average of three measurements.

3.2.10 Photoreactor

A Rayonet type photoreactor equipped with 16 Philips 8W / O6 lamps emitting light nominally at 350 nm was used.

3.2.11 UV lamp

High pressure UV-lamp (OSRAM, 300W) was used.

3.3 Preparation Methods

3.3.1 General procedure for the synthesis of spherical silica nanoparticles

Silica nanoparticle (SNP) formation by Stöber process was conducted in a round-bottom flask equipped with a condenser. A typical procedure, for example to form 57 nm of silica nanoparticles was as follows; 1.5 mL of TEOS was added directly into the solution of 3.8 mL NH_3 in 50 mL of absolute ethanol. The mixture was stirred for 24 h at constant temperature of 60 °C and stirring speed of 300 rpm. When the synthesis of the silica nanoparticles was completed, then milky solution was cooled to the room temperature. Silica nanoparticles were collected by centrifugation and redispersion in

ethanol several times and water as last. For the synthesis of SNPs with different sizes and structures, the same procedure was also applied to with different concentrations of the reactants and also at room temperature in addition to 60 °C.

3.3.2 Modification of silica nanoparticles

3.3.2.1 Isocyanate functionalization of silica nanoparticles

Bare silica nanoparticles dried under vacuum at 120 °C overnight were dispersed in dry toluene by ultrasonication. 2.5 mL of excess TDI and catalytic amount of dibutyltin dilaurate (DBTL) were added to a three-necked round bottom flask, equipped with a nitrogen inlet and a condenser, containing 0.9 g of silica nanoparticles in 12 mL of toluene. Surface functionalization reaction was carried out at 60 °C for 8 h. Functionalized silica nanoparticles were then isolated by centrifugation, and in order to remove unreacted, physically absorbed TDI redispersed several times in dry toluene and centrifuged.

3.3.2.2 Benzoin functionalization of silica nanoparticles

Isocyanate functionalized silica nanoparticles (Si-TDI) were dispersed in dry DMF by ultrasonication. 2.7 mL of benzoin and catalytic amount of DBTL were added via a syringe to a three-necked round bottom flask equipped with a condenser, containing 0.8 g of Si-TDI in 8 mL of DMF, under nitrogen. The reaction was carried out at 70 °C for 16 h. Benzoin functionalized silica nanoparticles (Si-Ben) that which is designed as SNP-photo macroinitiator were then isolated by centrifugation and washed repeatedly with DMF and toluene as last.

3.3.3 Synthesis of silica nanoparticle hybrid materials

3.3.3.1 Photopolymerization of MMA with SNP-photo macroinitor

Benzoin grafted silica nanoparticles (SNP-photo macroinitiator) were dried overnight in vacuum at room temperature. 0.5 g of Si-Ben dispersed with 3 mL of DMF in a vial, then 2.7 mL of freshly distilled methylmethacrylate (MMA) was added under nitrogen. Two different vial for two different polymerization period were prepared containing the same formulation. Photopolymerization proceeded by the irritation of a UV-photoreactor (λmax = 365 nm, equipped with 16 Philips 8W / O6 lamps) in two different vial for 2 h and 4 h respectively, at room temperature. The reaction mixtures

were precipitated into methanol yielding poly(methyl methacrylate) (PMMA) grafted silica nanoparticles (Si-PMMA), then several times washed with methanol and centrifuged. Ungrafted PMMA extracted by acetone from the grafted Si-PMMA and recollected with the evaporation of acetone and precipitation into methanol.

3.3.3.2 Synthesis of bisphenol A type epoxy acrylate

A 100mL three-necked round bottom flask equipped with a condenser and a magnetic stirrer, a dropping funnel and a nitrogen inlet, was charged with 20 g bisphenol A type epoxy resin with epoxy value of 0.54 (Marepoks 1721), 0,35 ml of triethylamine (TEA) (1phr of resin) as a catalyst and 0.01 g hydroquinone (500 ppm) as a radical scavenger to prevent spontaneous polymerization. All reactants were stirred until homogenous mixture was obtained and temperature was raised to 70 ^{o}C with the progress of the reaction under nitrogen. Then 7,4 ml of acrylic acid was added into the flask drop wise. After the addition was completely charged, the reaction mixture was kept at 80 ^{o}C during additional 8 h allowing the acid value to reach less than 2.5 (mg KOH/g) for the resin. A clear, viscous product (EA) was obtained. The resin was stored in a dark bottle until use.

3.3.3.3 Preparation of epoxy acrylate/Si-TDI hybrid resin (EA-Si)

In a three-necked round bottom flask, equipped with a condenser and ultrasonic sonicator, Si-TDI particles and hexane diol diacrylate (HDDA) were introduced under nitrogen and well dispersed by sonication for 20 min. at room temperature. Synthesized EA resin and catalytic amount of DBTL were added into the sonicating mixture and after 10 min of sonication, ultrasonic sonicator replaced with the magnetic stirrer and reaction mixture was stirred and heated at 55 ^{o}C for 6 h. Amount of the reactants charged in a typical procedure for the formulation of EA resin covalently interacted with Si-TDI (EA-Si) were as follows: 6.5 g of EA, 1.3 g of HDDA 20% of EA) and according to total amount of acrylates (EA and HDDA) 0.07 g, 0.15 g and 0.22 g of Si-TDI corresponding to 1%, 2% and 3% of the acrylates. As a control formulation, EA-control was also prepared with the same procedure without reacting with Si-TDI.

3.3.3.4 UV-curing application of EA/Si-TDI hybrid resin (EA-Si)

Irgacure 184 (1-Hydroxycyclohexyl phenyl ketone) as the photo initiator with a ratio of 3%/w of whole formulation was added into the prepared EA-Si and EA formulations which were in the vials of dark colour covered with aluminium foil to be protected from light. The vials of the formulations were sonicated for 5 min in a dark room in order to dissolve irgacure 184 and kept under gentle vacuum for 20 min to remove the air bubles. After the homogenization, viscous formulations were poured on to a Teflon™ mold and before irradiation, covered by a transparent Teflon™ film in order to prevent oxygen inhibition. A quartz glass plate was also placed over the Teflon™ films to obtain a smooth surface of cured film. As last, the formulations were irradiated 240 s under a high pressure UV lamp (OSRAM, 300 W).

3.3.4 Synthesis and application of amide-urethane alkoxy silane precursor

3.3.4.1 Synthesis of N^1,N^4-bis(3-hydroxyphenyl)terephthalamide (TPAP)

Terephthaloyl chloride was synthesized by the reaction of terephthalic acid with excess thionyl chloride ($SOCl_2$) being refluxed overnight. As the next step, 1.5 g of obtained terephthaloyl chloride (7.4 mmol) in 6 mL of THF was added dropwise into the two-necked round bottom flask equipped with nitrogen inlet, containing 2.2 g of excess 3-aminophenol (20 mmol) and 1.3 mL of pyridine in 8 mL of THF at 0-10 ^oC. The flask with the mixture was placed into ice bath after the complete addition of terephthaloyl chloride, the reaction was carried out for 4h at room temperature. The reaction mixture precipitated into hexane and filtered. Resulting TPAP was purified by dissolving in ethanol and precipitating into water.

^{1}H-NMR (500 MHz, DMSO) δ 10.23 (s, 2 NH), 9.42 (s, 2 OH), 8.04 (s, 4H), 7.35 (s, 2H), 7.16 (d, J = 8.7 Hz, 2H), 7.11 (t, J = 8.0 Hz, 2H), 6.51 (d, J = 7.9 Hz, 2H) ppm.

3.3.4.2 Synthesis of amide-urethane alkoxy silane precursor (TPAP-Si)

0.6 g (1.7 mmol) of TPAP, 3 mL (12 mmol) of 3-(Triethoxysilyl)propyl isocyanate (IPTES) and 10 mL of DMF were added into the three-necked round bottom flask, equipped with nitrogen inlet and condenser. Catalytic amount of (DBTL) was added to the reaction mixture. The temperature was increased to 65 ^oC and reaction was carried out for 6 h. The reaction mixture precipitated into hexane and filtered then washed with hexane.

^{1}H-NMR (500 MHz, DMSO) δ 10.46 (s, 2NH), 8.06 (s, 4H), 7.77 (t, J = 5.7 Hz, 2H), 7.62 (t, J = 2.0 Hz, 2NH), 7.59 (d, J = 8.2 Hz, 2H), 7.34 (t, J = 8.1 Hz, 2H), 6.84 (dd, J = 8.1 / 1.6 Hz, 2H), 3.74 (q, J = 7.0 Hz, 12H), 3.03 (q, J = 6.8 Hz, 4H), 1.54 – 1.48 (m, 4H), 1.14 (t, J = 7.0 Hz, 18H), 0.58 – 0.55 (m, 4H) ppm.

3.3.4.3 Preparation of sol-gels

Sol-gel components are prepared by the hydrolysis mixtures of organosilanes of 3-(Trimethoxysilyl)propyl methacrylate (MAPTMS) and amide-urethane alkoxy silane (TPAP-Si).

Component A was composed of the hydrolysis mixture of TPAP-Si (7.6 g, 9 mmol), MAPTMS (0.75 g, 3 mmol) and water (0.57 g, 30 mmol) of water/silicone ratio as r=1.5 for hydrolysis and condensation in a minimum amount of THF (2 ml) in order to dissolve TPAP-Si, without addition of any catalysis. After stirring for 4 h, the mixture was left to age for 24 h.

Component B was prepared by the same procedure of component A and composed of the hydrolysis mixture of MAPTMS (1 g, 4 mmol), ethanol (1 ml) and water (0.1 g, 6 mmol). The pH of the mixture was adjusted with acetic acid as 4. After stirring for 4 h, the mixture was left to age for 24 h.

3.3.4.4 Preparation of UV-cured epoxy acrylate/sol-gel hybrid resin film

Hybrid EA-solgel resin formulations were prepared by mixing the required amount of acrylates composed of EM 621A-80 (Bisphenol A type epoxy acrylate resin diluted in 20 wt% TPGDA) and additional HDDA (10 wt% of EM 621A-80) in the vials of dark colour with the required amount of sol-gels as component A and component B, obtaining EA-TPAP-Si and EA-Si hybrid resins, respectively. The formulations were completed with the addition of 3 wt% of 1-Hydroxycyclohexyl phenyl ketone (Irgacure 184) as photoinitiator. The vials of the formulations were sonicated for 5 min in a dark room in order to obtain the homogenious mixtures and kept under gentle vacuum for 15 min to remove the air bubles. After the homogenization, viscous formulations were poured on to a Teflon™ mold and before irradiation, covered by a transparent Teflon™ film in order to prevent oxygen inhibition. As last, the formulations were irradiated 240 s under a high pressure UV lamp (OSRAM, 300 W).

4. RESULTS AND DISCUSSIONS

The first part of the thesis was the preparation of spherical, monodispersed, well-defined silica nanoparticles with the evaluation of the effect of the concentration of reactants and reaction condition on the structure and properties of silica nanoparticles (SNP). Secondly, SNPs were grafted with toluene diisocyanate owning isocyanate functionality (Si-TDI) and further SNPs also modified with benzoin moieties (Si-Ben) over Si-TDI. Following, modified SNPs were used to form SNP hybrid materials. For this purpose, benzoin modified SNPs (SNP-Ben) were designed as photo macroinitiator in order to initiate MMA photopolymerization over its surface and isocyanate functionalized SNPs (SNP-TDI) were incorpareted into epoxy acrylate resin formulations following UV curing process. In the last part of the study for the thesis, the amide-urethane alkoxy silane precursor (TPAP-Si) was designed for the synthesis of hybrid materials formed by sol-gel process. TPAP-Si based sol-gel was incorparated into epoxy acrylate resin formulations following UV curing process.

4.1 Synthesis of Bare Silica Nanoparticles

Spherical, monodispersed SNP were prepared by the sol–gel process based on the Stöber method using tetraethoxysilane (TEOS) as a starting material and ammonia (NH_3) as the base catalyst. The overall reaction takes place as seen in Figure 4.1, yielding in SNPs of different sizes and structure depending on the reactant concentrations and temperature mainly.

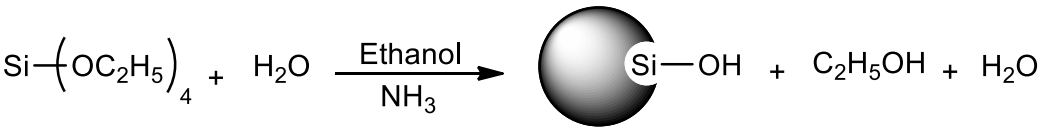

Figure 4.1 : General process for the synthesis of silica nanoparticles.

Reactions performed with the variable concentrations of TEOS and NH_3 in batches of 50 ml or 100 ml ethanol for 24 hours at 60 °C and at room temperature. The reaction temperatures, concentrations of the reactants and the diameter of the corresponding

SNPs are presented in Table 4.1. SNP samples formed at 60 °C and room temprature are represented with the initials Si1 and Si2, respectively.

Stöber process is a physical chemistry process as a result of a dynamic effect determined by the two competing processes; nucleation and growth. The form of resulting silica polymer particles is governed by the relative rates of hydrolysis and polycondensation. Silanol groups were formed by the hydrolysis of tetraethoxysilane monomers and undergo condensation forming siloxane bond (Si-O-Si), as seen in Figure 4.2. Hydrolysis process is a rate limiting process for the growth of silica particles effecting the nucleus concentration and final particle size. The same factors that determine the hydrolysis rate also affect the rate of growth and SNP generation is highly dependant on the reaction condition and concentration of reactants resulting in a variety of particle size. Synthesis of spherical, monodispersed and nanometer scale SNPs (Figure 4.3-4.5) was achieved by controlling and adjusting such parameters (Table 4.1) which also effect the relative rate of the hydrolysis and condensation processes enabling to reach the controlled growth .

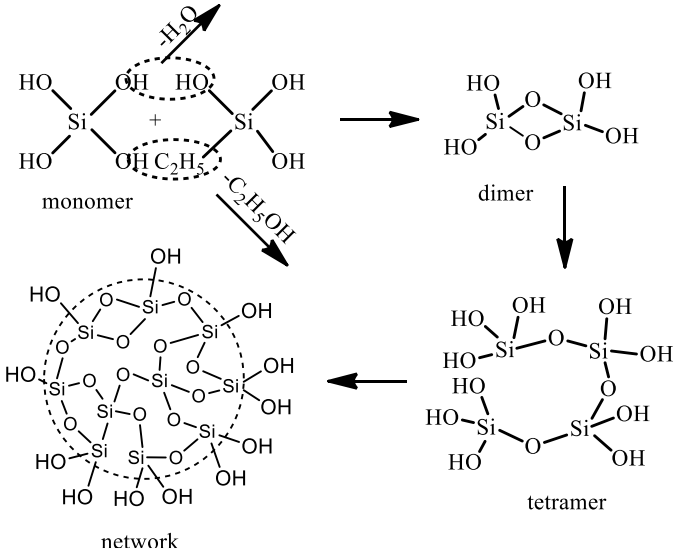

Figure 4.2 : Growth of silica nanoparticles forming spherical networks.

Ammonia, basic catalyst for the process was used as amonium hydroxide solution (25% aq NH_3) and NH_3 concentrations (Table 4.1) were calculated regarding to the solution. In all of the experiments, the only water source was from amonium hydroxide solution which was well above of the stoichiometric ratio 4/1 (water/teos) for the complete hydrolysis of TEOS, moreover, the condensation reaction of the TEOS monomer and precusors are also resulted in the elimination of water beside ethanol

molecules as seen in Figure 4.2, hence, the effect of the water concentration on the formation and final size of SNPs is not evaluated in this thesis.

Table 4.1 : Reactant concentrations and corresponding diameters of SNPs.

Sample*	TEOS (M)	NH_3 (M)	Diameter SEM (nm)
Si11	0.14	0.85	95
Si12	0.14	1.07	200
Si14	0.12	0.91	160
Si15	0.12	0.92	170
Si16	0.14	0.50	57
Si19	0.16	0.95	120
Si24	0.14	1.18	280
Si25	0.14	1.07	265
Si26	0.13	0.85	170
Si29	0.16	0.95	190
Si212	0.14	0.96	185
Si213	0.16	1.06	205

* SNP samples formed at 60 °C and room temprature are represented with the initials Si1 and Si2, respectively.

4.1.1 Shape, size and distribution properties of bare silica nanoparticles

The shape and the diameter of the resulting particles were determined using SEM and TEM. Observation of the images of electron microscopes clearly showed that all synthesized SNPs of Table 4.1 are spherical and monodispersed if not very nearly monodispersed. SEM images of SNPs; Si11 and Si26 with the particle sizes of 92 and 170, respectively, are shown in Figure 4.3. TEM images of SNPs; Si12 and Si210 with the particle sizes of 180 and 310, respectively, are shown in Figure 4.4. SEM and TEM images of Si19 are seen in Figure 4.5 indicating the approximate particle sizes of 115 and 105 respectively. Observation of the small difference between the TEM and SEM analysis for the size of same SNP, Si19, might be attributed to shrinkage of the nanoparticles under the electron beam of TEM resulting in slightly smaller size.

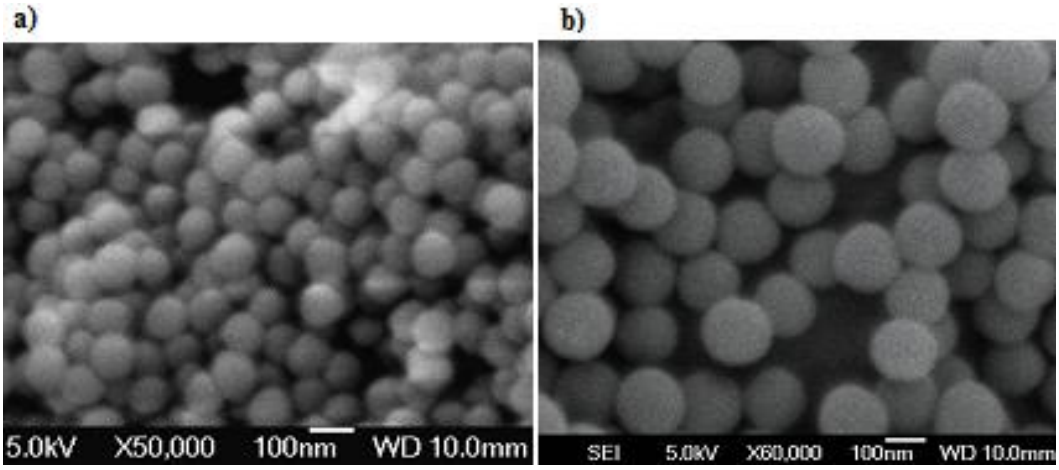

Figure 4.3 : SEM images of bare SNP a) Si11 and b) Si26.

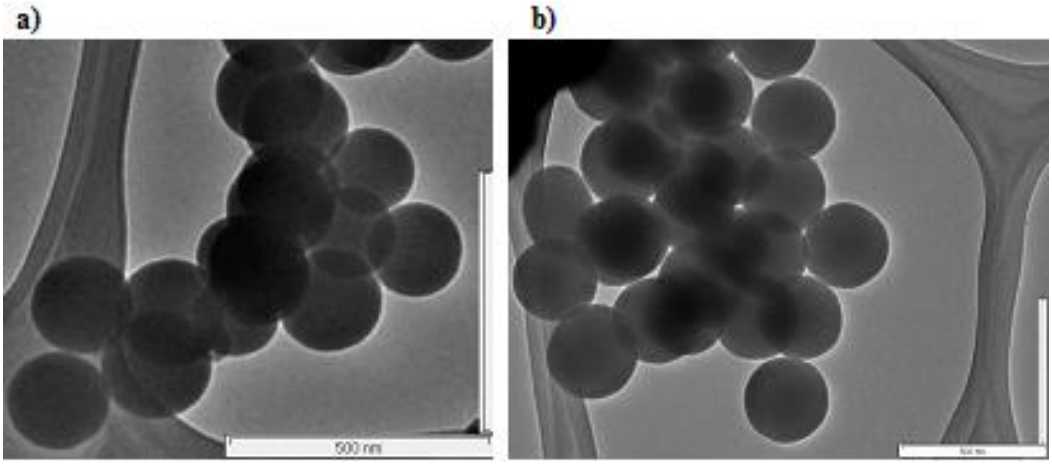

Figure 4.4 : TEM images of bare SNP a) Si12 and b) Si210

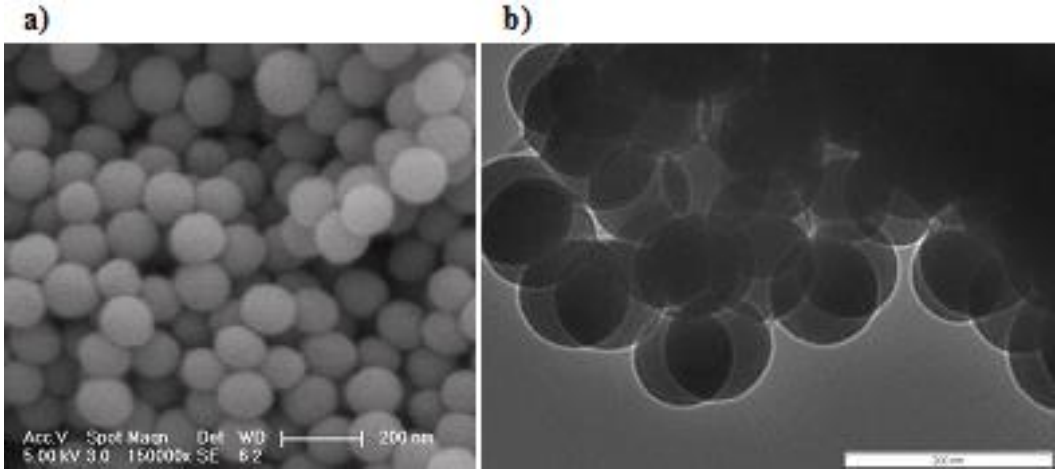

Figure 4.5 : a) SEM and b) TEM images of SNP Si19.

The effect of relative rate of polycondensation process to hydrolysis process on the growth of silica particles is also supported by the uniform, spherical structure of the resulting particles (Figure 4.3- 4.5). Spherical particles were obtained with the efficient concentrations of ammonia in the initial reaction medium, and the final particle size of

SNPs mainly depended on the adjusting the concentrations of tetraethoxysilane, water and ammonia and temperature of the reaction. Changing reaction medium thus allow for changes in the particle size and structure, due to changes in the nature of the siloxane chains formed as the reaction proceeds.

Effect of temperature on the size of SNPs:

In this thesis, the effect of the temperature on the size of SNPs through altering the hydrolysis rate can be clearly seen. SNP samples in Table 4.1 were synthesized at 60 °C and room temprature being represented with initials Si1 and Si2 respectively. The synthesis of SNP series of 60 °C; Si11, Si12, Si14, Si15, Si16, Si19 resulted in much more smaller particle sizes than their corresponding SNP series of room temperature; Si24, Si25, Si26, Si29, Si212, Si213 which synthesized by the same or nearly same concentrations of NH_3 and TEOS. Smaller size of SNP as a result of higher nucleation concentration must be attributed to the higher hydrolysis rate under higher temperature that leads to faster kinetics.

Effect of the reactant concentrations on the size of SNPs:

Since ammonia promote both the rate of hydrolysis and polymerization of TEOS, increacing the ammonia consentration results in faster kinetics and larger sizes of SNP. In this work, Table 4.1 displays the effect of ammonia concentration for the synthesis of SNP according to Stöber process. When the ammonia/teos ratio was increased at both tempratures of the synthesis, the final particle size of SNP was also relatively larger. The apparent effect of higher ammonia concentration on the formation of larger SNP as seen in Table 4.1 is consistent with the result of faster hydrolysis and condensation rate. However, again according to Table 4.1, size enlargement of SNP based on the ammonia concentration only occurs when TEOS concentrations is also increased or stayed constant with the increase of ammonia concentration. For example, ammonia and TEOS concentrations of sample Si29 are 0,95 and 0,16 respectively and of sample Si12 are 0,96 and 0,14 respectively. And corresponding ammonia/teos ratios for samples Si29 and Si212 are 6 and 7 respectively. Depending on the higher ammonia/teos ratio and ammonia concentration, the particle size of Si212 sample would be expected to be larger than the size of Si19 sample, however, the particle sizes of sample Si19 and Si12 are 185 nm and 205 nm respectively. The smaller particle size of Si212 sample, contrary to the higher ammonia concentration and ammonia/teos

ratio, is connected with the lower TEOS concentration of Si212. It is apparent that, along with the ammonia/teos ratio, the concentraion of TEOS itself also has the effect on the particle size of SNP. Even with the sufficient concentration of ammonia, the decrease in TEOS concentration result in the decrease of SNP size. Formation of particle nuclei; growth of nuclei and addition of monomer to nuclei determining the size of the SNP also depend on the TEOS concentration. This approach is consistent with the smaller particle size of sample Si212 compared to Si29 in Table 4.1 as a result of decreased concentration of TEOS even with the higher ammonia concentration and ammonia/teos ratio.

4.1.2 Structural properties of silica nanoparticles

The FTIR spectrums of bare SNPs with and without residual ethoxy group are shown as (a) and (b) respectively, in Figure 4.6. Small amount of ethoxy groups ($-OC_2H_5$) of TEOS might remain un-hydrolyzed during growth of silica particles depending on the reactant concentrations and synthesis condition. Both spectrums of (a) and (b) showed characteristic peaks of Si-O-Si at 1160 cm^{-1} (asym) and 1050 cm^{-1} (sym), of Si-OH at 940 cm^{-1}, of Si-O at 800 cm^{-1} and broad peak of free, bridged and H_2O absorbed SiO-H group at 3350-3700 cm^{-1}. The peak of H_2O at 1630 cm^{-1} in both spectrums indicated water absorption character of SNPs.

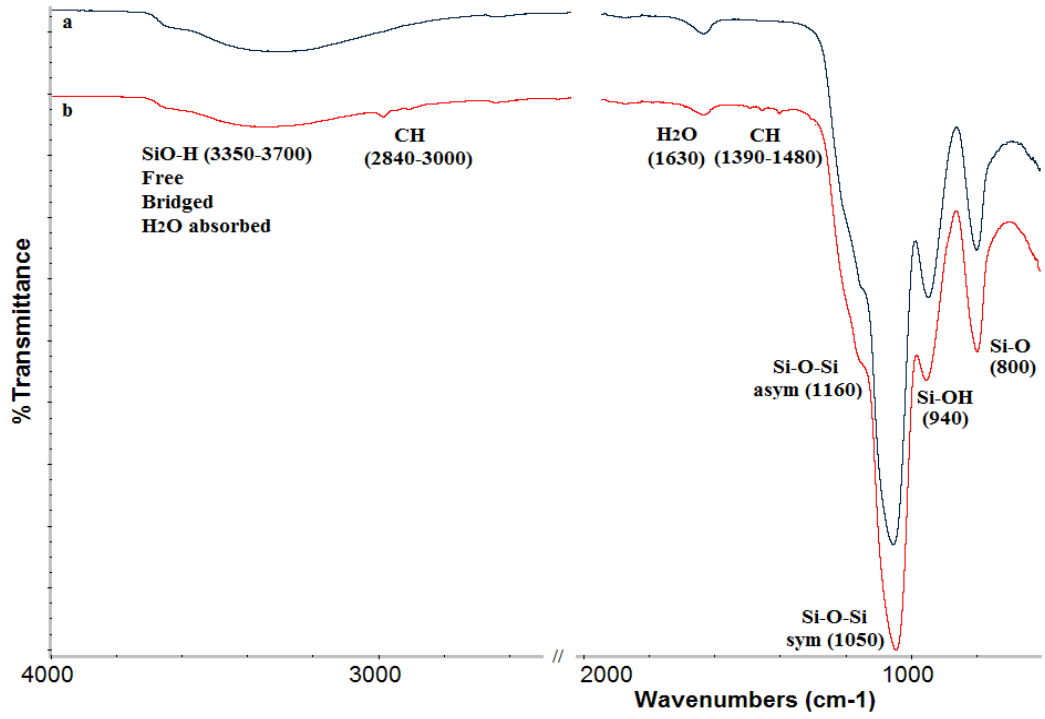

Figure 4.6 : FTIR spectrum of bare silica particles a) completely hydrolyzed b) carbon containing.

Thermal behavior of silica particles also examined by FTIR, the spectrum of each samples obtained after treating for 3 h at 150 ºC (b), 400 ºC (c), 600 ºC (d) and 800 ºC (e), respectively are shown in Figure 4.7. The intensity of characteristic H_2O absorbtion bands of SNPs at 3300-3700 cm^{-1} and 1630 cm^{-1} decreased with the increased temperature of the heat treatment. The H_2O peaks disappeared at the temperature of 800 ºC. The trace of H_2O peak at 1630 cm^{-1} in the spectrum of Figure 4.7 (d) at 600 ºC indicated the little amount of water trapped even at high temperatures. Such water molecules most likely trapped in the inner part of silica particles rather than the surface of the particles resulting in difficulty of evaporation. The peaks of silanol (-SiOH) groups at 3300-3700 cm^{-1} and 940 cm^{-1} also decreased with the increased temperature representing the siloxane (Si-O-Si) formation with the merge of silanol groups releasing water.

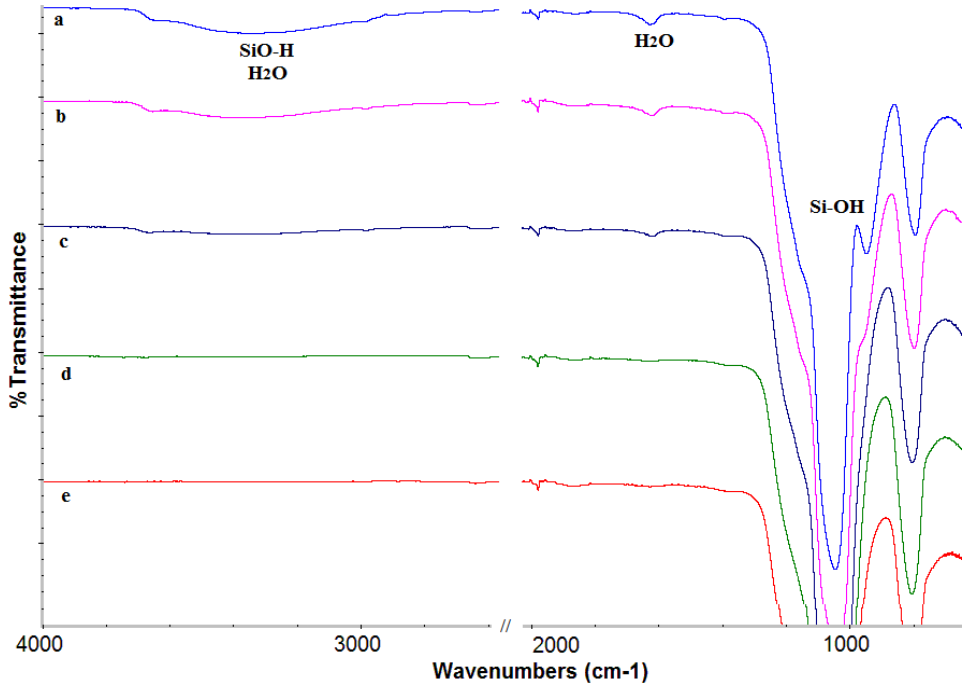

Figure 4.7 : FTIR spectrums of thermally untreated a) and treated at b) 150 ºC c) 400 ºC c) 600 ºC and d) 800 ºC.

The ^{29}Si MAS-NMR was employed to investigate the surface chemistry of bare SNPs, the general spectrum of the nanoparticles (Figure 4.8) exhibited prominent peaks at around -112, -103, -91 ppm are assigned to the siloxane group Q^4 $[(SiO)_4Si]$ and silanol groups of free Q^3 $[(SiO)_3Si(OH)]$ and geminal Q^2 $[(SiO)_2Si(OH)_2]$ respectively. The spectra of bare silica nanoparticles show that Q^3 peak intensity is less than Q^4 peak intensity and Q^2 peak is very small for bare silica nanoparticles. The smaller the diameter the bigger the surface area of the particle is resulting in a higher number of

silanols on the surface of SNPs. For the smaller particles with higher number of silanol groups, it is possible to obtain the peak intensity of silanol groups close to the peak intensity of siloxane bridges in ^{29}Si MAS-NMR spectrums. In Figure 4.8 of ^{29}Si MAS-NMR spectrum, we could also observe the peak intensity of free silanols Q^3 being very close to siloxane ones Q^4 indicating the nanometer scale of silica particles of this study with corresponding high specific surface areas for non-porous SNPs (table 4.2).

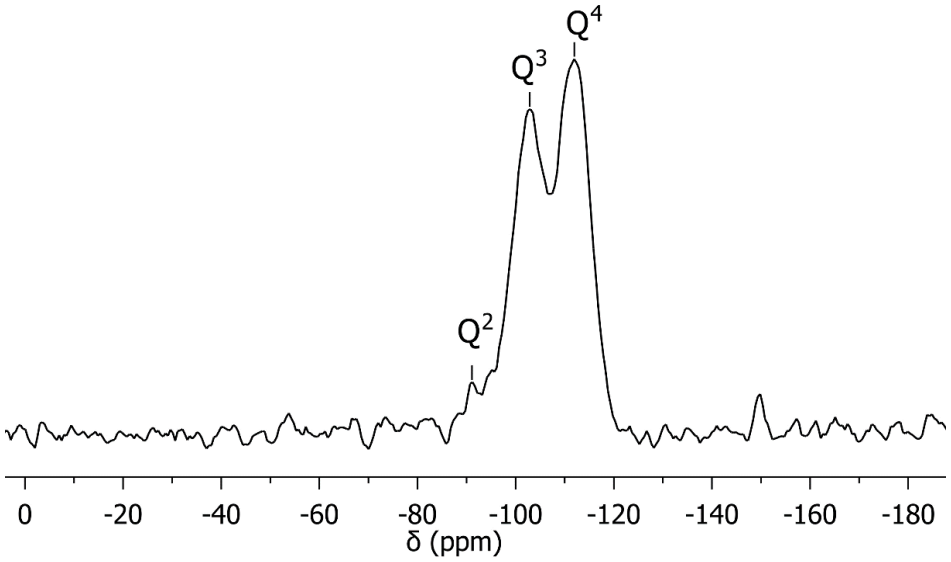

Figure 4.8 : ^{29}Si MAS-NMR spectra of bare silica nanoparticles.

4.1.3 Specific surface area of SNPs

Specific surface area (S) of Stöber SNPs was determined by BET model (N_2 adsorption at 77K), samples preheated at 160 ^oC for 2 h and degassed and the results are given in table 4.2. Specific geometric surface area, S_G, can be simply calculated making some assumption about the particle shape and taking the particle density (ρ) and size (D) into account using the following formula:

$$S = 6000 / \rho \times D \qquad (4.1)$$

The density of amorphous, spherical Stöber silica is accepted to be in the range of 1.9 g/cm^3 - 2.2 g/cm^3 because of the hexagonal shape and non-porous structure assumption of silica particles. In our work suggesting the density of Stöber SNPs as 2 g/cm^3, S_G values of the samples with different particle sizes were calculated according to the formula 4.1 and given in Table 4.2.

The measured S_{BET} values and the calculated S_G values of our SNP samples (Table 4.2) are in a very good agreement except for the samples Si11 and Si16 of which S_{BET} values are still very close to S_G values and in an acceptable range. The higher S_{BET}

values for the SNPs Si11 and Si16 with the sizes less than 100 nm, being 95 nm and 57 nm respectively might be attributed to possible porous structures of smaller particles resulting in higher specific surface areas. Even though S_G values of the SNPs in Table 4.2, were calculated according to formula for non-porous structures, some Stöber SNPs might have slightly porous structure resulting in higher specific surface areas measured by BET.

Table 4.2 : Specific surface (S) and specific geometric surface (S_G) areas of SNPs.

Sample	Particle size SEM (nm)	S (BET) ($m^2 g^{-1}$)	S_G ($m^2 g^{-1}$)
Si11	95	46.8	31.6
Si14	160	16.0	18.8
Si15	170	15.6	17.6
Si16	57	61.3	52.6
Si24	280	7.9	10.7
Si25	270	8.2	11.1
Si26	160	18	18.8
Si29	190	16.7	15.8
Si213	200	20.3	15

Furthermore, there are other methods in addition to BET method for specific surface area measurement, also in case of BET method there are other appropriate gases and temperatures in addition to N_2 and 77K, respectively. BET measurements based on N_2 adsorbtion at 77K might fail to give accurate results for some Stöber silica particles known as non-porous but owning microporous or ultra-microporous structures with higher specific surface areas. The possible reasons of this failure were explained in many studies and mainly attributed to micropores of some silica particles that cannot be accessed by N_2 at low temperatures. Therefore, measured S_{BET} values of our samples might even be less than the real S values of some samples in Table 4.2 if they also own ultramicropores. This approach might be also consistent with the high hydroxyl number results for some of our SNP samples in Table 4.3, as a result of possible existence of ultra-micropores that could not be accessed by N_2 at low temperatures of the BET method used in this thesis.

Still, ignoring the possibility of micro-porous structure for some silica particles, BET technique with the good aggreement of S_{BET} and S_G values in Table 4.2, allowed us to confirm the monodispersity, uniformity and reproducibility of our SNPs synthesized under certain reaction conditions.

4.1.4 Hydroxyl number (silanol) of SNPs

Hydroxyl group content and thermal behavior of bare silica nanoparticles were determined with thermogravimetric analysis (TGA) (30-1000^{o}C), under nitrogen, with a heating rate of 20 ^{o}C/min. The TGA thermograms of bare SNP are shown in Figure 4.9 and some thermal characteristics are presented in Table 4.3.

In case of complete hydrolysis and condensation, the weight loss of bare SNPs evaluated from TGA is due to the water release as a result of two processes; the release of physically-structurally absorped water and silanol group condensation. It is necessary to determine T_B, boundary temperature that separates two processes in order to distinguish hydroxyl group content and molecularly absorbed water of SNPs. The substantial discrepancy for T_B (120-600 ^{o}C) in literature might be attributed to possible porous or ultramicroporous structure of some Stöber silica particles that result in the need for higher temperatures to release the trapped water from the inner micropores of the SNPs.

Table 4.3 : Hydroxyl content (n_{OH} (mmol/g)) of SNPs evaluated from TGA.

Sample	Size SEM (nm)	S (BET) (m^2 g^{-1})	Residue (%) (^{o}C) 200	Residue (%) (^{o}C) 900	n_{OH} (mmol/g) (^{o}C) 30-200	n_{OH} (mmol/g) (^{o}C) 200-900
Si11	95	46.8	9.8	90.9	3.5	6.7
Si14	160	16.0	97.7	93.1	2.6	5.1
Si15	170	15.6	94.1	89.7	6.5	4.9
Si16	57	61.3	93.9	86.6	6.8	8.2
Si25	270	8.2	94.0	89.9	6.6	4.7
Si26	160	18	93.0	88.3	7.8	5.3
Si29	190	16.7	93.7	87.3	7.0	7.2
Si213	200	20.3	94.5	88.1	6.1	7.1

The hydroxyl group content (n_{OH}), determined as the moles of hydroxyls per gram of silica can be calculated at any temperature according to following formula:

$$n_{OH}\ (mol/g\ SiO_2) = 2\ n_{H2O} = 2(W_0\text{-}W_f\ )\ /100\ M_{H2O} \qquad (4.2)$$

Where the residue difference, W_0-W_f corresponds to the weight loss in any temperature region (T_0-T_{final}) and M_{H2O} is the molar mass of water. In this thesis, we accepted T_B as 200 ^oC and n_{OH} values of the silica samples in Table 4.3 were calculated by the corresponding weight losses of the samples during thermal anaysis (Figure 4.9) according to formula 4.2.

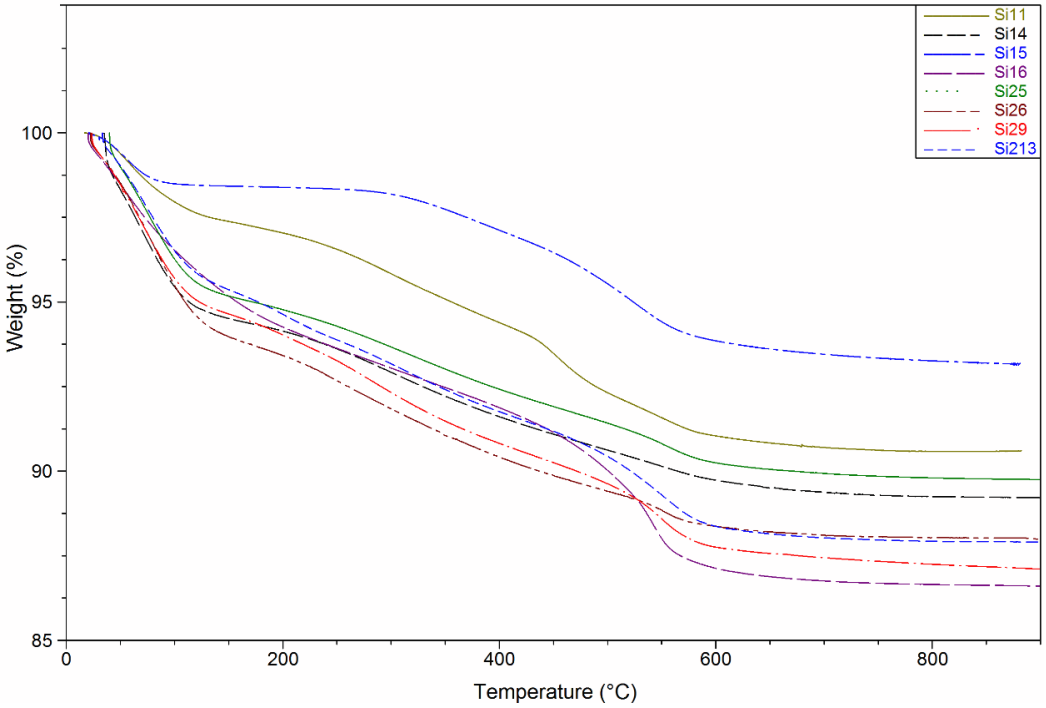

Figure 4.9 : TGA thermogram of bare silica nanoparticles.

The weight losses of the silica samples up to 200 ^oC and between the temperatures of 200-900 ^oC correspond to water content and hydroxyl (silanol) groups of SNPs, respectively. The larger specific surface areas (S) of SNP samples caused the higher n_{OH} values of the temperature region of 200-900 ^oC in Table 4.3 and samples (Si14-Si15 and Si29-Si213) with similiar particle sizes and S values also resulted in similiar n_{OH} values confirming the direct relation of hydroxyl content and specific surface area of the SNPs. However, calculated n_{OH} values for temperature region of 30-200 ^oC which represent the water content of SNPs did not show a direct relation between the specific surface areas and hydroxyl group content of the SNPs. This result is consistent with the water absortion behavior of the SNPs that the amount of absorbed water does

not only depend on the structure of the particles such as having ultramicropores but also on storage condition and pre-treatment of the particles.

Mole of hydroxyl groups per gram of silica (n_{OH}) can be converted to silanol number (α_{OH}) determined as the number of hydroxyl group per nm^2 of SNP with the following equation:

$$\alpha_{OH} = n_{OH} \times 10^{-18} \times N / S \qquad (4.3)$$

Where N is Avagadro number and S is the specific surface area (m^2/g) of the particles. When the surface of silica nanoparticle is hydroxylated to the maximum degree, independent of the origin and structural characteristics of the amorphous silica particles, α_{OH} is ranged from 4.3 up to 5.8 OH per nm^2 and this value is considered to be a physico-chemical constant known as Kiselev Zhuravlev constant [84].

According to calculations of TGA analysis (Figure 4.9) of SNP samples of Table 4.3, corresponding α_{OH} numbers are obtained out of the range (4.3-5.8 per nm^2) owning in some cases almost in 10 times higher values than the exceptedrange. The parameters applied in the formulations 4.2 and 4.3, repectively are independent of the possible porous structures of the particles. However, also according to BET measurements we consider that some of the SNPs might have ultra or micro porous structure even though in literature it is accepted as non-porous structure for Stöber silica particles. Such possible porous structure of the SNPs might result in larger S, so the higher number of hydroxyl groups that observed in TGA analysis. Moreover, such ultramicropores trap molecular water inside the SNPs which result in the need for higher temperatures (up to 450 ^oC) in order to release water. In such case, the calculations based on the T_B being 200 ^oC might fail to give accurate results of α_{OH}.

4.2 Modification of SNPs and Their Incorporation in Hybrid Materials

The widely used and seemingly effective coupling reactions of silica particles with alkoxy silane coupling agents may become challenging owning some disadvantages and limitations (see section 2.4.3). Direct functionalization of silica nanoparticles with reactive organic moieties can overcome such problems of silane coupling reactions. In this thesis, we aimed to use toluen diisocyanate (TDI) as the organic moiety in order to eliminate the disadvantages of silane coupling agent graftings and enable high number of attachment of functional isocyanate groups for further reactions on the

surface of SNPs. Secondly, well dispersed, isocyanate grafted silica nanoparticles (Si-TDI) reacted with benzoin molecules designing SNP macro-photoinitiator and subsequently formed SNP macroinitiators were employed to initiate photopolymerization of methyl methacrylate onto the surface of SNPs. As last, well determined Si-TDI also incorporated into epoxyacrylate resin over the covalent bond.

4.2.1 Functionalization of SNPs with toluen diisocyanate

2,4-Toluene diisocyanate (TDI) having two reactive isocyanate group takes the place of being a very effective organic moiety for surface grafting of SNPs and also for further effective reactions over the isocyanate groups. TDI functionalized silica nanoparticles (Si-TDI) were synthesized as shown in Figure 4.10.

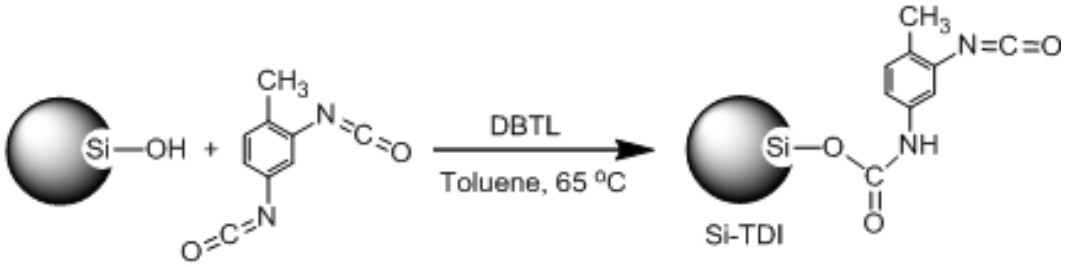

Figure 4.10 : Toluene diisocyanate functionalization of SNPs.

Spherical, well-defined and uniform bare silica nanoparticles (Si16) with an average diameter of 57 nm, were modified with TDI moeity. The high reactivity of TDI molecule increase the ability of grafting so the concentration of functional isocyanate groups on the surface of SNPs. Grafting of TDI on the surface of silica nanoparticles was achieved by the reaction of silanol groups of SNPs and isocyanate groups of TDI molecules forming urethane linkage. Since the sensitivity of isocyanate groups towards moisture is very high, prior to grafting reaction, it was essential to remove all types of water absorbed by the particles. It was assumed that most of the urethane linkages formed by p-isocyanate group of TDI molecule considering para located isocyanate group of TDI to be much more reactive than its o-isocyanate group. Furthermore, excess TDI was used to ensure that more reactive p-isocyanate groups react preferentially with the silanol groups of SNPs. The other reason for the preservation of o-isocyanate group during TDI functionalization is the steric hindrance caused by the size of the SNPs.

The FTIR spectrums of the bare and TDI grafted silica nanoparticles are shown in Figure 4.11(A and B). The appearance of a new band at 3302 cm^{-1}, which is

characteristic for –NH group, confirms the urethane bond formation between the silica nanoparticles and TDI. The strong absorption at 2268 cm^{-1} shows the existence of unreacted o-isocyanate group of Si-TDI.

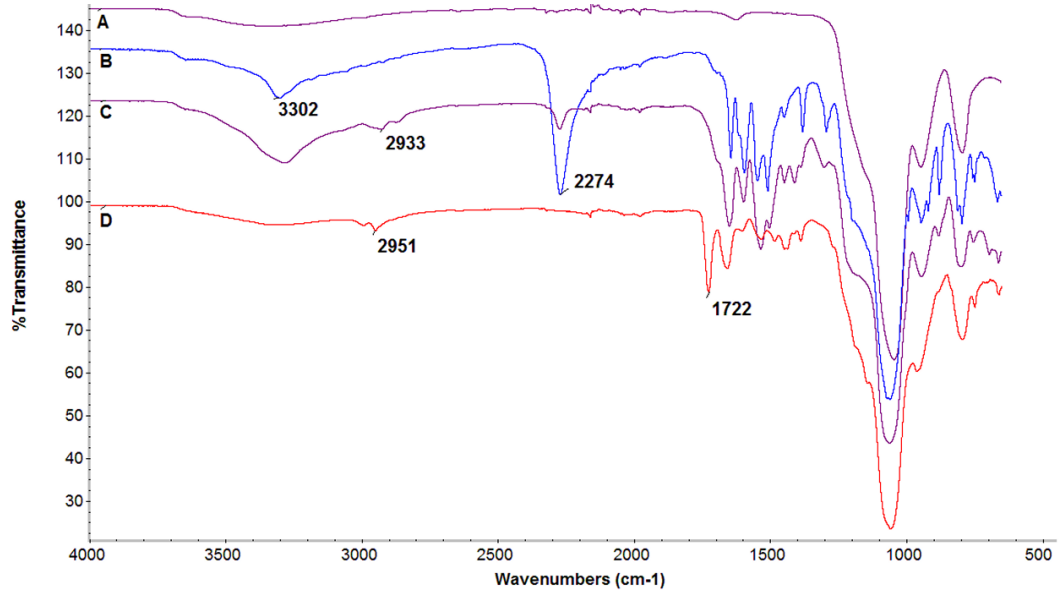

Figure 4.11 : FTIR spectra of SiO_2 (A), Si-TDI (B), Si-Ben (C) and Si-PMMA (D).

The ^{29}Si MAS NMR spectra of bare silica nanoparticles (Figure 4.12A) exhibited prominent peaks at around -112, -103, -91 ppm assigned to the siloxane group Q^4 $[(SiO)_4Si]$) and free Q^3 $[(SiO)_3Si(OH)]$ and geminal Q^2 $[(SiO)_2Si(OH)_2]$ silanol groups respectively. The ^{29}Si MAS NMR spectra of Si-TDI (Figure 4.12B) exhibited the same Q^3 and Q^2 peaks of bare silica with the reduced intensities related to TDI functionalization on the surface of silica nanoparticles. The peak intensities of Q^3 and Q^2 became much smaller compared to the Q^4 peak of Si-TDI while an increase in Q^4 peak intensity was observed indicating the reaction of TDI with the silanol groups of silica nanoparticles.

^{13}C CP/MAS NMR spectrum of Si-TDI (Figure 4.13) shows the characteristic peaks of grafted TDI moiety. The carbonyl peak at 151 ppm is indicative of urethane formation confirming TDI bonding on silica nanoparticles. The other carbonyl peak at 116 ppm is assigned to isocyanate group of TDI confirming the remaining free isocyanate functionality of TDI. In addition to evaluation of Si-TDI structure by ^{29}Si MAS NMR, the three peaks at 110, 112, 128 ppm correspond to unsubstituted aromatic carbons of TDI and the peaks at 125, 130, 131 ppm correspond to substituted aromatic carbons of TDI. The characteristic methyl peak of TDI appears at 13 ppm.

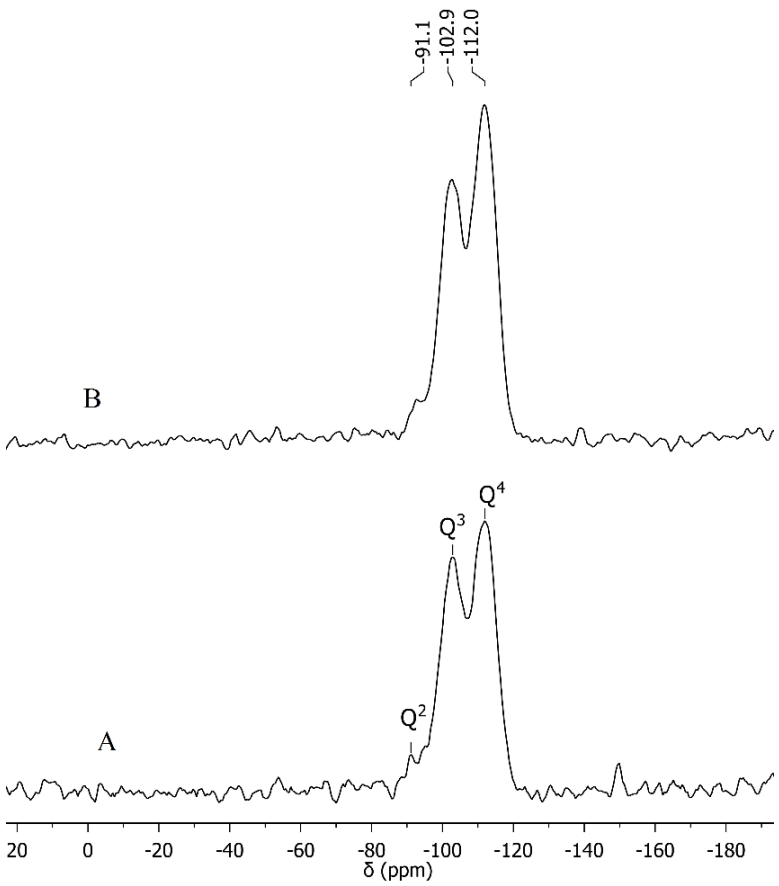

Figure 4.12 : ^{29}Si MAS NMR spectra of bare SiO_2 (A) and Si-TDI (B) nanoparticles.

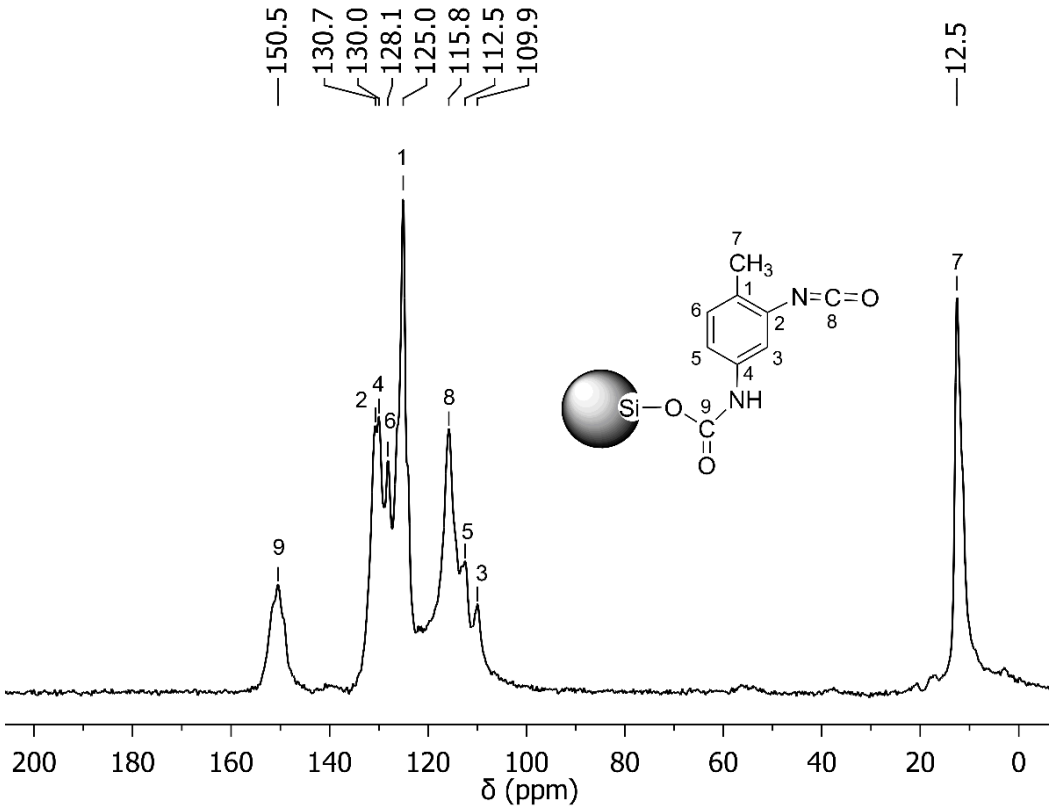

Figure 4.13 : ^{13}C CP/MAS NMR spectra of Si-TDI.

4.2.2 Synthesis of benzoin grafted SNPs and photopolymerizaiton of MMA via designed SNP-photo macrointiator

Benzoin and derivatives are well known photoinitiators which also find commercial application in UV curable coatings. Upon irradiation, these molecules undergo Norrish Type I cleavage and yield radicals (Figure 4.14) which are capable of initiating the free radical polymerization of vinyl monomers [146, 147]. In this thesis, benzoin grafted silica nanoparticles (Si-Ben) were designed as SNP-photo macroinitiators to achieve the graft polymerization of methyl methacrylate (MMA).

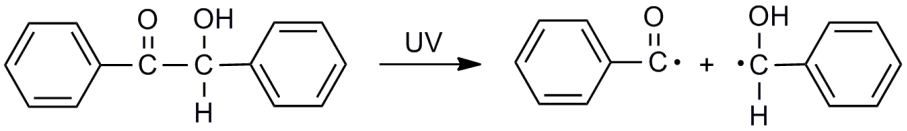

Figure 4.14 : The cleavage of photo active benzoin initiator.

The succesful attachment of TDI moiety onto the surface of SNPs with a high concentration of functional isocyanate groups (Si-TDI) further enabled the SNPs to react with benzoin molecules. The introduction of benzoin groups onto the surface of SNPs was achieved by the formation of second urethane linkage between previously attached free o-isocyanate group of SNPs and hydroxyl group of benzoin molecules. The overall reaction for the synthesis of Si-Ben is represented in Figure 4.15.

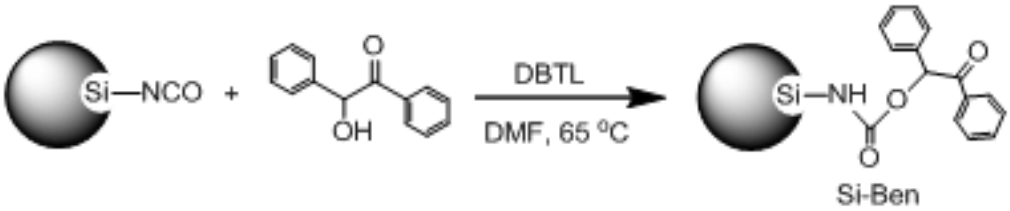

Figure 4.15 : Benzoin functionalization of SNPs.

As seen in the FTIR spectrums of Si-TDI and Si-Ben (Figure 4.11 B and C), the increased intensity of the absorption at 3302 cm^{-1} (Figure 4.11C) indicates the increasing –NH group formation due to the reaction between benzoin molecules and free o-isocyanate groups of TDI that previously grafted onto SNPs. In addition, the dramatic weakening of –NCO absorption at 2241 cm^{-1} also confirms the same free isocyanate reaction with benzoin.

TGA was performed to investigate the grafting content of SNPs and thermograms are shown in Figure 4.17. All samples were heated up to 800 ^{o}C with a heating rate of 20

°C/min under nitrogen. Relative mole of grafted organic content calculated according to the weight loses at 700°C by the following equation;

$$(\eta_{grafting} = \% W_{loss}/100\ MW_{organic\ component}) \quad (4.4)$$

The weight losses of 33.1 % (Figure 4.17B) and 51.8 % (Figure 4.17C) obtained by TGA analysis, corresponded to covalently attached TDI moeity of Si-TDI and the organic content (consisting of TDI and benzoin moieties) of Si-Ben, respectively. Relative mole of grafted TDI and benzoin initiator, calculated according to the formula 4.4 by the weight loses at 700°C, the results revealed that 72 % of the free isocyanate groups on the surface of SNPs reacted with benzoin moieties. Evaluated by TGA, remaining approximately 28 % of surface isocyanate groups as unreacted was in the agreement with the appearance of residual -NCO absorption at the FTIR spectrum of Si-Ben (Figure 4.11C) indicating not all of the free isocyanate groups to be reacted with hydroxyl groups of benzoin moieties. This maybe attributed to relatively less reactivity of o-isocyanate group compared to p-isocyanate group of TDI.

In the second stage, benzoin grafted silica nanoparticles (Si-Ben) were used as photo-macroinitiators for the graft polymerization of methyl methacrylate from the surface of SNPs, the process is represented in Figure 4.16. MMA monomer polymerized under UV in the presence of benzoin grafted silica nanoparticles (SNP-Photo macroinitiator) dispersed in DMF. Two vials of polymerization mixture were prepared with the same amount of reactants to be subjected to UV treatment in different periods as 2h and 4h, respectively, in order to observe the initiator effect of SNP- Photo macroinitiator by the different yileds of formed polymethylmethacrylate (PMMA).

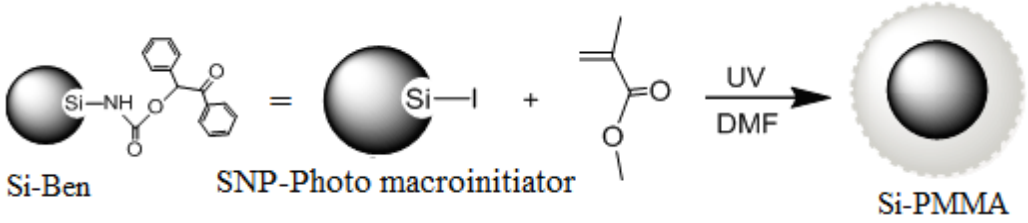

Figure 4.16 : PMMA grafting of Si-Ben Macroinitiator SNPs.

After the photopolymerizaiton of MMA, PMMA grafted SNPs (Si-PMMA-2h and Si-PMMA-4h) were obtained by precipitating into methanol and in order to remove un-grafted PMMA from the grafted Si-PMMAs, the cured products were extracted with acetone. Furthermore, the extracted un-grafted PMMA was recollected by the evaporation of acetone and precipitation into methanol.

The absorption bands belong to Si-PMMA can be seen in the FTIR spectrum of Figure 4.11D. The new absorption band of acrylate group (-COO) at 1722 cm^{-1} is referred to PMMA grafted onto surface of SNPs. Moreover, the partially sharp –NH band of urethane groups of Si-Ben at 3300 cm^{-1}, Figure (4.11C), was also observed significantly broad, such difference on the absortion band might be attributed to the coverage of Si-TDI particles by grafted PMMA.

The observed mass losses of TGA were attributed to pyrolysis of grafted organic components on the surface of SNPs referring the remaining incombustible residue to SNPs (Figure 4.17). The complete pyrolysis of ungrafted PMMA resulted in remaining no incombustible residue (Figure 4.17F). The weight losses of 77 % (Figure 4.17D) and 84.4 % (Figure 4.17E), correspond to grafted PMMA ratios of Si-PMMA-2h and Si-PMMA-4h, respectively and indicated the increase rate of photopolymerization along with the period of UV exposure which also confirms the macroinitiator role of benzoin functionalized SNPs for the synthesis of hybrid Si-PMMA.

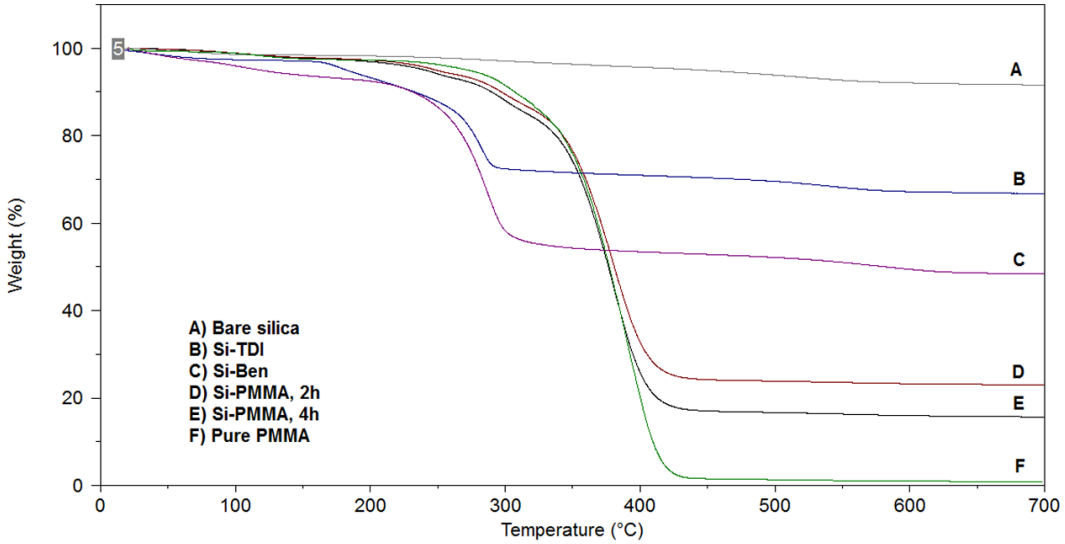

Figure 4.17 : TGA spectra of bare SNP (A), Si-TDI (B), Si-Ben (C) Si-PMMA-2h (D) Si-PMMA-4h (E) and un-grafted PMMA (F).

The SEM images of bare Si16 and Si-PMMA-4h are shown in Figure 4.18. While the average diameter of Si16 bare nanoparticles was 57 nm, the average diameter of Si-PMMA hybrid was 105 nm as seen by the SEM analysis of Figure 4.18 (A) and (B), respectively. The noticeably increased size of SNP-PMMA with retaining the spherical form of the SNP perfectly confirmed the photopolymerization of MMA yielding PMMA that grafted onto surface of SNPs and also confirmed the photomacroinitiator property of benzoin grafted SNPs.

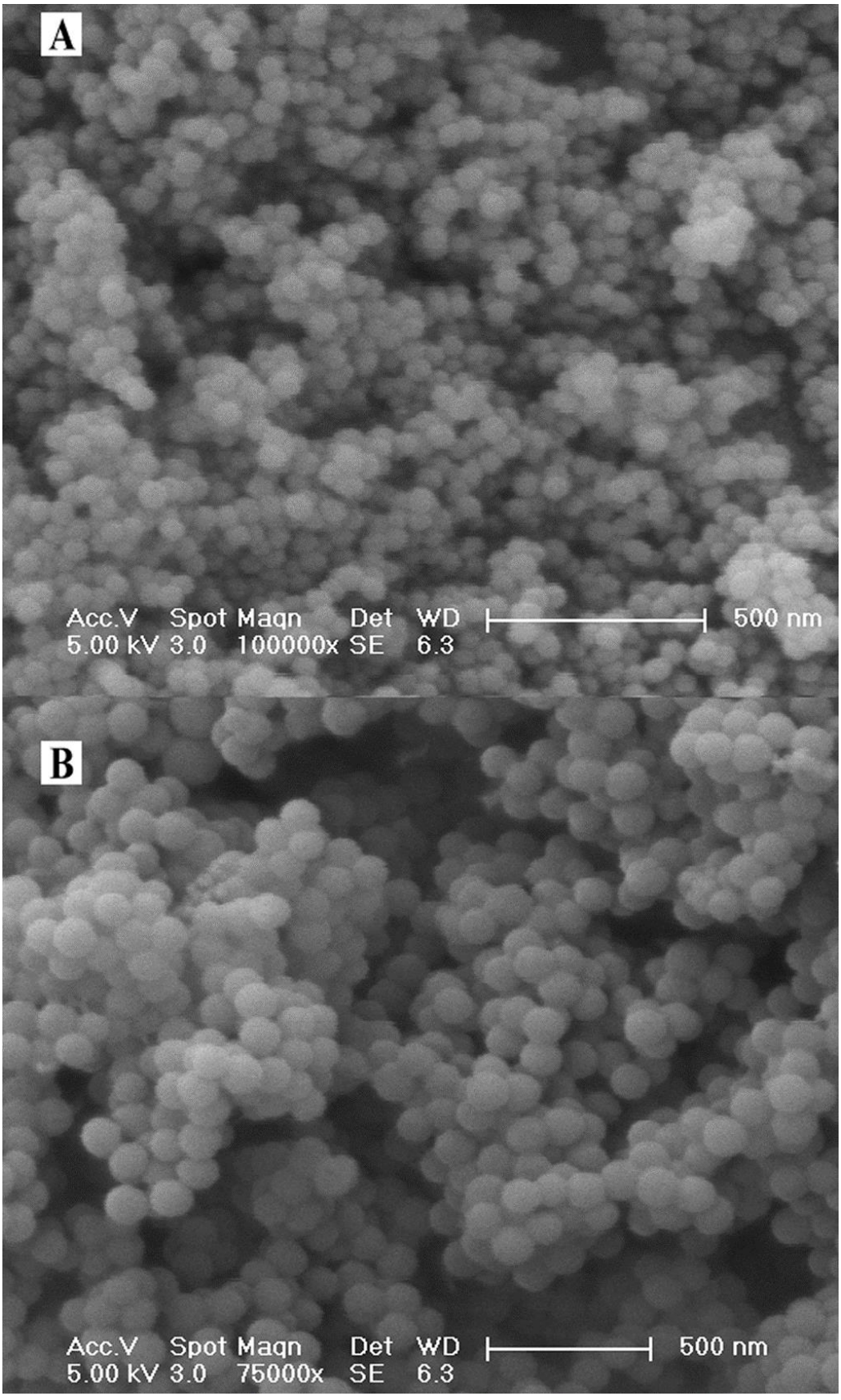

Figure 4.18 : SEM images of bare (A) and PMMA grafted silica nanoparticles (B).

TEM image of Si-PMMA-4h is shown in Figure 4.19. The degradation of organic PMMA component of Si-PMMA hybrid was observed and the possible reason for it is attributed to the high voltage of TEM analysis which also reduce the image quality. Under the electron beam of TEM, SNPs as the core part of Si-PMMA seemed to be embedded in PMMA shell-matrix with a slight deformation and shrinkage compared to the SEM images of Si-PMMA. The observation of TEM image of Si-PMMA clearly showed that aggregation of SNPs was prevented despite the relatively high surface area of SNPs indicating the PMMA shell structure of hybrid Si-PMMA.

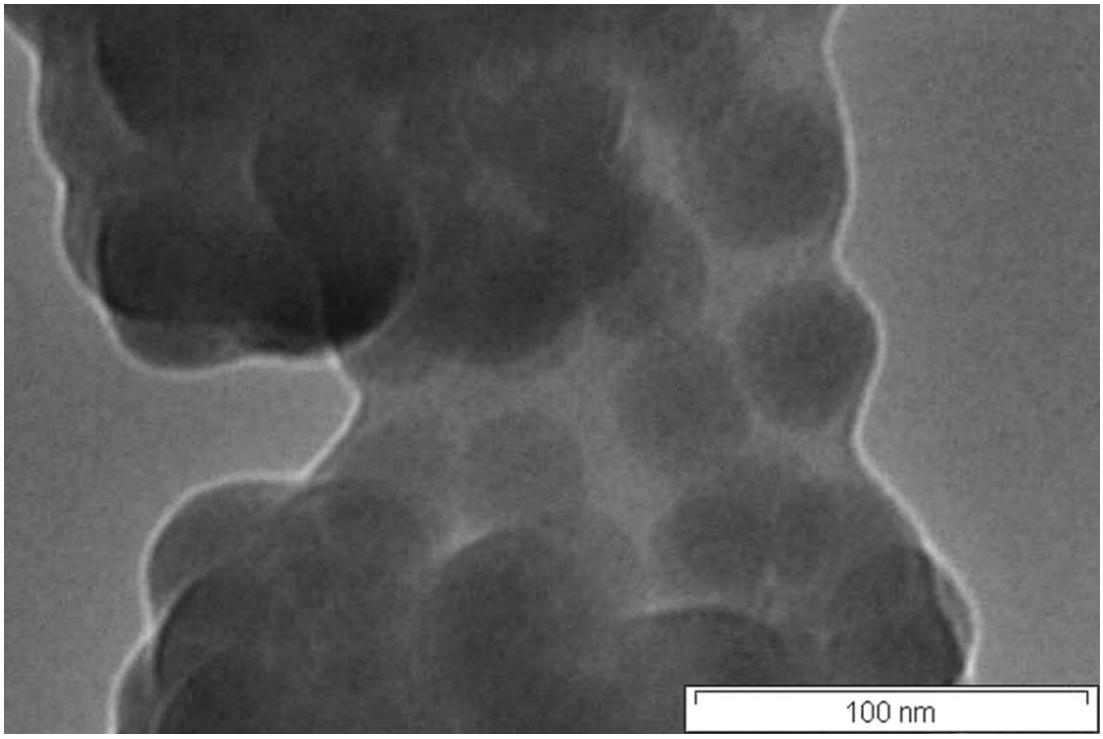

Figure 4.19 : TEM images of PMMA grafted silica nanoparticles.

Photoinitiator migration from a polymer matrix can be defined with diffusion and cleavage processes. Such processes may result in limitations for the use of photopolymerized materials in some applications such as food packaging. In this thesis, synthesized and applied benzoin grafted SNP is also considered as rewarding photo macroinitiator candidate being grafted to inorganic SNPs to reduce the risk of photoinitiator migration. Our published work is based on this study of the thesis [148].

4.2.3 UV-cured organically modified SNP/EA hybrid resin (EA-Si)

Isocyanate functionalized SNPs (SNP-TDI) were incorpareted into epoxy acrylate resin formulations following UV curing process. Bisphenol A type, solvent free epoxy resin with low viscosity (Marepoks 1721) was reacted with acrylic acid for the synthesis of epoxy-acrylate resin (EA). Then, EA resin (diluted with 20% HDDA) was reacted with Si-TDI nanoparticles in order to obtain SNP/epoxyacrylate hybrid resin (EA-Si). As the last step, EA-Si hybrid resin was cured under UV radiation. The synthetic route for the whole process is shown in Figure 4.20.

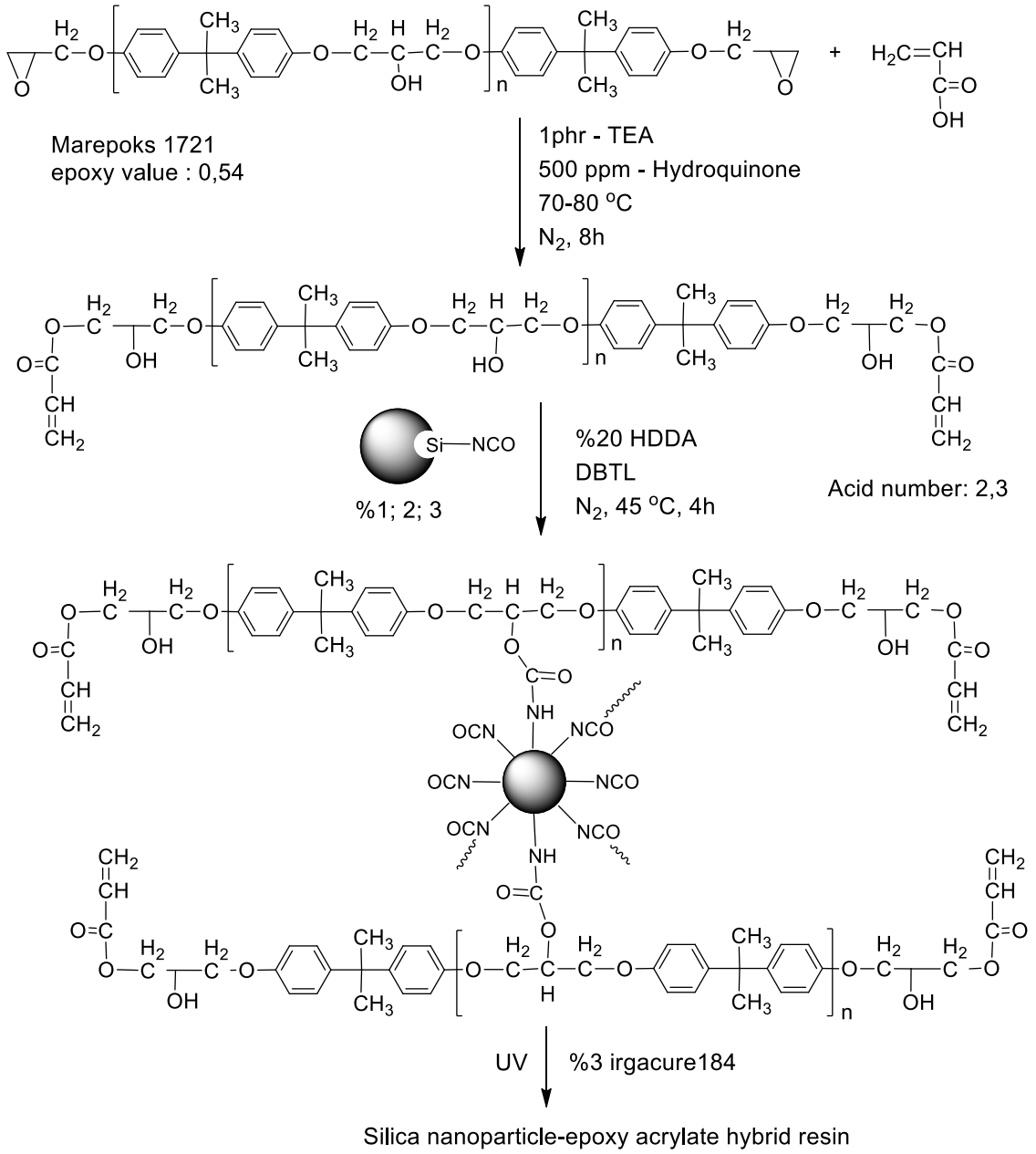

Figure 4.20 : The synthetic route for silica nanoparticle/epoxyacrylate hybrid resin.

The epoxide equivalent weight (EEW) of Marepoks 1721 was calculated from the epoxide value (EV) determined as the number of moles of epoxy groups per 100 g of resin by the following equation :

$$\text{Epoxide value} = 100 / \text{epoxide equivalent weight.} \quad (4.5)$$

The given EV for Marepoks 1721 by the manufacturer is ~0.54 and the EEW of the resin was calculated according to equation 4.5 as ~185. The equivalent concentrations of all the reactants such as TEA and acrylic acid were determined according to calculated EEW of the Marepoks 1721 resin.

The ring opening reaction of epoxy resin by acrylic acid was followed by measuring the acid value of the epoxy resin and observing epoxy ring absorption band FTIR analysis. Acid value (mgKOH/resin) expressed by potassium hydroxide in mg required to neutralize free acid in 1g of substance, measured by titration with 0.1 N KOH in ethanol and phenolphthalein as indicator. The reaction was continued till acid value reached 2.3 mg KOH/epoxy resin indicating that almost all acidic groups were quantitatively reacted with the epoxy groups of Marepoks 1721.

Table 4.4 : Ratios of the components of EA-Si hybrid resin formulations.

Sample	EA resin (%w)	HDDA (%w)*	Si-TDI (%w)	Irgacure-184 (%w)
EA-Si 0%	80.8	16.2	0	3
EA-Si 1%	80	16	1	3
EA-Si 2%	79	15.8	2	3
EA-Si 3%	78.3	15.7	3	3

* 20% of EA resin

Acrylate functionalized Marepoks 1721 resin (EA) was well mixed with HDDA in %20 weight ratio of EA in order to dilute EA and increase the acrylate functionality. Si-TDI nanoparticles with 1%, 2% and 3% corresponding weight ratios of total acrylates (EA and HDDA) were well dispersed in HDDA by ultrasonication and reacted with EA. Prepared hybrid resins with the addition of irgacure-184 photoinitiator were successfully cured under UV radiation. EA-control resin (EA-Si 0%) also prepared without the addition of Si-TDI and cured under UV. The ratios for the components of EA-Si hybrid resin formulations are given in Table 4.4.

Figure 4.21 shows the FTIR spectrums of Marepoks 1721 epoxy resin (A), EA resin (B), and UV cured EA-control resin (C). The appearance of the new bands at 1637 cm^{-1} and 1724 cm^{-1}, which are characteristic for -C=C and -COO groups, respectively and disappearance of the bands at 919 cm^{-1} and 1366 cm^{-1} that belong to epoxy ring confirmed the esterification reaction between epoxy and acrylic acid. And the complete disapperance of epoxy band indicated that almost all of the epoxy groups acrylated by acrylic acid which is consistent with the acid value of 2.3 mg KOH/epoxy resin. After the curing treatment, FTIR spectrum (Figure 4.21 C) of the formed film of EA-control resin exhibited the disappearance of -C=C absorption band at 1637 cm^{-1} and the increasing intensity of $-CH_2$ absorption band around 2900 cm^{-1} relatively to the intensity of –COO absorption band at 1724 cm^{-1} confirming the complete curing process.

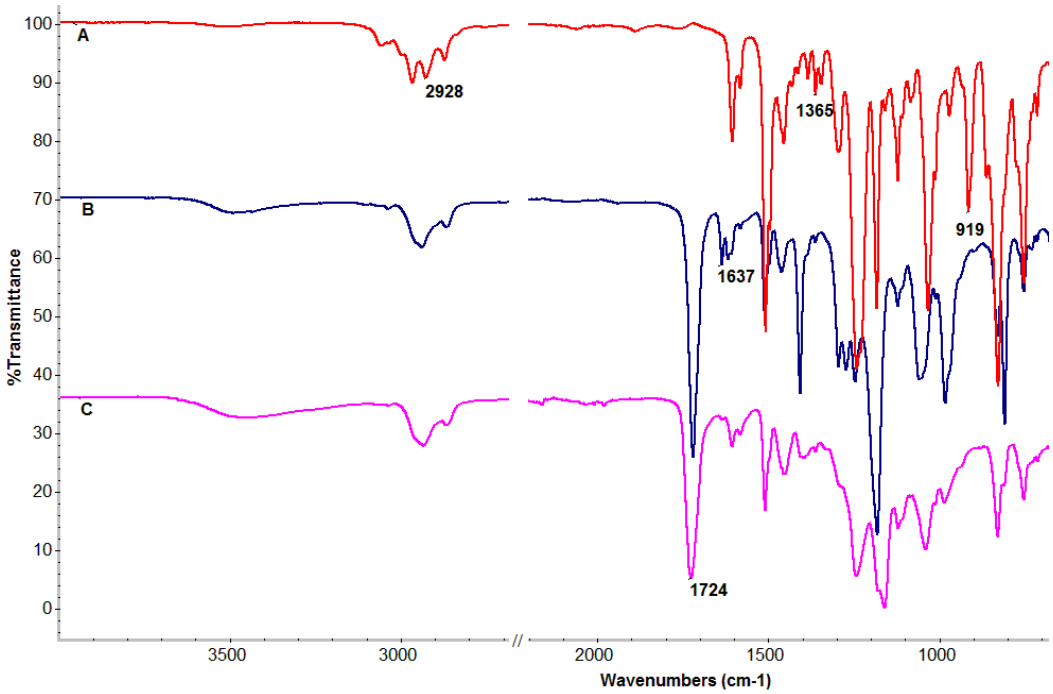

Figure 4.21 : FTIR spectra of Marepoks 1721 epoxy resin (A), EA resin (B), UV-cured EA-control resin (C).

Figure 4.22 shows the FTIR spectrum for cured EA-Si resins. In addition to all of the characteristic absorption bands of cured EA-control resin, the broaden apperance of the band at 3425 cm^{-1} is observed in Figure 4.22 (C) and attributed to -NHCOO group absorptions of Si-TDI. The appearance of the new bands at 1182 cm^{-1} and 1071 cm^{-1}, which are characteristic for Si-O groups, also indicated Si-TDI incorporation into EA resin. And the complete disapperance of the band at 2264 cm^{-1} that belongs to free –

NCO groups of Si-TDI nanoparticles indicated that there is not any unreacted isocyanate group remained.

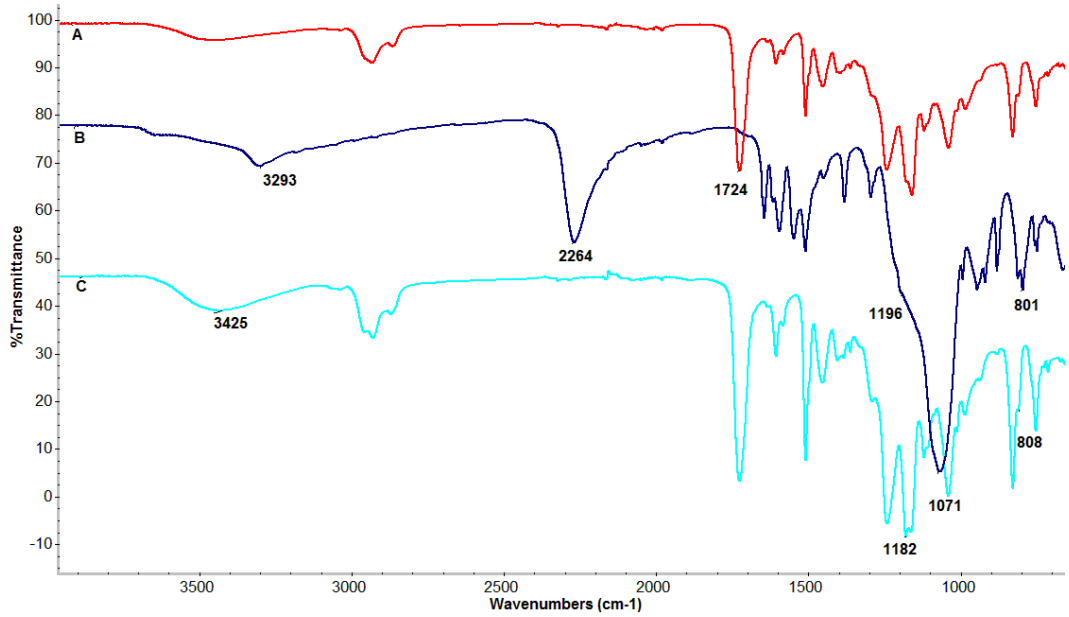

Figure 4.22 : FTIR spectra of UV cured EA-control resin (A), Si-TDI (B), UV cured EA-Si %2 hybrid resin (C).

The glass transition temperature (T_g) of the cured control EA resin film and SNP-EA hybrid resin films were analyzed by DSC and thermograms are seen in Figure 4.23. It was found from the DSC thermograms that control EA and silica-EA hybrid resins showed two T_g values corresponding to transitions of acrylate and epoxy regions. As seen in Figure 4.23A, T_g values of acrylate and epoxy regions were 82.5°C and 209°C, respectively for control EA resin. The both T_g values of acrylate and epoxy regions of the SNP-EA hybrid films increased with the increasing content of Si-TDI nanoparticles reaching to approximately 102.2 °C and 221.4 °C, reprectively for 3% Si-TDI content Figure 4.23D. The significant and consistent increase in T_g values of the hybrid films were both atributed to monodispersed incorporation of inorganic Si-TDI nanoparticles and the effect of the increased crosslinking density. Diisocyanate funcionalty of Si-TDI nanoparticles acts as cross-linking points of EA-Si hybrid resin because of the reaction between isocyanate groups of Si-TDI and hydroxy groups of EA resin.

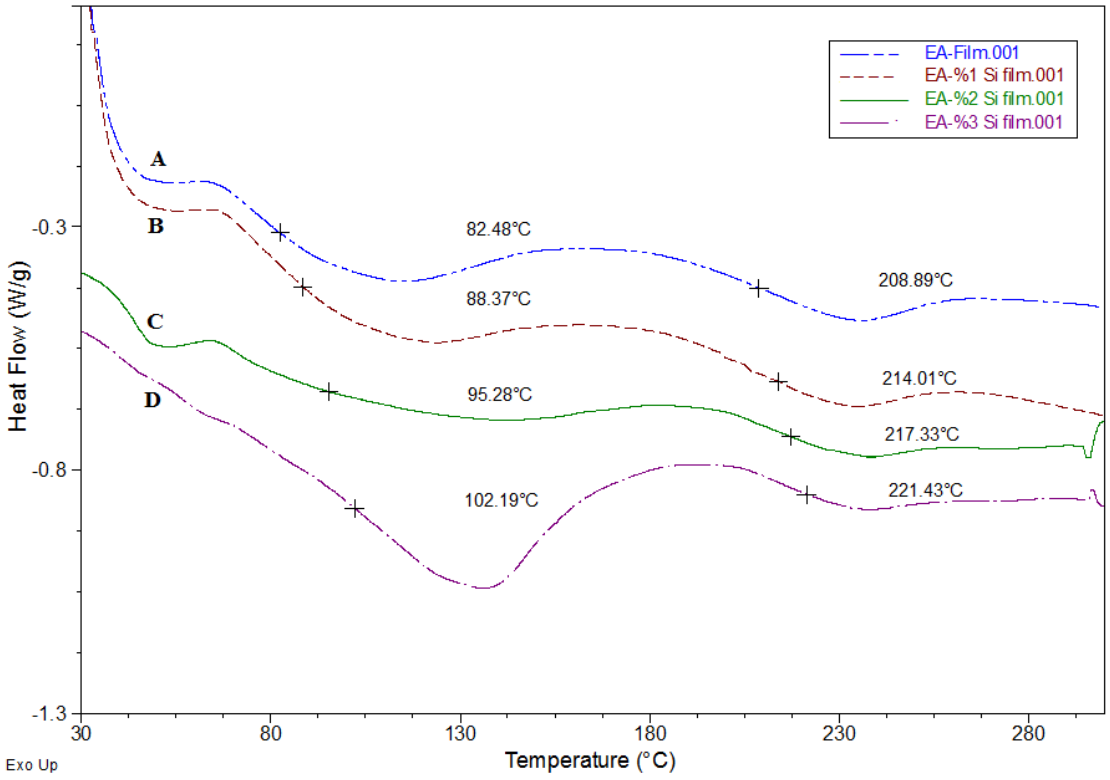

Figure 4.23 : DSC thermogram of UV-cured EA-control film (A), %1 (B), %2 (C), %3 (D) UV cured EA-Si nano hybrid films.

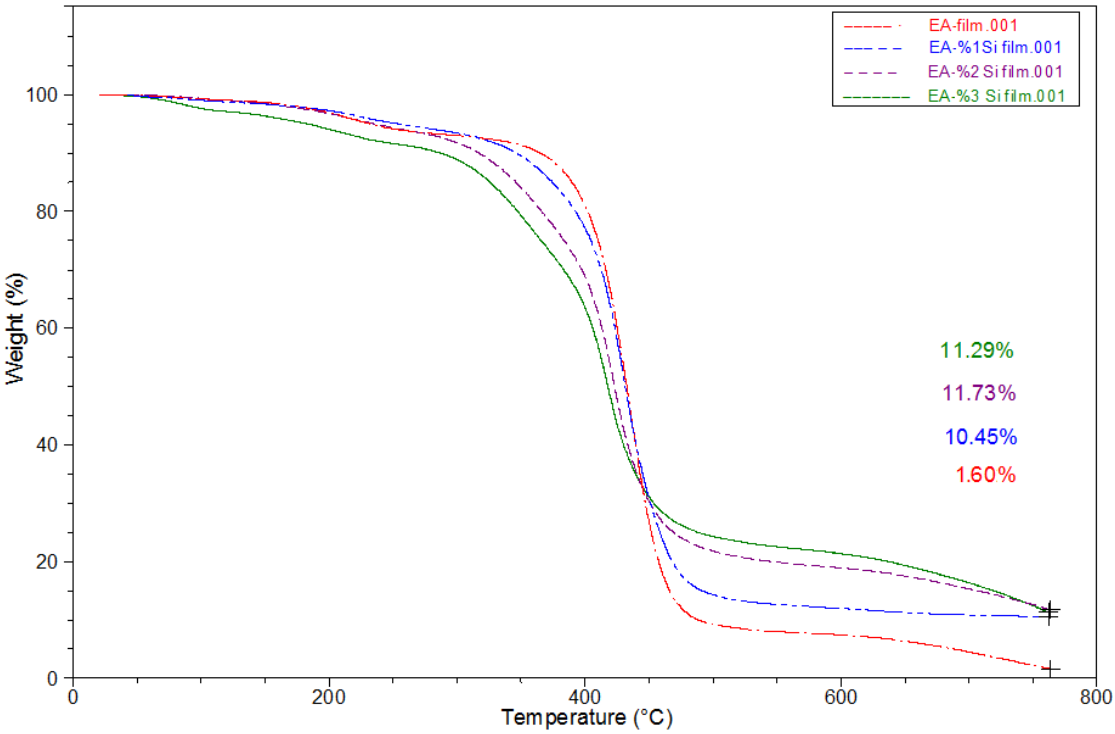

Figure 4.24 : TGA thermogram of cured EA-control film (A),), %1 (B), %2 (C), %3 (D) UV cured EA-Si nano hybrid films.

The TGA thermograms of cured EA-control film and EA-Si hybrid films are shown in Figure 4.24. The samples were heated up to 800°C by the rate of 20°C/min. The weight

loss at the temperature less than 280°C can be attributed to trapped volatile content of the cured resins which is less than 5%. Then the thermal decomposition of the cured EA film continued up to 450 °C due to aromatic and aliphatic structure of the resin. The temperatures above 450°C indicated the complete thermal degradation of the cured films. The residue of cured EA-control film at 800°C was 1.6% and such residue for totally organic structure might be attributed to inert nitrogen atmosphere of thermal analysis. The increased content of Si-TDI nanoparticles in cured EA-Si hybrid films resulted in the increase of residues at 800°C as 10.5%, 11.7% and 11.3% for 1% Si-TDI, 2% Si-TDI and 3% Si-TDI, respectively. It was obveously seen that incorporation of Si-TDI nanoparticles into EA-Si hybrid film had a significant effect on the residue content of the hybrid films resulting in much higher char content than Si-TDI nanoparticles' own proportions. The results evaluated from TGA (Figure 4.24) confirmed the synergistic effect of Si-TDI nanoparticles on cured EA-Si hybrid film that SNPs promote char formation by forming of protective coat over the organic content of the hybrid film. The small decrease in the residue of EA-Si 3% film (11.3%) compared to the residue of EA-Si 2% film might indicate the optimum proportion of Si-TDI nanoparticles in EA-Si hybrid resin to be 3% above which the residues will not increase.

Table 4.5 : Mechanical properties of UV-cured EA-Si hybrid resins.

Sample	E-Modulus (MPa)	Tensile Strength (MPa)	Elongation at Break (%)
EA-Si %0	2437	23	1.4
EA-Si %1	2748	28	1.2
EA-Si %2	3342	34	0.8
EA-Si %3	3527	36	0.7

The application of nano hybrid materials is highly dependent on tensile properties, particularly modulus, tensile strength and elongation. These properties are also related to the crosslinking density of the resins as well as to the chemical structures. The mechanical specification of UV-cured EA-Si nano hybrid resin films of 50x10x1mm dimensions made with the measurement of stress-strain values. In Table 4.5, evaluated stress-strain data of UV-cured Si-TDI modified epoxy acrylate resins are given as ultimate tensile strength, elongation at break and modulus. As it can be seen in Table

4.5., both e- modulus and tensile strength of EA-Si resins increase with the increasing silica nanoparticle content because of increased photocrosslinking ability of the cured system. Thus, resins become more rigid and elongation values decrease with the increasing Si-TDI content.

The SEM image of UV-cured EA-Si 3% nano hybrid resin is shown in Figure 4.25. The observation of the SEM image clearly showed that aggregation of SNPs was prevented despite the relatively high surface area of SNPs. Morover, mainly homogenous dispersion of SNPs in EA resin was achieved. Obviously, the reason to that is attributed to TDI functionalization of SNPs which is further incorporated into EA resins. The isocyanate functionality together with the aromatic nature of Si-TDI particles was chosen as the appropriate structure for an optimum compatibility with bisphenol-A based epoxy acrylate resin. Also, isocyanate functionality of Si-TDI nanoparticles was aimed to react with the hydroxyl groups of EA resin by covalent bonding, regardless of the complete achivement of the aim, the SEM image in Figure 4.25 clearly indicated that Si-TDI nanoparticles in EA resin dispersed mainly homogenous without aggregation.

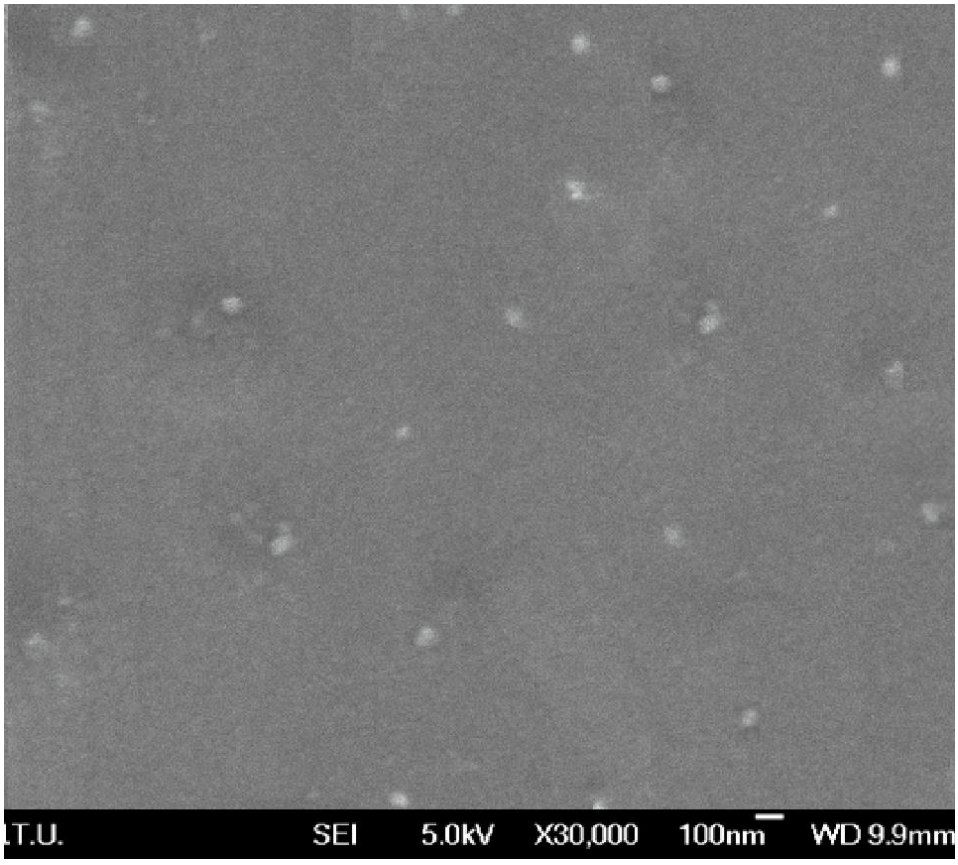

Figure 4.25 : SEM image of UV-cured EA-Si 3% hybrid resin.

4.3 Synthesis and Application of Amide-Urethane Alkoxy Silane Precursor

Alkoxy silane precursors with their wide variety of organic functional groups have been widely used as coupling agents, silane crosslinkers and organic polymer modifiers commonly being followed by the application of sol-gel process that is resulted in the formation of hybrid materials with the silicon dioxide networks. Such hybrid materials gain improved thermal, mechanical, optical, surface etc. properties depending on the strructure, chemistry and the morphology of newly formed material. In this thesis, alkoxysilane precursor of aromatic amide-urethane structure (TPAP-Si) was synthesized as a novel structure for the synthesis of hybrid materials formed by sol-gel process. Such precursor has the potential to form hybrid materials by owning the organic and inorganic component in the same monomer. TPAP-Si based sol-gel was incorparated into epoxy acrylate resin formulations following UV curing process.

4.3.1 Synthesis of N^1,N^4-bis(3-hydroxyphenyl) terephthalamide (TPAP)

Aromatic diamide structure with dihydroxy end groups (TPAP) was synthesized as shown in Figure 4.26.

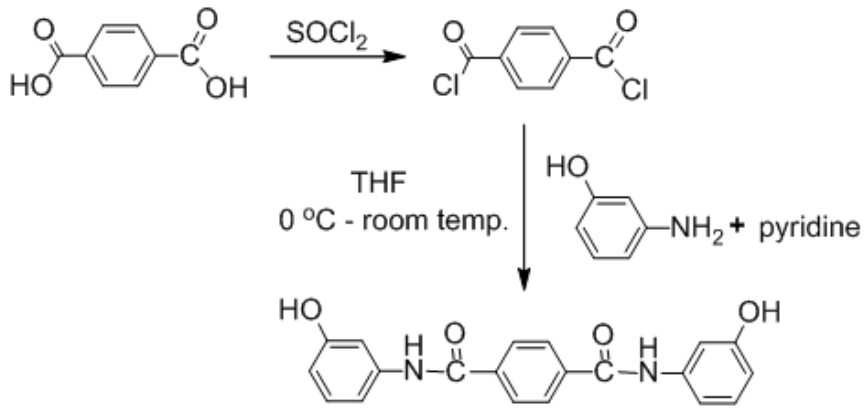

Figure 4.26 : The synthesis route for N^1,N^4-bis(3-hydroxyphenyl) terephthalamide.

Terephthaloyl chloride was successfully and easily formed by the reaction of terephthalic acid in excess $SOCl_2$. The formation of aromatic diamide structure with diphenol end groups (TPAP) was achieved in a high yield by the reaction of reactive terephthaloyl chloride with m-aminophenol. Excess m-aminophenol was used in order to prevent possible oligomeric or polymeric formation leading to form monomeric diphenol. Furthermore, both the higher reactivity of amine group over hydroxy group of m-aminophenol towards to reactive terephthaloyl chloride and the synthesis condition disabled the possible ester bond formation.

The ^{1}H-NMR spectra of TPAP in Figure 4.27 confirms the amide formation after the reaction of terephthaloyl chloride with m-aminophenol. The peak at 10.23 ppm belongs to the protons attached to the nitrogens of amide groups. Hydroxyl functionalities attached to the aromatic rings appear at 9.42 ppm. The same integration ratios of -OH and -NH protons indicates that two m-aminophenols were attached from the amine groups to form amide functions on the terephthaloyl body. Because of the high symmetry of the synthesized structure, the protons of the middle benzene ring all gave the same signal at 8.04 ppm, as expected. The integrations of aromatic protons also support the expected structure. There is no peak of the starting materials or any possibly formed side structure on the NMR spectra indicating that the material is obtained in high purity.

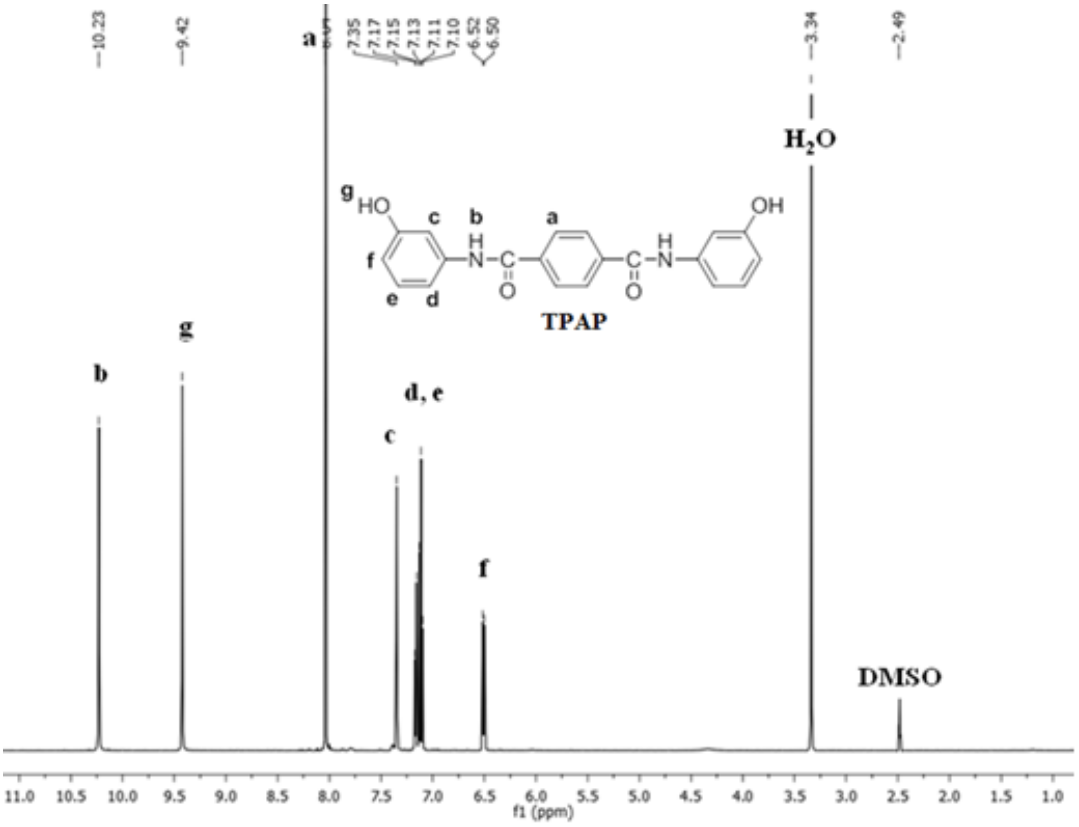

Figure 4.27 : ^{1}H-NMR spectra of TPAP.

As seen in the FTIR spectrum (Figure 4.29 A), characteristic amide (-NHCO) band at 1617 cm^{-1} and sharp-broad band at 3350 cm^{-1} region which represents both –OH and –NH functionalities also indicated the predicted structure of N^{1},N^{4}-bis(3-hydroxyphenyl) terephthalamide (TPAP).

4.3.2 Synthesis of amide-urethane alkoxy silane precursor (TPAP-Si)

Aromatic amide-urethane alkoxy silane monomeric precursor (TPAP-Si) was synthesized as represented in Figure 4.28. N^1,N^4-bis(3-hydroxyphenyl) terephthalamide of high purity was reacted with 3-(Triethoxysilyl)propyl isocyanate (IPTES) with the addition of catalytic amount of DBTL in mild condition yielding aromatic amide-urethane alkoxy silane monomer (TPAP-Si) by the formation of urethane bond.

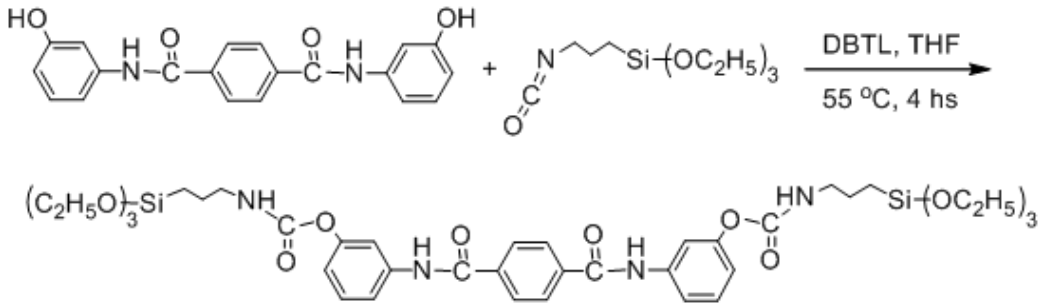

Figure 4.28 : The synthesis route for N^1,N^4-bis(3-hydroxyphenyl) terephthalamide-urethane alkoxy silane precursor (TPAP-Si).

During the synthesis reaction of TPAP-Si, both the possible hydrolysis of alkoxy silanes and undesired side reactions of reactive isocyanate group of IPTES were prevented by the purity of reacted TPAP and the use of organic solvent in mild and dry reaction condition.

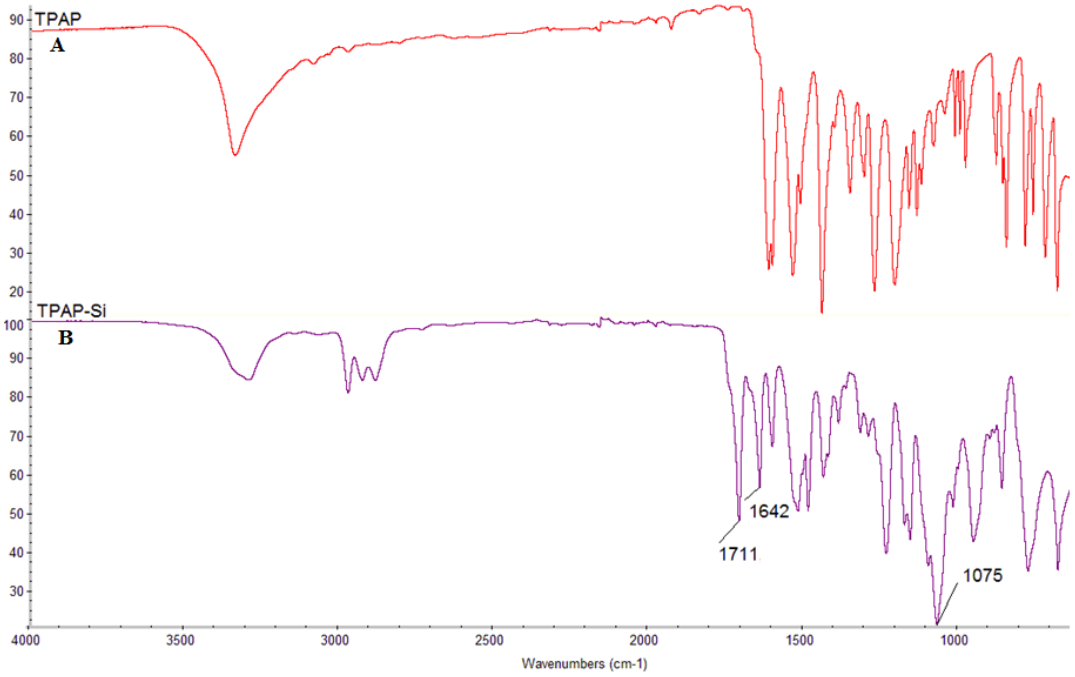

Figure 4.29 : FTIR spectrums of TPAP (A) and TPAP-Si (B).

Figure 4.29 (B) shows the FTIR spectrum of TPAP-Si. The appearance of the urethane (-NHCOO) band at 1711 cm^{-1} in addition to neighbour band of amide group at 1642 cm^{-1} confirmed the urethane reaction of TPPA with IPTES forming TPPAP-Si. Furthermore, it is clearly indicated that the new bands of $–CH_2$ group at the region of 2900 cm^{-1} and of -Si-O-C group at 1075 cm^{-1} belong to IPTES, as expected.

^{1}H-NMR spectra of TPAP-Si is seen in Figure 4.30 confirming the structure. The peak at 10.46 ppm is assigned to -NH groups of the amide linkages between the aromatic rings. Aromatic protons are seen clearly with expected integrations of the structure. As an addition to the previous TPAP structure (Figure 4.27), proton signals appeared at the higher field of NMR spectrum indicating the attached aliphatic protons of IPTES. Signals of attached NH protons are seen at 7.62 ppm. Furthermore, the signal between 0.55-0.58 ppm belongs to $–CH_2$ group next to Si atom. The overall integration ratios of the protons perfectly consistent with the expected structure of TPAP-Si. The absence of any peak as an addition to expected peaks of NMR spectrum of TPAP-Si also indicated the high purity of synthesized N^1,N^4-bis(3-hydroxyphenyl) terephthalamide-urethane alkoxy silane precursor.

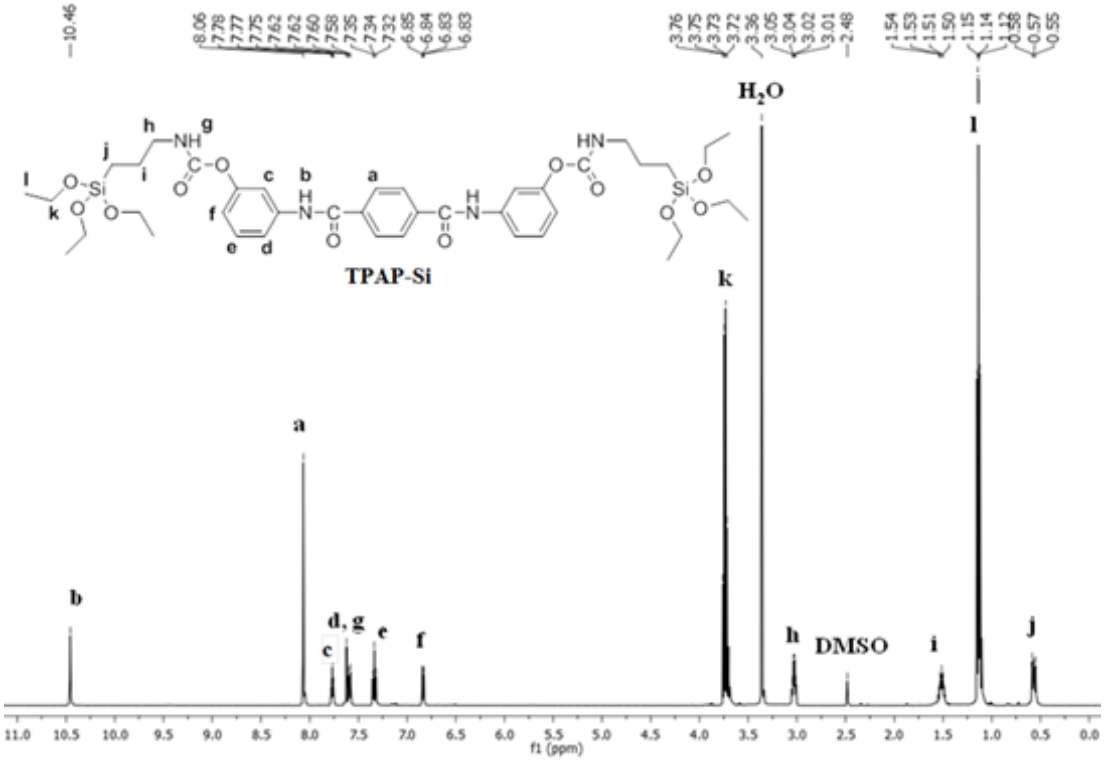

Figure 4.30 : ^{1}H-NMR spectra of TPAP-Si.

4.3.3 UV-cured epoxyacrylate/solgel hybrid resin (EA-TPAP-Si)

Aromatic amide-urethane alkoxy silane precursor (TPAP-Si) synthesized in the study of this thesis is considered as a suitable novel candidate for the synthesis of hybrid materials with improved properties having two alkoxy silane and two aromatic amide functionality per molecule. For this purpose, sol-gel of TPAP-Si and MAPTMS as component A, was prepared and incorparated into EA resin (epoxy acrylate, EM 621A-80) obtaning EA-TPAP-Si hybrid resin formulation. As a comparing compound sol-gel of only MAPTMS as component B, was also prepared and mixed with EA resin forming EA-Si hybrid resin formulation. Sol-gel/EA hybrid resin films of EA-TPAP-Si and EA-Si were obtained by UV curing process of the formulations. In order to characterize and compare the properties of UV-cured hybrid resins, EA-TPAP-Si and EA-Si, epoxy acrylate formulation without the addition of any sol-gel content was also prepared and photopolymerized obtaining UV-cured control EA resin. The synthetic route for the whole process is represented in Figure 4.31.

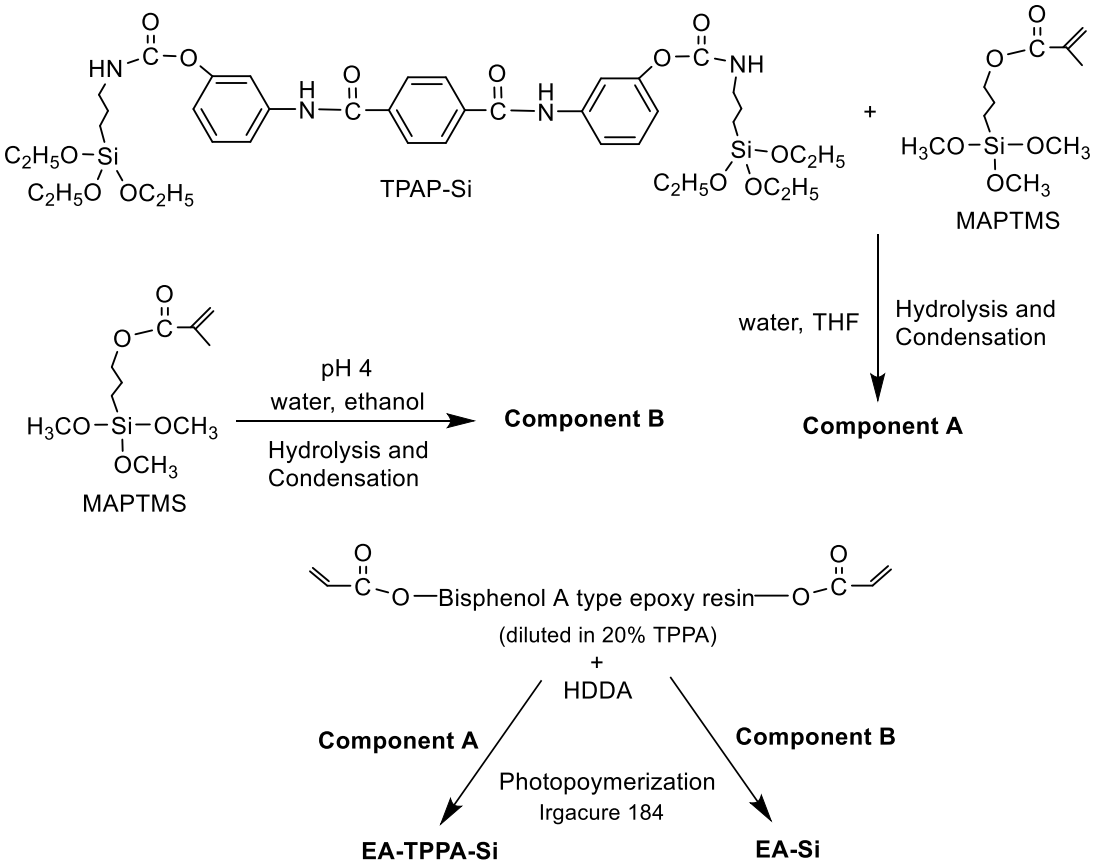

Figure 4.31 : The synthetic route for UV-cured EA/solgel hybrid resins.

Carrying two amide functionality TPAP-Si was considered as a self catalyser for the sol-gel formation and for the purpose of investigating its such property, no catalyst

was added in the sol-gel formulation of component A. Contrary, acid catalyst was used for the sol-gel formulation of component B. The ratios for the components of EA hybrid resin formulations are given in Table 4.6. After photopolymerization, UV-cured resin film samples were heated up to 100°C under vacuum for 2 h in order to remove used solvents and by products of sol-gel process.

Table 4.6 : Ratios of the components of EA hybrid resin formulations.

Sample Formulations	EA resin* (%w)	HDDA (%w)	Component A (%w)	Component B (%w)
EA	87	10	0	0
EA-Si	72	10	0	15
EA-TPAP-Si	72	10	15	0

* EM 621A-80 (diluted in 20%wt TPGDA)
3%wt of Irgacure-184 was used as photoiniator in all of the formulations of the samples.

The expected chemical structures of UV cured EA resins were confirmed by FT-IR characterization. FT-IR spectra of UV-cured resins; EA (A), EA-Si (B), and EA-TPPA-Si (C) are shown in Figure 4.32. As seen in the spectra, characteristic absorption peaks of broad -OH at the region of 3330 cm^{-1}, acrylate C=O at 1725 cm^{-1} and aromatic –C=C– at 1600 cm^{-1} which belong to BisphenolA type EA resin are common in spectrums of (A), (B) and (C) of Figure 4.32. In addition to common characteristic absorption peaks of EA resin, sharper absorption peak of –NH at 3342 cm^{-1}, amide C=O at 1620 and -NH bending at 1541 cm^{-1} are seen in the spectrum of EA-TPAP-Si (Figure 4.30 C) indicating amide-urethane alkoxy silane structure of TPAP-Si. The complete disapperance of the characteristic absorption peak of -Si-O-C- at 1075 cm^{-1} and the appearance characteristic absorption peak of -Si-O at 1162 cm^{-1} in the both spectrums of Figure 4.32 (B) and (C) confirmed the successful hydrolysis and condensation process of silanol groups in EA/Si and EA/TPAP-Si.

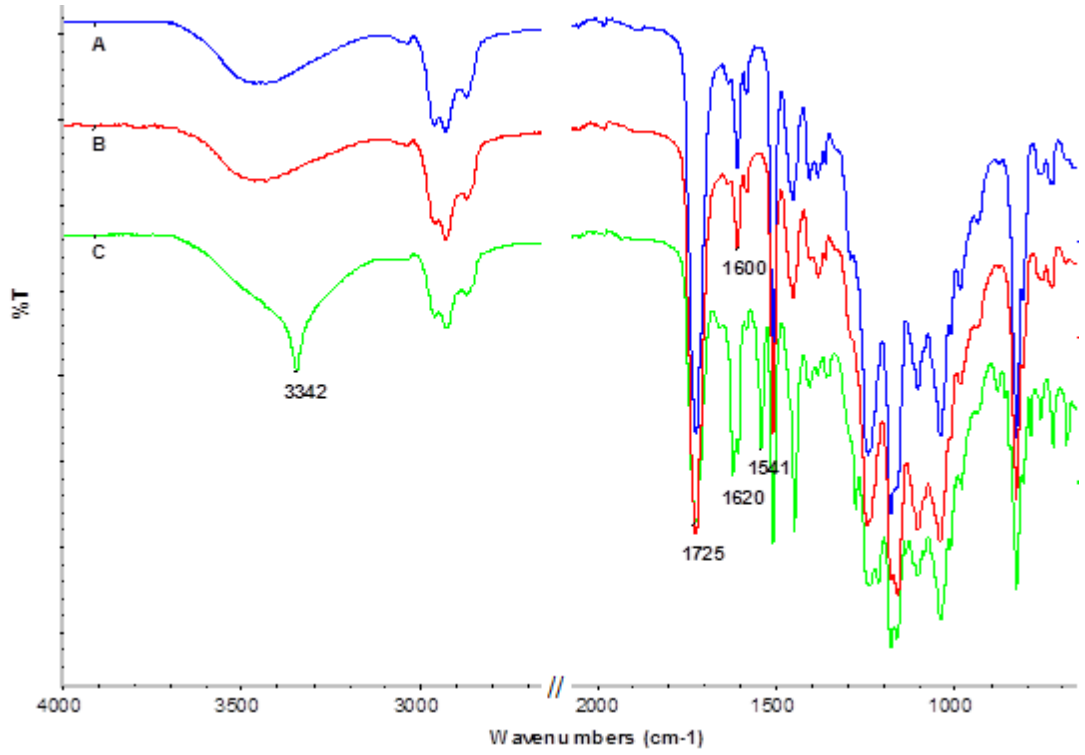

Figure 4.32 : FTIR spectrums of UV cured resins; EA (A), EA-Si (B) and EA-TPPA-Si (C).

The TGA thermograms of UV-cured EA and EA-hybrid films are shown in Figure 4.33. Since UV-cured EA resins were thermally treated at 100°C under vacuum for 4hrs before TGA analysis, the weight losses up to 130 °C were below 1 % for all of the film samples as seen in the thermograms. There is not a significant difference between the rapid weight loss temperatures of the UV-cured EA films and tempereatures were assigned as 368 °C, 364 °C and 356 °C for UV-cured EA, EA-Si and EA-TPAP-Si films, respectively. The weight losses are below 5 % for both EA and hybrid EA-Si resin at decomposition temperature of 365 °C, whereas it is approximately 13 % for hybrid EA-TPAP-Si film. The higher (13 %) weight loss of EA-TPAP-Si between 120-360 °C is attributed to continuing condensation process of partially condensed silanol groups of TPAP-Si sol during thermal analysis which is consistent with the analysis of FTIR spectrum (Figure 4.32 B). The residues at 900°C are 2 %, 11.9 % and 13.6 % for UV-cured EA, EA-Si and EA-TPAP-Si films, respectively. It was obviously seen that incorporation of MPTES and TPAP-Si sols into EA resin as inorganic network had a significant effect on the char yield of UV-cured hybrid EA films. Besides, synergistic effect of silica network was also assigned by the higher char yields of EA hybrid films than possible silisium dioxide content that was formed by sol-gel content of the hybrid resin formulations.

Moreover, according to TGA thermogram in Figure 4.33 the flame retardant behavior of TPAP-Si structure may be also evaluated. Contrary to fact that the ratio of inorganic SiO_2 content of EA-TPAP-Si was lower than that of EA-Si and condensation process of silanol groups of TPAP-Si significantly continued during thermal analysis, EA-TPAP-Si hybrid resin resulted in a higher char yield at 900°C. This contradiction may indicate the improving effect of aromatic amide structure of TPAP-Si on flame retardancy.

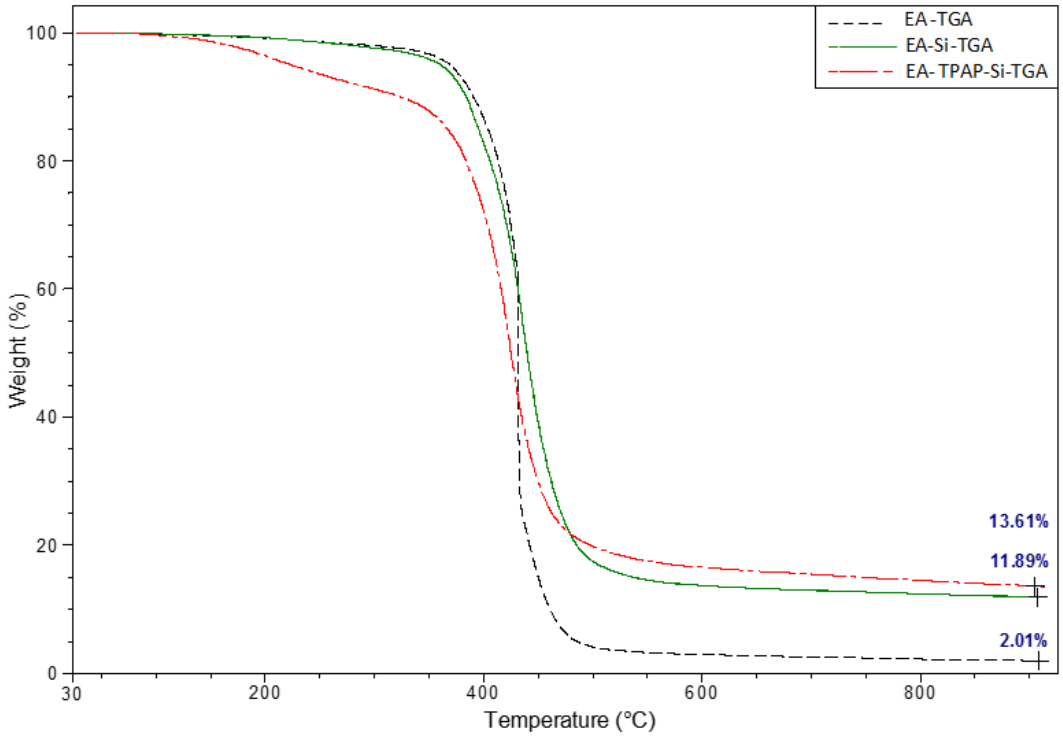

Figure 4.33 : TGA thermogram of UV-cured EA, EA-Si and EA-TPAP-Si films.

SEM examination of UV-cured EA-Si and EA-TPAP-Si hybrid resin films was performed and micrographs are shown in Figure 4.34 (A) and (B), respectively. As seen in Figure 4.32, the surface of EA-TPAP-Si hybrid resin exhibits smoother and more homogenous transitions than the surface of EA-Si hybrid resin. SEM images of EA-Si film appears as heterogeneous and particulate-like structure. This is clearly evidence that aromatic amide-urethane structure of TPAP-Si is compatible with bisphenol a type EA resin and improves the missibility and morphlogical properties of EA-TPAP-Si hybrid resin. Moreover, the higher rate of the condensated silanol groups of EA-Si is also confirmed by the SEM images in Figure 4.34 having small aggregated regions contrary to possibly linear like network structure of EA-TPAP-Si as a result of its less condensed silanol groups. Evaluating by SEM observation, the morphology

difference because of the condensation rates of silanol groups of the hybrid resins is also consistent with the results of FTIR and TGA analysis of the hybrid resin films.

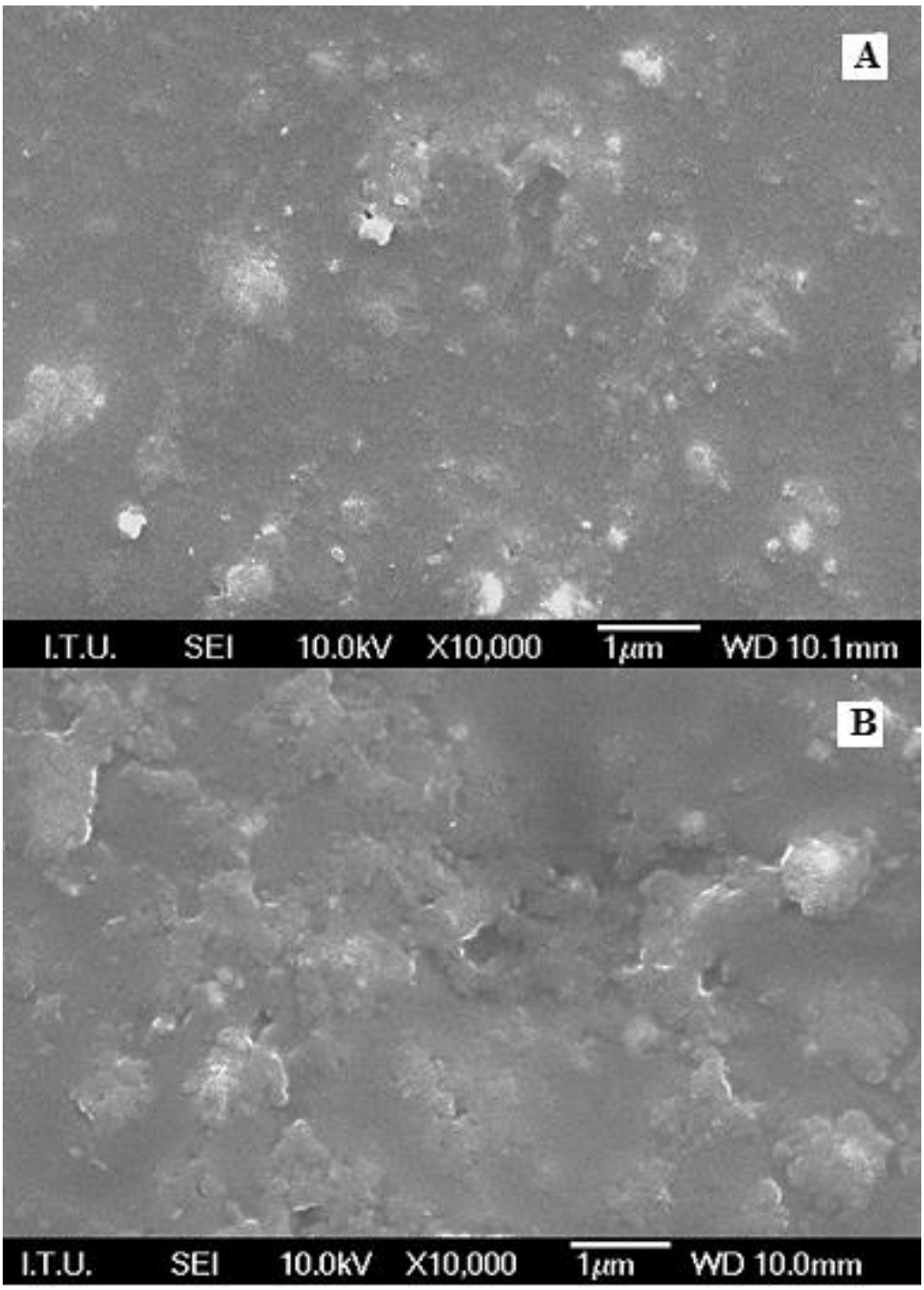

Figure 4.34 : SEM images of UV-cured EA-Si (A) and EA-TPAP-Si (B) films.

5. CONCLUSIONS

The structures and the properties of all of the synthesized compounds and materials were characterized and evaluated by the instruments based on the spectral (^{1}H-, ^{13}C-CP/MAS, and ^{29}Si MAS-NMR, IR) thermal (DSC, TGA) and microscopic (SEM and TEM) and stress-strain calculationg methods.

As the first part of this thesis well-defined, monodisperse, uniform silica nanoparticles synthesized by Stöber process. Adjusting the reaction conditions such as temperature, concentration of TEOS and ammonia their effect on the size and structure of the SNPs were evaluated. Physical and chemical structure of the the synthesized nanoparticles such as particle size, specific surface area and hydroxyl number were characterized clarifying their surface properties for the modification of silica nanoparticles.

During the modification of silica nanoparticles by alkoxy silane coupling agents, the possible formation of a siloxane network layer on the surface of SNPs and also different type of attachments of alkoxysilanes leading in inadequate and variety of concentration of functional groups were aimed to prevent in this thesis, by using effective toluene diisocyanate molecule instead of seemingly effective alkoxy silane coupling agents. After the well definition of SNPs, surface modification of the silica nanoparticles was achieved with the reaction over p-isocyanate groups of toluen di-isocyanate (TDI) obtaining Si-TDI nanoparticles in order to gain both improved dispersion of SNPs in organic phase and ability for further possible reactions over the free m- isocyanate group of TDI.

In most of monomer grafted nanoparticle hybrid systems, the polymerization proceeds both by monomers attached on the surface of nanoparticles, and the free monomers existing in polymerization medium resulting in a high yield of ungrafted polymer. For this reason, initiator grafted nanoparticles may be considered as the rewarding structure in order to obtain higher grafting ratios of polymers onto the nanoparticles surfaces. In this thesis, for the role of SNP macro initiator, benzoin grafted SNP

structure was designed and synthesized aiming of higher grafting ratios and restriction of photoinitiator migration in polymeric matrices. High reactive di-isocyanate groups of Si-TDI enabled the covalent attachment of benzoin molecules on the surface of silica nanoparticles acting as a bridge between SNPs and benzoin photoinitiator. Consequantly, benzoin grafted SNPs (Si-Ben) initiated the photopolymerization of MMA under UV irradiation becaming the core part of Si-PMMA hybrid nanoparticles. SEM observations exhibited the PMMA grafting on the surface of SNPs core with the increased volume closely to spherical form of silica nanoparticles indicating the structure of inorganic silica core and outer layer of PMMA. By this study, macroinitiator SNPs, formed by covalent grafting of benzoin was considered as a "grafting from" system enabling either the direct synthesis of polymer silica nanoparticle hybrids with the desired UV active monomers or incorporation of polymer grafted nanoparticles into the formation of composites.

Well defined Si-TDI nanoparticles were also incorporated into preformed epoxy-acrylate resin over the urethane bond formed between hydroxyl groups of EA resin and free isocyanate groups of Si-TDI creating inorganic crosslinking points. The curing process of EA hybrid resin film was performed under UV irradiation and thermal properties of the cured films were investigated by DSC and TGA. Two different T_g values were observed for EA films and that is attributed to existence of two different region of EA resin as epoxy and acrylate. The increase in Si-TDI content of EA hybrid resins resulted in the consistent increase of T_g values of hybrid films indicating both monodispersed incorporation of inorganic Si-TDI nanoparticles into hybrid resin and crosslinker effect of Si-TDI nanoparticles. The results evaluated from TGA confirmed the synergistic effect of Si-TDI nanoparticles on cured EA-Si hybrid film significantly promoting the char formation most likely due to the protective coat occured by silica nanoparticles over the organic content. The observation of the SEM image clearly confirmed that aggregation of SNPs was prevented despite the relatively high surface area of SNPs. Moreover, mainly homogenous dispersion of SNPs in EA resin was achieved. Evaluating stress-strain data of UV-cured Si-TDI modified epoxy acrylate resins, it could be seen that both e- modulus and tensile strength of EA-Si resins increase with the increasing silica nanoparticle content because of increased photocrosslinking ability of the cured system. Thus, resins become more rigid and elongation values decrease with the increasing Si-TDI content.

In this thesis, the design of alkoxysilane precursor of aromatic amide-urethane structure was also aimed for the formation of silicon dioxide network domains and polymeric matrix simultaneously together as hybrid material. For this purpose, preformed terephthalic acid chloride was reacted with m-amino phenol yielding aromatic amid containing dihydroxy monomer, N^1,N^4-bis(3-hydroxyphenyl), and the reaction of the synthesized monomer with amino propyl trimethoxysilane (IPTES), formed alkoxysilane containing aromatic amide-urethane macromonomer, over the urethane linkage. Synthesized macromonomer precursor, characterized by ^{1}HNMR indicating the high purity, has the potential to form hybrid materials by sol-gel process owning the organic and inorganic precursor in the same precursor. TPAP-Si based sol-gel was prepared and incorparated into epoxy acrylate resin formulations following UV curing process. The expected structure of obtained UV-cured EA-TPAP-Si hybrid film was determined by FTIR. It was obviously seen that incorporation of TPAP-Si sol-gels into EA resin formulations had a significant effect on the char yield of UV-cured hybrid EA films not only because of silisium dioxide network of the precursor but also aromatic amide structure of TPAP-Si. Evaluating the SEM image of EA-TPAP-Si hybrid, the surface of the hybrid resin was oberved as smooth and having homogenous transitions. This is clearly evidence that aromatic amide-urethane structure of TPAP-Si is compatible with bisphenol a type EA resin and improves the missibility and morphlogical properties of EA-TPAP-Si hybrid resin beside its thermal properties.

REFERENCES

[1] **Schottner, G.** (2001). Hybrid sol-gel-derived polymers: Applications of multifunctional materials, *Chem. Mat., 13*, 3422-3435.

[2] **Sanchez, C., Soler-Illia, G., Ribot, F., Grosso, D.** (2003). Design of functional nano-structured materials through the use of controlled hybrid organic-inorganic interfaces, *C.R. Chim., 6*, 1131-115.

[3] **Rahman, I. A., Padavettan, V.** (2012). Synthesis of Silica Nanoparticles by Sol-Gel: Size-Dependent Properties, Surface Modification, and Applications in Silica-Polymer Nanocomposites, *Journal of Nanomaterials, 2012*, 1-15.

[4] **Sanchez, C., Ribot, F.** (1994). Design of hybrid organic-inorganic materials synthesized via sol-gel chemistry, *New J. Chem., 18*, 1007-1047.

[5] **Stöber, W., Fink, A., Bohn, E.** (1968). Controlled growth of monodisperse silica spheres in the micron size range, *J. Colloid Interface Sci., 26*, 62-69.

[6] **Park, S. K., Kim, K. D., Kim, H. T.** (2002). Preparation of silica nanoparticles: determination of the optimal synthesis conditions for small and uniform particles, *Colloids Surf., A, 197*, 7-17.

[7] **Surivet, F., Lam, T., Pascault, J., Pham, Q.** (1992). Organic inorganic hybrid materials .1. hydrolysis and condensation mechanisms involved in alkoxysilane-terminated macromonomers, *Macromolecules, 25*, 4309-4320.

[8] **Bengtsson M., Oksman K.** (2006). Silane crosslinked wood plastic composites: processing and properties, *Compos. Sci. Technol, 66*, 2177–2186.

[9] **Ashby, M. F., Brechet, Y. J. M.** (2003). Designing hybrid materials, *Acta Mater., 51*, 5801–5821.

[10] **Kickelbick, G.** (2007). *Hybrid Materials. Synthesis, Characterization, and Applications,* Wiley-VCH, Weinheim.

[11] **Patrick, J., Clement, S.** (1996). Hybrid organic–inorganic materials: a land of multidisciplinarity, *J. Mater. Chem., 6*, 511-525.

[12] **Steinhoff, K., Weidig, U., Scholtes, B., Zinn, W.** (2005). Innovative flexible metal forming processes based on hybrid thermo-mechanical interaction, *Steel Res. Int., 76*, 154-159.

[13] **Oki, A.; Qiu, X., Alawode, O., Foley, B.** (2006). Synthesis of organic-inorganic hybrid composite and its thermal conversion to porous bioactive glass monolith, *Mater. Lett., 60*, 2751-2755.

[14] **Aura, S., Jokinen, V., Laitinen, M., Sajavaara, T., Franssila, S.** (2011). Porous inorganic-organic hybrid material by oxygen plasma treatment, *J. Micromech. Microeng., 21*, 1-8.

[15] **Blanc, D., Zhang, W., Massard, C., Mugnier, J.** (2006). Synthesis and characterisation of tantalum-incorporating silica hybrid sol-gel thin films for optical application, *Opt. Mater., 28*, 331-335.

[16] **Costacurta, S., Malfatti, L., Falcaro, P., Innocenzi, P.** (2007). Photocurable silica hybrid organic-inorganic films for photonic applications, *J. Sol-Gel Sci. Technol., 44*, 59-64.

[17] **Usuki, A.; Kato, M., Okada, A., Kurauchi, T.** (1997). Synthesis of polypropylene-clay hybrid, *J. Appl. Polym. Sci., 63*, 137-139.

[18] **Lan, T., Pinnavaia, T.** (1994). Clay-reinforced epoxy nanocomposites, *Chem. Mater., 6*, 2216-2219.

[19] **Usuki, A., Kojima, Y., Kawasumi, M., Okada, A., Fukushima, Y., Kurauchi, T., Kamigaito, O.** (1993). Synthesis of nylon 6-clay hybrid, *J. Mater. Res., 8*, 1179-1184.

[20] **Krug, H., Schmidt, H.** (1994). Organic-inorganic nanocomposites for micro optical applications, *New J. Chem., 18*, 1125-1134.

[21] **Guo, Y., Mylonakis, A., Zhang, Z., Yang, G., Lelkes, P., Che, S., Lu, Q., Wei, Y.** (2008). Templated synthesis of electroactive periodic mesoporous organosilica bridged with oligoaniline, *Chem. Eur. J., 14*, 2909-2917.

[22] **Fei, J., Lim, K., Palmore, G.** (2008). Polymer composite with three electrochromic states, *Chem. Mater., 20*, 3832-3839.

[23] **Ochi, M., Nii, D., Harada, M**. (2011). Preparation of epoxy/zirconia hybrid materials via in situ polymerization using zirconium alkoxide coordinated with acid anhydride, *Mater. Chem. Phys., 129*, 424-432.

[24] **Caruso, F., Shi, X., Caruso, R., Susha, A.** (2001). Hollow titania spheres from layered precursor deposition on sacrificial colloidal core particles, *Adv. Mater., 13*, 740-744.

[25] **Lee, R., Hsiue, G., Jeng, R.** (2001). Organically modified inorganic sol-gel materials for second-order nonlinear optics, *J. Appl. Polym. Sci., 79*, 1852-1859.

[26] **Hannula, S., Turunen, E., Koskinen, J., Soderberg, O.** (2009). Processing of hybrid materials for components with improved life-time, *Curr. Appl Phys., 9*, 160-166.

[27] **Hofacker, S., Mechtel, M., Mager, M., Kraus, H.** (2002). Sol-gel: a new tool for coatings chemistry, *Prog. Org. Coat., 45*, 159-164.

[28] **Groenewolt, M.** (2008). Highly scratch resistant coatings for automotive applications, *Prog. Org. Coat., 61*, 106-109.

[29] **Ren, T.; Yuan, Z., Su, B.** (2007). Direct blue dye-encapsulated mesostructured MCM-41 composites: Microwave-assisted preparation and characterization, *Colloids Surf., A, 300*, 88-93.

[30] **Faustini, M., Nicole, L., Boissiere, C., Innocenzi, P., Sanchez, C., Grosso, D.** (2010). Hydrophobic, Antireflective, Self-Cleaning, and Antifogging Sol-Gel Coatings: An Example of Multifunctional Nanostructured Materials for Photovoltaic Cells, *Chem. Mater., 22*, 4406-4413.

[31] **Bisanda, E. T. N, Ansell, M. P.** (1991). The effect of silane treatment on the mechanical and physical properties of sisal–epoxy composites, *Compos. Sci. Technol., 41*, 165–178.

[32] **Mammeri, F., Le Bourhis, E., Rozes, L., Sanchez, C.** (2005). Mechanical properties of hybrid organic-inorganic materials, *J. Mater. Chem., 15*, 3787-3811.

[33] **Tang, Y., Zhuge, J., Gou, J., Chen, R., Ibeh, C., Hu, Y.**, (2011). Morphology, thermal stability, and flammability of polymer matrix composites coated with hybrid nanopapers, *Polym. Adv. Technol., 22*, 1403-1413.

[34] **Langer, R.** (1998). Drug delivery and targeting, *Nature, 392*, 5-10.

[35] **Heinemann, S., Ehrlich, H., Knieb, C., Hanke, T.** (2007). Biomimetically inspired hybrid materials based on silicified collagen, *Int. J. Mater. Res., 98*, 603-608.

[36] **D'Agostino, A., Colella, M., De Rosa, M., De Rosa, A., Lanza, A., Schiraldi, C.** (2009). Chemico-physical characterization of hybrid composites based on hydroxyethyl methacrylate and nanosilica, *J. Polym. Res., 16*, 561-567.

[37] **Cramer, N.B., Stansbury, J.W., Bowman, C.N.** (2011). Recent Advances and Developments in Composite Dental Restorative Materials, *J. Dent. Res., 90*, 402-416.

[38] **Komarneni, S.** (2007). Porous materials: Science and engineering, *Mater. Res. Innovations, 11*, 106-107.

[39] **De Matteis, F., Prosposito, P., Sarcinelli, F., Casalboni, M., Pizzoferrato, R., Furlani, A., Russo, M., Vannucci, A., Varasi, M.** (1999). Silica-based sol-gel films optically functionalized through doping with organic molecules, *J. Non-Cryst. Solids, 245*, 15-19.

[40] **Jena, K. K., Narayan, R., Raju, K.V.S.N.** (2013). New high performance waterborne organic–inorganic hybrid materials from UV curing, *Prog. Org. Coat., 76*, 1418-1424.

[41] **Mark, J. E.** (2006). Some novel polymeric nanocomposites, *Acc. Chem. Res., 12*, 881-888.

[42] **Jang, E. S, Khan, S. B., Seo, J., Akhtar, K., Choi, J., Kim, K. I., Han, H.** (2011). Synthesis and characterization of novel UV-Curable PU-Si hybrids: Influence of silica on thermal, mechanical, and water sorption properties of polyurethane acrylates, *Macromol. Res., 19*, 1006-1013.

[43] **Sanchez, C., Julian, B., Belleville, P., Popall, M.** (2005). Applications of hybrid organic-inorganic nanocomposites, *J. Mater. Chem., 15*, 3559-3592.

[44] **Barrer, R. M., Rideal, E. K.** (1939). Permeation, diffusion and solution of gases in organic polymers, *Transaction of the Faraday Society, 35*, 628-643.

[45] **Jia, J., Tang, M., Chen, X., Qi, L., Dong, S.** (2003). Co-immobilized microbial biosensor for BOD estimation based on sol-gel derived composite material, *Biosens. Bioelectron., 18,* 1023-1029.

[46] **Ulrich, R., Zwanziger, J., De Paul, S., Reiche, A., Leuninger, H., Spiess, H., Wiesner, U.** (2002). Solid hybrid polymer electrolyte networks: Nano-structurable materials for lithium batteries, *Adv. Mater., 14,* 1134-1137.

[47] **Gomez-Romero, P., Chojak, M., Cuentas-Gallegos, K., Asensio, J., Kulesza, P., Casan-Pastor, N., Lira-Cantu, M.** (2003). Hybrid organic-inorganic nanocomposite materials for application in solid state electrochemical supercapacitors, *Electrochem. Commun., 5,* 149-153.

[48] **Nam, S., Kim, S., Kang, Y., Lee, J., Lee, K.** (2008). Preparation of Nafion/sulfonated poly(phenylsilsesquioxane) nanocomposite as high temperature proton exchange membranes, *J. Membr. Sci., 322,* 466-474.

[49] **Giannelis, E.** (1996). Polymer layered silicate nanocomposites, *Adv. Mater., 8,* 29-35.

[50] **Allis, D., Rarig, R., Burkholder, E., Zubieta, J.** (2004). A three-dimensional bimetallic oxide constructed from octamolybdate clusters and copper-ligand cation polymer subunits. A comment on the stability of the octamolybdate isomers, *J. Mol. Struct., 688,* 11-31.

[51] **Zhu, C., Fang, Y., Wen, D., Dong, S.** (2011). One-pot synthesis of functional two-dimensional graphene/SnO_2 composite nanosheets as a building block for self-assembly and an enhancing nanomaterial for biosensing, *J. Mater. Chem., 21,* 16911-16917.

[52] **Kiselev, A. V.** (1936). The structure of silicic acid gels. *Kolloidn. Zh., 2,* 17-26.

[53] **Carman, P. C.** (1940). Constitution of colloidal silica, *Transactions of the Faraday Society, 36,* 964-973.

[54] **Hench, L., West, J.** (1990). The sol-gel process, *Chem. Rev., 90,* 33-72.

[55] **Novak, B. M.** (1993). Hybrid Nanocomposite Materials between inorganic glasses and organic polymers, *Adv. Mater., 5,* 422-433.

[56] **Yano, S., Nakamura, K., Kodomari, M., Yamauchi, N.** (1994). Preparation and properties of poly(vinyl acetate)/silica-gel microhybrids, *J. Appl. Polym. Sci., 54,* 163-176.

[57] **Malay, O., Yilgor, I., Menceloglu, Y.Z.** (2013). Effects of solvent on TEOS hydrolysis kinetics and silica particle size under basic conditions, *J. Sol-Gel Sci. Technol., 67,* 351-361.

[58] **Eisenberg, P., Erra-Balsells, R., Ishikawa, Y., Lucas, J. C., Mauri, A. N., Nonami, H., Riccardi, C. C., Williams, R. J. J.** (2000). Cagelike Precursors of High-Molar-Mass Silsesquioxanes Formed by the Hydrolytic Condensation of Trialkoxysilanes, *Macromolecules, 33,* 1940-1947.

[59] **Donescu, D., Serban, S., Gosa, K., Peteu, C.** (2005). Polymer-Titanium hybrids obtained by radical polymerization and Sol-Gel process, *Cent. Eur. J. Chem., 3,* 10-27.

[60] **Levy, D., Einhorn, S., Avnir, D.** (1989). Applications of the sol-gel process for the preparation of photochromic information-recording materials - synthesis, properties, mechanisms, *J. Non-Cryst. Solids*, *113*, 137-145.

[61] **Vacassy, R., Flatt, R. J., Hofmann, H., Choi, K. S., Singh, R. K.** (2000). Synthesis of Microporous Silica Spheres, *J. Colloid Interface Sci.*, *227*, 302-315.

[62] **Brinker, C. J.** (1988). Hydrolysis and condensation of silicates: Effects on structure, *J. Non-Cryst. Solids*, *100*, 31-50.

[63] **Badley, R., Ford, W., McEnroe, F., Assink, R.** (1990). Surface modification of colloidal silica, *Langmuir*, *6*, 792-801.

[64] **Abdelmouleh, M., Boufi, S., Belgacem, M. N., Dufresne, A.** (2007). Short natural-fibre reinforced polyethylene and natural rubber composites: effect of silane coupling agents and fibres loading, *Compos. Sci. Technol.*, *67*, 1627-1639.

[65] **Allauddin, S., Narayan, R., Raju, K. V. S. N.** (2013). Synthesis and Properties of Alkoxysilane Castor Oil and Their Polyurethane/Urea–Silica Hybrid Coating Films, *ACS Sustainable Chem. Eng.*, *1*, 910-918.

[66] **Brunauer, S., Emmett, P. H., Teller, E.** (1938). Adsorption of Gases in Multimolecular Layers, *J. Am. Chem. Soc.*, *60*, 309-319.

[67] **Matijevic, E.** (1986). Monodispersed Colloids - Art and Science, *Langmuir*, *2*, 12-20.

[68] **Tilgner, I., Fischer, P., Bohnen, F., Rehage, H., Maier, W.** (1995). Effect of acidic, basic and fluoride-catalyzed sol-gel transitions on the preparation of sub-nanostructured silica, *Microporous Mater.*, *5*, 77-90.

[69] **LaMer, V. K., Dinegar, R. H.** (1950). Theory, Production and Mechanism of Formation of Monodispersed Hydrosols, *J. Am. Chem. Soc.*, *72*, 4847-4854.

[70] **Silva C. R., Airoldi C.** (1997). Acid and Base Catalysts in the Hybrid Silica Sol–Gel Process, *J. Colloid Interface Sci.*, *195*, 381-387.

[71] **Pileni, M. P.** (2003). The role of soft colloidal templates in controlling the size and shape of inorganic nanocrystals, *Nat. Mater.*, *2*, 145-150.

[72] **Malay, O., Oguz, O., Kosak, C., Yilgor, E., Yilgor, I., Menceloglu, Y.Z.** (2013). Polyurethaneurea-silica nanocomposites: Preparation and investigation of the structure-property behavior, *Polymer*, *54*, 5310-5320.

[73] **Liao, W., Teng, H., Qu, J., Masuda, T.** (2011). Fabrication of chemically bonded polyacrylate/silica hybrid films with high silicon contents by the sol-gel method, *Prog. Org. Coat.*, *71*, 376-383.

[74] **Daniels, M. W. Sefcik, J., Francis, L. F., McCormick, A. V.** (1999). Reactions of a Tri-Funcitional Silane Coupling Agent in the Presence of Colloidal Silica Sols in Polar Media, *J. Colloid Interface Sci.*, *219*, 351–356.

[75] **Salon, M. B., Belgacem, M. N.** (2010). Competition between hydrolysis and condensation reactions of trialkoxysilanes, as a function of the amount

of water and the nature of the organic group, *Colloids Surf., A, 366*, 147–154.

[76] **Paquet, O., Salon, M. B., Zeno, E., Belgacem, M. N.** (2012) Hydrolysis-condensation kinetics of 3-(2-amino-ethylamino)propyl-trimethoxysilane, *Mater. Sci. Eng. C, 32*, 487–493.

[77] **Guo, J. J., Liu, X. H., Cheng, Y. C., Li, Y., Xu, G. J., Cui P.** (2008). Size Controllable Synthesis of Monodispersed Colloidal Silica Nanoparticles via Hydrolysis of Elemental Silicon, *J. Colloid Interface Sci., 326*, 138–142.

[78] **Balthis, J. H. Mendenhall, P.** (1989). Preparation of sols from finely divided silicon, *United States Patent*, No: 2614994 dated 1952.

[79] **Vansant, E. F., Van Der Voort, P., Vrancken, K. C.** (1995). *Characterization and chemical modification of the silica surface*, Elsevier, Amsterdam.

[80] **Green, D. L., Lin, J. S., Lam, Y. F., Hu, M. Z., Schaefer, D. W., Harris, M. T**. (2003). Size, volume fraction, and nucleation of Stober silica nanoparticles, *J. Colloid Interface Sci., 266*, 346-58.

[81] **Matsoukas, T., Gulari**, **E.** ***(***1988). Dynamics of Growth of *Silica* Particles from Ammonia-Catalyzed Hydrolysis of Tetra-ethyl-orthosilicate, *J. Colloid Interface Sci., 124*, 252-261.

[82] **Park, S. K., Kim, K. D., Kim, H. T.** (2002). Preparation of silica nanoparticles: determination of the optimal synthesis conditions for small and uniform particles, *Colloids Surf., A, 197*, 7-17.

[83] **Pandey, S., Mishra, S.** (2011). Sol-gel derived organic-inorganic hybrid materials: synthesis, characterizations and applications, *J. Sol-Gel Sci. Technol., 59*, 73-94.

[84] **Zhuravlev, L. T.** (2000). The surface chemistry of amorphous silica, Zhuravlev model, *Colloids Surf., 173*, 1-38.

[85] **Kiselev, A. V., Lygin, V. I.** (1975). *Infrared Spectra of Surface Compounds*, John Wiley & Sons, New York.

[86] **Young, G. J.** (1958). Interaction of water vapor with silica surfaces, *J. Colloid Sci., 13*, 67-85.

[87] **Barby, D.** (1976). Characterization of powder surface, *Academic Press*, London.

[88] **Agzamkhodzhaev, A., Zhuravlev, L., Kiselev, A., Shengeliya, K.** (1974). Rehydroxylation of surface of amorphous silicas, *Colloid Journal of the Ussr, 36*, 1036-1039.

[89] **Iler, R. K.** (1979). *The Chemistry of Silica: Solubility, Polymerization, Colloid and Surface Properties, and Biochemistry*, John Wiley & Sons, Chichester.

[90] **Kiselev, A.V.** (1957). *Surface Chemical Compounds and Their Role in Adsorption Phenomena*, Moscow State University Press, Moscow.

[91] **Peri, J. B., Hensley, J. A L.** (1968). The Surface Structure of Silica Gel, *J. Phys. Chem., 72*, 2926-2933.

[92] **Harris, R. K., Mann, B. E.** (1978). *NMR and the Periodic Table*, Academic Press, New York.

[93] **Blinka, T. A., Helmer, B. J., West, R.** (1984). Polarization Transfer NMR Spectroscopy for Silicon-29: The INEPT and DEPT Techniques, *Adv. Organomet. Chem., 23*, 193-218.

[94] **Zhuravlev, L. T.** (1987). Concentration of hydroxyl groups on the surface of amorphous silicas, *Langmuir, 3*, 316-318.

[95] **Zhuravlev, L. T.** (1989). Structurally bound water and surface characterization of amorphous silica, *Pure Appl. Chem., 61*, 1969-1976.

[96] **Zhuravlev, L.T.** (1993). Surface characterization of amorphous silica-a review of work from the former USSR, *Colloids Surf., A, 74*, 71-90.

[97] **Langmuir, I.** (1916). The constitution and fundamental properties of solids and liquids. Part I. Solids, *J. Am. Chem. Soc., 38*, 2221-2295.

[98] **McClellan, A. L., Harnsberger, H. F.** (1967). Cross-sectional areas of molecules adsorbed on solid surfaces, *J. Colloid Interface Sci., 23*, 577-599.

[99] **Cook, M. A.** (1948). Theory of Adsorption of Gases on Solids, *J. Am. Chem. Soc., 70*, 2925-2930.

[100] **Carrott, P., Roberts, R., Sing, K.** (1988). Adsorption of neopentane by nonporous carbons and silicas, *Langmuir, 4*, 740-743.

[101] **Partyka, S., Rouquerol, F., Rouquerol, J.** (1979). Calorimetric determination of surface-areas - possibilities of a modified harkins and jura procedure, *J. Colloid Interface Sci., 68*, 21-31.

[102] **Wheeler, A.** (1951). Advances in Catalysis, *Academic Press*, New York, *3*, 250.

[103] **Gurvitsch L.G.** (1915). Physicochemical attractive force, *Russ. J. Phys. Chem., 47*, 805-827.

[104] **Elhamzaoui, H., Toupance, T., Maugey, M., Zakri, C., Jousseaume, B.** (2007). Particle growth of hybrid materials followed by dynamic light scattering, *Langmuir, 23*, 785-789.

[105] **Hong, B., Panagiotopoulos, A.** (2012). Molecular Dynamics Simulations of Silica Nanoparticles Grafted with Poly(ethylene oxide) Oligomer Chains, *J. Phys. Chem. B, 116*, 2385-2395.

[106] **Fripiat, J. J., Uytterhoeven, J.** (1962). Hydroxyl content in silica gel "Aerosil", *J. Phys. Chem., 66*, 800-805.

[107] **Armistead, C. G., Tyler, A. J., Hambleton, F. H., Mitchel, S. A., Hockey, J. A.** (1969). Surface hydroxylation of silica, *J. Phys. Chem., 73*, 3947-3953.

[108] **Michael, G., Ferch, H.** (2001). Basic characteristics of Aerosil, *Degussa Technical Bulletin Pigments, 11*, 41.

[109] **Gorski, D., Klemm, E., Fink, P., Horhold, H.** (1988). Investigation of quantitative SiOH determination by the silane treatment of disperse silica, *J. Colloid Interface Sci., 126*, 445-449.

[110] **Hoffmann, P., Knozinger, E.** (1987). Novel aspects of mid and far IR fourier spectroscopy applied to surface and adsorption studies on SiO_2, *Surf. Sci., 188*, 181-198.

[111] **Zhdanov, S., Kosheleva, L., Titova, T.** (1987). IR Study of hydroxylated silica, *Langmuir, 3*, 960-967.

[112] **Kellum, G. E., Smith, R. C.** (1967). Determination of water, silanol, and strained siloxane on silica surfaces, *Anal. Chem., 39*, 341-345.

[113] **Sindorf, D., Maciel, G.** (1983). Si-29 Nuclear magnetic-resonance study of hydroxyl sites on dehydrated silica-gel surfaces, using silylation as a probe, *J. Phys. Chem., 87*, 5516-5521.

[114] **Gilpin, R., Gangoda, M., Jaroniec, M.** (1997). Preparation and characterization of silica-carbon hybrids, *Carbon, 35*, 133-139.

[115] **Panasyuk, G., Budova, G., Lazarev, V.** (1979). Thermogravimetric investigation of the dehydration thermodynamics of amorphous silica after its hydrothermal and thermovaporous treatment, *J. Therm. Anal., 17*, 311-317.

[116] **DeFarias, R., Airoldi, C.** (1998) Thermogravimetry as a reliable tool to estimate the density of silanols on a silica gel surface, *J. Therm. Anal. Calorim., 53*, 751-756.

[117] **Lin, J. Chen, H. Ji, Y. Zhang, Y.** (2012) Functionally modified monodisperse core–shell silica nanoparticles: Silane coupling agent as capping and size tuning agent, *Colloids Surf., A, 411*, 111–121.

[118] **Bauer, F., Glasel, H. J., Decker, U., Ernst, H., Freyer, A., Hartmann, E., Sauerland, V., Mehnert, R.** (2003). Trialkoxysilane Grafting onto Nanoparticles for the Preparation of Clear Coat Polyacrylate Systems with Excellent Scratch Performance, *Prog. Org. Coat., 47*, 147–153.

[119] **Cousinié, S., Gressier, M., Alphonse, P., Menu, M. J.** (2007). Silica-based nanohybrids containing dipyridine, urethan or urea derivatives, *Chem. Mater., 19*, 6492-6503.

[120] **Rotzoll, R., Vana, P.** (2008). Synthesis of poly(methyl acrylate) loops grafted onto silica nanoparticles via reversible addition-fragmentation chain transfer, *J. Polym. Sci., Part A: Polym. Chem., 46*, 7656-7666.

[121] **Haensch, C., Hoeppenerand, S., Schubert, U. S.** (2010) Chemical modification of self-assembled silane based monolayers by surface reactions, *Chem. Soc. Rev., 39*, 2323-2334.

[122]**Zhang, P., Zhang, C., Zhao, Y.** (2012). Facile synthesis of highly pure block copolymers by combination of RAFT polymerization, click reaction and de-grafting process, *Polym. Chem., 3*, 1803-1812.

[123]**Atsushi, S., Kazufumi, K., Ryutaro, W., Yasuhiro, T., Yusuke, A., Masaki, K.** (2014). Utilization of Alkoxysilyl Groups for the Creation of Structurally Controlled Siloxane-Based Nanomaterials, *Chem. Mater., 26*, 211-220.

[124] **Jermouni, T., Smaihi, M., Hovnanian, N.** (1995). Hydrolysis and initial polycondensation of phenyltrimethoxysilane and diphenyldimethoxysilane, *J. Mater. Chem., 5,* 1203-1208.

[125] **Nachtigall, S. M. B., Cerveira, G. S., Rosa S. M. L.** (2007). New polymeric-coupling agent for polypropylene/wood–flour composites, *Polym. Test., 26*, 619–628.

[126] **Gassan, J., Bledzki, A. K.** (1997). Effect of moisture content on the properties of silanized jute-epoxy composites, *Polym. Compos., 18*, 179-184.

[127] **Matuana1, L. M., Woodhams, R. T., Balatinecz, J. J., Park, C. B.** (1998). Influence of interfacial interactions on the properties of PVC/cellulosic fiber composites, *Polym. Compos., 19*, 446-455.

[128] **Feng, X., Fryxell, G. E., Wang, L.-Q., Kim, A. Y., Liu, J., Kemner, K. M.** (1997). Functionalized Monolayers on Ordered Mesoporous Supports, *Science, 276*, 923-926.

[129] **Bayramoğlu, G., Kahraman, M. V., Kayaman-Apohan, N., Güngör, A.** (2006). Synthesis and characterization of UV-curable dual hybrid oligomers based on epoxy acrylate containing pendant alkoxysilane groups, *Prog. Org. Coat., 57*, 50-55.

[130] **Perro, A., Manoharan, V. N** (2010). Bulk Synthesis of Polymer-Inorganic Colloidal Clusters, *Langmuir, 26*, 18669-18675.

[131] **Matuana, L. M., Woodhams, R. T., Balatinecz, J. J., Park, C. B.** (1998). Influence of interfacialinteractions on the properties of PVC/cellulosic fiber composites, *Polym. Compos., 19*, 446–455.

[132] **Huang, Y., Hou, T., Cao, X., Perrier, S., Zhao, Y.** (2010). Synthesis of silica-polymer hybrids by combination of RAFT polymerization and azide-alkyne cycloaddition 'click' reaction, *Polym. Chem., 20*, 1615-1623.

[133] **Che, J., Xiao, Y., Wang, X., Pan, A., Yuan, W., Wu, X.** (2007). Grafting polymerization of polyacetal onto nano-silica surface via bridging isocyanate, *Surf. Coat. Technol., 201*, 4578-4584.

[134] **Carrot, G. Oberdisse, J. Jestin, J. Boué, F. El Harrak, A.** (2005). Atom transfer radical polymerization from silica nanoparticles using the 'grafting from'method and structural study via small-angle neutron scattering, *Polymer, 46*, 1095- 1104.

[135] **Kim, E. Kim, S. Kim, W.** (2005). Surface modification of silica nanoparticles by UV-induced graft polymerization of methyl methacrylate, *J. Colloid Interface Sci., 292*, 93-98.

[136] **Waddell, T. G., Leyden, D. E., DeBello, M. T.** (1981). The nature of organosilane to silica-surface bonding, *J. Am. Chem. Soc., 103*, 5303-5307.

[137] **Stenzel, M. H., Zhang, L., Huck, W. T. S.** (2006). Temperature-responsive glycopolymer brushes synthesized via RAFT polymerization using the Z-group approach, *Macromol. Rapid Commun., 27*, 1121-1126.

[138] **Torry, S.A. Campbell, A. Cunliffe, A. V., Tod, D.A.** (2006). Kinetic analysis of organosilane hydrolysis and condensation, *Int. J. Adhes. Adhes., 26*, 40-49.

[139] **Wight, A. P., Davis, M. E.** (2002) Design and preparation of organic−inorganic hybrid catalysts, *Chem. Rev., 102*, 3589-3614.

[140] **Parida, S. K., Dash, S., Patel, S., Mishra, B.K.** (2006). Adsorption of organic molecules on silica surface, *Adv. Colloid Interface Sci., 121*, 77-110.

[141] **Wang, Y. Pei, X. Yuan, K.** (2005). Reverse ATRP grafting from silica surface to prepare well-defined organic/inorganic hybrid nanocomposite, *Mater. Lett., 59*, 520– 523.

[142] **Kickelbick, G., Holzinger, D., Ivanovici,** (2008). *Organically Functionalized Silica Nanoparticles*, Materials Syntheses, Springer, Vienna.

[143] **Bachmann, S. Wang, H. Albert, K. Partch, R.** (2007). Graft polymerization of styrene initiated by covalently bonded peroxide groups on silica, *J. Colloid Interface Sci., 309*, 169-175.

[144] **Huang, Y., Liu, Q., Zhou, X., Perrier, S., Zhao, Y.** (2009). Synthesis of silica particles grafted with well-defined living polymeric chains by combination of RAFT polymerization and coupling reaction, *Macromolecules, 42*, 5509-5517.

[145] **Li, D. Sheng, X. Zhao, B**. (2005). Environmentally responsive "Hairy" nanoparticles: Mixed homopolymer brushes on silica nanoparticles synthesized by living radical polymerization techniques, *J. Am. Chem. Soc., 127*, 6248-6256.

[146] **Serhatli, I. E., Kacar, T., Önen**, **A.** (2003). Synthesis of Liquid Crystalline-Amorphous Block Copolymers by Combination of ATRP and Photoinduced Polymerization, *J. Polym. Sci., Part A: Polym. Chem., 42*, 1892-1903.

[147] **Demirhan, S., Serhatli , İ. E.**, **Önen**, **A.** (2007). Synthesis of Liquid Crystalline- Amorphous Block Copolymers by the Combination of Atom Transfer and Promoted Cationic Polymerization, *J. Appl. Polym. Sci., 106*, 568-575.

[148] **Karahasanoğlu, M., Önen, A., Serhatlı, İ. E.** (2014). Synthesis of hybrid materials via photopolymerization of benzoin functionalized silica nanoparticles, *Prog. Org. Coat., 77*, 1079-1084.

CURRICULUM VITAE

Candidate's full name: Müfide Duriye KARAHASANOĞLU

Place and date of birth: İSTANBUL, 23.08.1979

e-mail: karahasan5@itu.edu.tr

Universities and Colleges attended:

2006-2015 ***Philosophy of Doctorate,*** Chemistry
Istanbul Technical University, Istanbul, Turkey

2003-2005 ***Master of Science,*** Chemistry
Istanbul Technical University, Istanbul, Turkey

1998-2002 ***Bachelor of Science,*** Chemistry
Marmara University, Istanbul, Turkey

Professional Experience:

2006-2016 ***Research and Teaching Assistant,*** Chemistry
Istanbul Technical University, Istanbul, Turkey

Publications:

• Synthesis of hybrid materials via photopolymerization of benzoin functionalized silica nanoparticles. **Karahasanoğlu, M.**, Önen, A., Serhatlı, İ. E. (2014). *Prog. Org. Coat.,77,* 1079-1084.